UNIVERSITÀ DEGLI STUDI DI PADOVA

DIPARTIMENTO DI INGEGNERIA INDUSTRIALE

CORSO DI LAUREA MAGISTRALE IN INGEGNERIA ENERGETICA

Tesi di Laurea Magistrale in

Ingegneria Energetica

NUMERICAL SIMULATION OF FLOW CONSIDERING WATER INJECTION IN FRONT OF A RADIAL COMPRESSOR STAGE

Relatore: Prof. Giorgio Pavesi

Relatore: Prof. Friedrich-Karl Benra

Laureando: Mattia De Poli

ANNO ACCADEMICO 2016 – 2017

Contents

Abstract

Water injection has been used as an effective method to improve the compression process and the overall performance in gas turbines. In the process, evaporation of small droplets takes place and a reduction of the temperature rise through the compressor is obtained, lowering its power demand.

The method has been applied and studied mainly in axial machines, both in numerical and experimental investigations, whereas knowledge about the process in centrifugal compressors is limited and will require increased efforts in the future.

The aim of this work is to provide further information about the overall behaviour of the machine and analyse thermodynamic aspects related to water droplets injection in the compression process. Thus, a CFD analysis of a radial compressor stage has been performed to understand how the evaporation takes place through the stage, investigating its effects on temperature, pressure and power consumption.

A validation CFD case has been developed first, to test the behaviour of small droplets evaporation in free stream conditions, and has been compared with a 1D numerical model to check its validity.

In the radial compressor CFD model, different water injection rates and droplets sizes are tested, and their influence on the compressor performance is investigated. Some considerations about the efficiency and the specific work of the compressor are also presented. Moreover, a discrete particle distribution is used and the results are presented in comparison with the specified diameter cases analysed.

The effect of evaporation is analysed inside the impeller, and mean particle diameter, vapour mass fraction, pressure and temperature variations are described, using mass flow rate averages on a set of locations along the streamwise direction.

Lastly, starting from the investigation carried out, some considerations about further work to be done on the topic are given.

Sommario

L’iniezione di acqua è utilizzata come metodo efficace per migliorare la performance nelle turbine a gas. Durante la compressione si verifica l’evaporazione delle piccole gocce d’acqua, con una conseguente riduzione dell’incremento di temperature attraverso il compressore e una minor potenza richiesta dallo stesso.

Questa tecnica è stata utilizzata studiata principalmente in macchine assiali con analisi numeriche e sperimentali, mentre le conoscenze nell’ambito dei compressori centrifughi è limitata e richiederà maggiori sforzi in futuro.

Lo scopo di questo lavoro è fornire ulteriori informazioni riguardo al comportamento della macchina e analizzare gli aspetti termodinamici connessi all’iniezione di gocce d’acqua nella compressione. È stata quindi condotta un’analisi CFD su uno stadio per comprendere come avvenga l’evaporazione all’interno della girante e quali effetti essa abbia su pressione, temperatura e potenza richiesta.

Come prima cosa è stato sviluppato un modello CFD per la validazione, testando l’evaporazione di piccole gocce in condizioni indisturbate di flusso e confrontando i risultati con un modello analitico 1D.

Nel modello CFD della macchina sono state utilizzate diverse quantità d’acqua iniettata e diverse dimensioni delle particelle, analizzando come esse influenzino le prestazioni del compressore. Sono poi presentate, nell’analisi dei diversi parametri, alcune considerazioni relative all’effetto osservato su efficienza e lavoro specifico della macchina. Inoltre, una distribuzione di particelle aventi differenti dimensioni è utilizzata e i risultati sono presentati comparandoli ai precedenti, ottenuti con diametro uniforme.

Lo studio si concentra sulla variazione di diametro medio, frazione di vapore, pressione e temperatura attraverso la girante, comparando tra loro due diverse dimensioni delle particelle.

Infine sulla base dell’analisi condotta sono riportate alcune considerazioni riguardo a futuri sviluppi del modello utilizzato.

Acknowledgments

A voi, compagni di viaggio in questa avventura.

A special thanks to everyone who made my stay in Germany a great experience:
at the university, discovering new places, in front of a pc or sharing a beer together.

Chapter 1

Introduction

Chapter 1 describes the background and motivation for the work presented. In addition, the scope of the thesis, limitations and challenges related are presented.

1.1 Background and scope of the work

The use of water injection in gas compression processes has grown rapidly in recent years, driven by the need of improving the machine performance, and has been implemented with different techniques. The growing interest is mainly due to the power production field, where water injection is performed in gas turbines to lower the power demand of the compressor and improve the overall power production increasing the mass flow in the turbine section.

Wet compression refers generically to liquid water-gas two-phase flow in the field of gas compression. Water is involved in the process as small droplets are injected in the air stream and evaporate, providing a cooling effect and lowering the temperature rise through the machine. The two-phase fluid affects the compression process and the overall parameters that describe the compressor performance.

Many research efforts have been done to provide deeper understanding on the topic, by means of analytical, numerical and experimental works, in which thermodynamic and aerodynamic effects of water injection have been investigated. Those works provided, in addition to general statements about the overall performance of wet compression processes, further information about the influence of the way in which water is injected, concerning droplets size, amount of injected water, etc.
Moreover, some works investigated specific aspects inside the machine, such as increased stability of the flow, influence on compressor map, water film formation and droplets behaviour.

Nevertheless, the majority of investigation works concerning wet compression examine axial compressors, due to their use in gas turbines, while only few of them analyse the behaviour of centrifugal machines. Therefore, the aim of this work is to provide further knowledge about the process in a centrifugal compressor, analysing the thermodynamic aspects and the influence of water injection.

This task consist of several CFD simulations, performed at design point, using different water droplet sizes and different amount of water injected.

The overall target is to give some indications about the thermodynamics and evaporation inside the impeller, highlighting the behaviour of the wet case compared to the dry one, and to provide initial statements as a basis for further investigations about the topic.

1.2 Structure of the thesis

A short summary of the chapters of this work is given below.

Chapter 2 presents an overview about how wet compression has been developed in the past, from the first applications in aircraft engines during the 1950s to the recent works published.

Chapter 3 gives a short description of the theoretical background, presenting the parameters used in the analysis of the compressor performance.

Chapter 4 describes the machine, the boundary conditions and the settings implemented about the physics in the model.
Moreover, it presents all the information about the droplet sizes and injection rates used in the investigation.

Chapter 5 presents a validation case, whose scope is to verify the model trustworthiness. A 1D analytical calculation is compared to the CFD 3D free stream simulation.

Chapter 6 presents the mesh creation and explains the demands of the numerical simulations, providing further information about the model in terms of grid and choice of the settings.

Chapter 7 describes and discusses the results obtained, presenting the general investigation with monodiameter droplets, and then introducing the nozzle distribution. In addition, a through-the-impeller analysis is carried out, to investigate how thermodynamic parameters vary inside the machine as evaporation takes place.

Chapter 8 includes conclusions about the thesis and recommendations for further work.

Chapter 2

Wet compression

The injection of liquid water in the air intake system is a well-known method for performance enhancement in stationary gas turbines and aero engines.
The use of this technique has been evolving throughout the last 70 years, changing its features and applications. An overview of its development in the past is presented in the following sections of the chapter.

2.1 Brief history of water injection

The idea of water injection for system power enhancement was already developed in the early years of gas turbine technology. Due to the lack of an adequate liquid injection technology, the applicability of this method was entirely limited or restricted to short-term use; indeed, droplets exceeding a certain size and the formation of liquid phase sheets may lead to inacceptable erosion on the blades.
Further work was made with military aviation development and then transferred to civil aviation in the 1950ies, since compressor water injection was used to generate temporarily increased thrust during aircraft starting at high ambient temperatures or high altitude. The liquid phase injected was often a mixture of de-mineralized water and methanol [1].

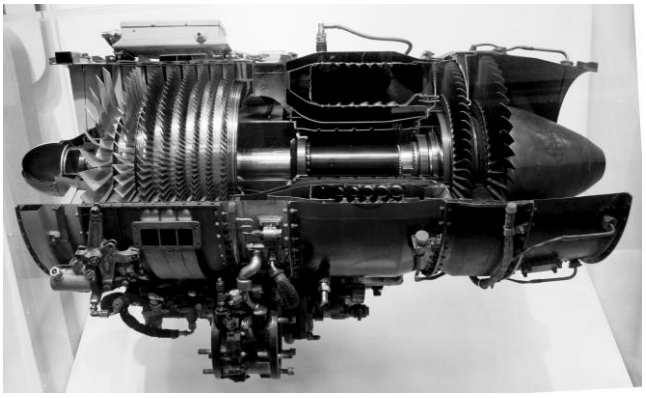

Figure 2.1. *Aircraft engine*

Research papers from National Advisory Committee for Aeronautics (NACA) investigated the application of water injection on axial flow compressor in gas-turbine engine, observing a lower specific work and higher compression ratios in the machine [2]. Beede et al. [3] conducted an analysis on the performance of a centrifugal machine, in which increasing water-air ratios were tested, showing an increase of total pressure

ratio and air mass flow, and a reduction of the efficiency as well. The work showed the connection between the evaporation magnitude and the performance of the compressor.
Therefore, interest about wet compression concerned both axial and centrifugal machines since the first application steps of the technology.

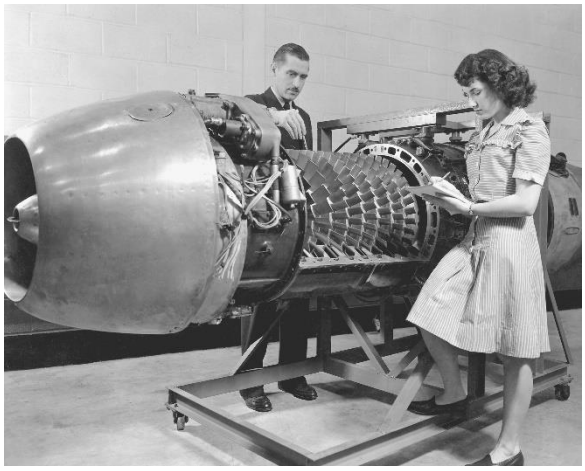

Figure 2.2. *1950´s axial compressor*

Further development of the injection technology was achieved in several industrial branches until the 1990ies.
The growth of the worldwide energy market and the associated energy cost led to the rediscovery of the method of water injection for power boosting in stationary gas-turbines. The need for cost-effective long-term water injection systems to employ in the intake sections of gas turbines increased the publication of research works, focusing on one side on the droplets size suitable to avoid erosion phenomena and keep maintenance costs reduced, and on the other side on the amount of water to get an efficient evaporation through the machine.
Therefore, due to the increasing energy demand in emerging markets, where higher ambient temperatures are common and climate conditions imply the coupling between phases of highest power demand and highest temperature, the research work rose significantly around 2000 to investigate the use of liquid phase injection in stationary gas turbines.

2.2 Recent research works about the topic

The amount of papers published in the last decade shows the interest on this technique. Many different aspects related to multiphase flow in compressors have been investigated, looking for deeper knowledge and deeper understanding of the complex phenomena associated with wet compression.

2.2.1 General and axial compressors investigation

Among the research efforts, the majority of them consider the effects of water injection on axial compressors, as its utilisation is intended to boost the power output of gas turbines. Although they refer to different machines from the one that has been investigated in this work, their contribution to the knowledge of the topic is important and deserves to be mentioned.

Zheng et al. [4] have proposed a thermodynamic model of wet compression process, in which several aspects as ideal wet compression process, actual wet compression process characteristics, water droplet evaporation rate, wet compression work and compression efficiency are discussed. The results show that the reduction of compression work can be reduced and be lower than that of a dry air isentropic process, and therefore a new wet compression efficiency is proposed to evaluate the performance. Evaporative rate, time and aerodynamic breaking of water particles have proven to be important for wet compression.

The impact of evaporative processes on compressor operation has been examined by White and Meacock [5], focusing particular attention on cases with substantial overspray, where significant evaporation takes place within the compressor itself rather than in the inlet (inlet fogging). The work describes a simple numerical method for computation, based on a combination of droplets evaporation and mean-line calculations, and this method is applied to a generic compressor geometry in order to investigate the off-design behaviour that results from evaporative cooling. A shift of compressor characteristics towards higher mass flow and compression ratio is shown.

Bharghava and Meher-Homji [6] developed an analysis on the effects of inlet fogging on a wide range of existing gas turbines, considering both evaporative and overspray fogging conditions, and showed correlation between performance and gas turbine key design parameters due to inlet fogging effects. Moreover, a sensitivity study has been carried out to examine the effects of varying climatic conditions and to see if the general qualitative trends noted are modified.

Among latest works about water injection in axial compressors, Schnitzler et al. [7] investigated numerically and experimentally the effects of water droplets on the operating behaviour of a four stage axial compressor. Increased mass flow is assessed. Negative effects on the global performance occur for water-air mass ratio of 2%, with lower pressure ratio and mass flow values, compared to the dry case.

Several more works analysed different aspects inside the machine, such as separation of the flow [8], liquid particle erosion [9] and droplets interaction with the blades [10], adding more knowledge about the effects of water in the machine.

2.2.2 Centrifugal compressors investigation

About centrifugal machines, fewer efforts have been put into investigating their behaviour, due also to their different and less common applications, compared to axial ones in the power generation sector.
Nevertheless, some application fields may need further knowledge about evaporation and liquid phase existence inside the machines, as the oil and gas industry, where wet gas compression is performed with hydrocarbons.

Among the limited literature about wet compression in centrifugal machines, Hundseid et al. [11] developed an analysis about both wet gas and hydrocarbon gas - water mixture compression, showing a relevant influence of liquid properties on the compressor performance. Suitable wet gas performance parameters are presented. The need of improved fundamental understanding on the topic is pointed out, as also in other several works published by the Norwegian University of Science and Technology.

Considering air-water two-phase flow, only few research works investigated the behaviour of the machine and the influence of water parameters on the compression process. Bertoneri et al. [12] developed performance tests for subsea applications on a two stage centrifugal compressor with a mixture of air and water at suction pressures of 20 bar. Under these boundary conditions, an increase of liquid injected showed a decreased polytropic head together with an increased absorbed power by the compressor because of deterioration of its efficiency. On the other hand, the discharge temperature of the compressor reduces significantly.

Abdelwahab [13] investigated the use of water injection technology in industrial centrifugal compressors, providing a numerical method based on both droplet evaporation and compressor mean-line calculations. The assessment shows that wet compression can successfully be applied in industrial centrifugal compressors, even though droplet radii smaller than 5 μm need to be used. This means sophisticated fogging technologies need to be employed.
On the other hand power reductions up to 5% per stage can be achieved, and water injection rates up to 3% of the dry gas flow rate can be used successfully to reduce the

compressor work requirements. The benefits of wet compression are more pronounced at high inlet compressor temperatures typical of hot day conditions.
Increasing the compressor pressure ratio by increasing the individual stages pressure ratio using higher rotational speeds leads to deteriorating wet compression effects.

Surendran and Kim [14], who presented a computational fluid dynamics method to investigate the wet compression effects on a low speed centrifugal compressor, made further work on the topic, finding that significant power saving can be obtained with water droplet injection ratios above 3%, up to 10%. The interaction of water droplets with the air helps to reduce the recirculation zone near the diffuser vane, improving stall behaviour. The work shows that with a decrease in the mean droplet diameter wet compression becomes more effective, while most of the large droplets are collected on the impeller walls. With a smaller mean diameter, the droplets are distributed more evenly inside the compressor and the evaporation is more effective. Moreover, at design condition the efficiency is shown to vary linearly with injection ratio.

2.3 Motivation of the work

Further understanding is therefore needed on the topic, especially concerning high-speed centrifugal compressors, as few investigations have been developed about them. The study of the overall parameters that characterize the machine behaviour and performance, together with the influence of water droplets size and injection rate, plays an important role in giving a more complete overview of wet compression, setting the basis for further investigations on the topic and on its many aspects.
Hence, the aim of this work is to provide information about the thermodynamics of the process by means of a numerical CFD investigation, understanding how water evaporation takes place and how relevant are its beneficial effects on the process.

Chapter 3

Theoretical background

The thermodynamic analysis of the centrifugal compressor requires the definition of some parameters used in the investigation. Before introducing the numerical model, a brief description of these parameters is presented.

3.1 Evaporation model

The evaporation of small droplets, injected inside the machine, involves heat and mass transfer. The liquid droplet is in a gaseous environment, namely humid air, whose components include water vapour. Therefore, at the interface between the liquid and gaseous phase, e.g. the droplet surface, heat and mass flow occur. Both flows can be described using conservation equations.

In the case investigated the liquid temperature is lower than the gas one, therefore heat is transferred from the gas phase to the droplet surface first, and then from the surface inside the droplet. Figure 3.1 shows a single droplet heat flows. The gas-surface heat flux q_g depends on the temperature difference between air and the droplet surface, whereas the internal heat flux q_i depends on the temperature value at the centre and at the outer radius of the particle.

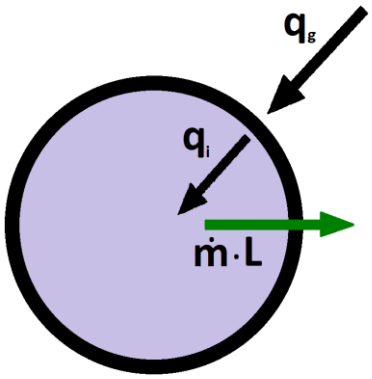

Figure 3.1 *Evaporation of a droplet, heat flows.*

This aspect is relevant to describe how the mass flow is generated. Assuming no thermal resistance at the droplet surface, the two heat flows can be considered equal in magnitude. As the droplet is heated up, the temperature difference inside it starts to decrease, and in the same way the internal heat flux is reduced. The mass flow is

generated by the energy imbalance at the droplet surface: the liquid starts to evaporate, water vapour arises and latent heat balances the heat flow coming from the gas phase.

The convective heat transferred q_g and q_i can be expressed as follows:

$$q_g = \pi \cdot d_{dr} \cdot \lambda_g \cdot Nu_g \left(T_g - T_s\right) \quad (1)$$

$$q_i = \pi \cdot d_{dr} \cdot \lambda_l \cdot Nu_l \left(T_s - T_i\right) \quad (2)$$

Where the convective coefficient α has been replaced introducing the Nusselt number definition:

$$Nu = \frac{\alpha\, d_{dr}}{\lambda} \quad (3)$$

For laminar forced convection around a spherical particle, theoretical analysis shows that Nu=2 [15].

If the heat flows are known, it is also possible to calculate the evaporation rate from the energy balance:

$$q_g + q_i = \dot{m}L \quad (4)$$

And the expression obtained is:

$$\dot{m} = \frac{q_i + q_g}{L} = \frac{dm_{dr}}{dt} \quad (5)$$

Where the last term represents the variation of droplet (liquid) mass in time.

Moreover, the conservation of mass along a streamline can be expressed as:

$$\frac{d\dot{m}_g}{dt} + N_{dr} \cdot \frac{d\dot{m}_{dr}}{dt} = 0 \quad (6)$$

Where N_{dr} is the number of droplets that take part to evaporation along the streamline.

3.2 Sauter mean diameter

The most important parameter in a water injection application is the droplet size. The characterization of the spray requires a suitable and concise way to describe the droplet size distribution and its variation as evaporation occurs. Assuming a spherical shape of the particles, several diameter definitions are available, such as the arithmetic

diameter d_{10}, the surface mean diameter d_{20}, the volume mean diameter d_{30}, etc. The most suitable and common choice with a particle distribution is the Sauter Mean Diameter d_{32} (or SMD), defined as the diameter of a sphere that has the same volume/surface area ratio as the entire spray (or as a particle of interest, depending on the case where it is applied).

3.2.1 Single particle

Its definition, considering a single droplet, is strictly related to the surface and volume diameter. The surface diameter is defined as:

$$d_{20} = d_s = \sqrt{\frac{A_p}{\pi}} \quad (7)$$

where A_p and V_p are the surface area and volume of the particle, respectively, while the volume diameter is obtained from:

$$d_{30} = d_v = \left(6\frac{V_p}{\pi}\right)^{\frac{1}{3}} \quad (8)$$

The Sauter Mean Diameter for a given particle is defined as:

$$d_{32} = \frac{d_v^3}{d_s^2} \quad (9)$$

3.2.2 Particle distribution

The definition of the Sauter Mean Diameter for a discrete particle size distribution is obtained from the surface and volume mean diameters in a similar way, taking into account the different droplet size d_i and their number n_i in each class.

The surface mean diameter is obtained with:

$$d_{20} = \left(\frac{\sum n_i d_i^2}{\sum n_i}\right)^{\frac{1}{2}} \quad (10)$$

And the volume mean diameter similarly

$$d_{30} = \left(\frac{\sum n_i d_i^3}{\sum n_i}\right)^{\frac{1}{3}} \quad (11)$$

Thus, the Sauter Mean Diameter is given as follows:

$$d_{32} = \frac{d_{30}^3}{d_{20}^2} = \frac{\sum n_i d_i^3}{\sum n_i d_i^2} \quad (12)$$

In this way, the diameter of a droplet having the same volume/surface area ratio as the spray is obtained. A reduction of the droplet size in the whole distribution can be assessed examining the mean diameter calculated.

3.3 Performance parameters

The scope of water injection is reducing the temperature during the compression and the power consumption needed by the machine. The analysis of the compressor performance is carried out not only considering the power, but it also includes two more parameters to describe the process from the thermodynamic point of view: the isothermal efficiency and the polytropic index.

3.3.1 Power consumption

The power needed by the compressor is used to increase the fluid pressure, reducing its volume. Considering an adiabatic process, where no heat is exchanged with the environment, the compressor head can be written as:

$$H = \frac{\gamma\, p_1}{\gamma - 1}\left[\left(\frac{p_2}{p_1}\right)^{\frac{\gamma-1}{\gamma}} - 1\right] \qquad (13)$$

Where γ is the ratio of specific heats c_p/c_v.

The head multiplied by the volumetric flow of gas (Q) gives the compressor power equation:

$$P = Q\,\frac{\gamma\, p_1}{\gamma - 1}\left[\left(\frac{p_2}{p_1}\right)^{\frac{\gamma-1}{\gamma}} - 1\right] \qquad (14)$$

Moreover, the power can be expressed in terms of total enthalpy, as the mass flow rate multiplied by the total enthalpy difference between the inlet and outlet sections:

$$P = \dot{m}\,(h_2^0 - h_1^0) = \dot{m}\,\Delta h^0 \qquad (15)$$

However, in the model the power is calculated using the torque on the single blade, available as a parameter, and the rotational velocity ω' [rev min^{-1}] of the compressor:

$$P = M \cdot \omega = M_b \cdot n_b \cdot \frac{2\pi\,\omega'}{60} \qquad (16)$$

Where ω is expressed in rad s^{-1} and n_b is the number of blades.

3.3.2 Isothermal efficiency

Isentropic efficiency and polytropic efficiency are commonly used to evaluate the compressor performance, when only a gaseous fluid is handled by the machine. In a

wet compression process, due to the cooling effect provided by liquid droplets injected in the machine, the common efficiency definition is not suitable to describe the machine performance, as it could give values above 1.0[4].
Thus, a new efficiency definition is needed. As the scope of water injection is to reduce the temperature rise inside the machine, the compressor work can be compared with the work needed in an isothermal process, to evaluate in a clear manner the effect of evaporation in lowering it and approaching the isothermal one.
The isothermal efficiency considers the specific isothermal work [J/kg], expressed as:

$$w_{isoth} = RT\ ln\left(\frac{p_2}{p_1}\right) \quad (17)$$

And is defined as follows:

$$\eta_{isoth} = \frac{w_{isoth}}{w_c} \quad (18)$$

Where w_c is the compressor specific work calculated in the model.

3.3.3 Polytropic index

The polytropic index is a parameter used to describe a polytropic process, whose law is $pV^n = const.$

Its value can vary according to the considered process; for an isothermal process dT=0 determines n=1, as it can be inferred by equation (19):

$$n = \frac{ln\frac{p_2}{p_1}}{ln\frac{p_2}{p_1} - ln\frac{T_2}{T_1}} \quad (19)$$

Thus, the stronger the effect of water evaporation is, the lower *n* value is obtained, coming closer to the isothermal value. It can be observed that when the outlet temperature is lowered, the logarithm value decreases (it is zero for $T_2=T_1$) and the denominator is bigger, lowering the *n* value.

Chapter 4

Numerical model

In the present work, a centrifugal compressor is considered. The geometry is given and tested under specific boundary conditions that will be described in the following sections.
The model set up used in the numerical simulations is also presented in the chapter.
At a later stage, after the model description and validation chapters, the mesh generation process is described and some comments about it are reported (see Chapter 6).

4.1 Geometry

The given geometry of the compressor is typical of a big machine, and very similar to the design of a commercial one.
Some meaningful dimensions of the case used are given in Table 4.1.

Table 4.1. *Geometry characteristic parameters.*

Dimension	Value
External Impeller Diameter D_ext	1300 mm
Impeller Inlet Diameter	1000 mm
Radial distance of the walls at the inlet	450 mm
Number of blades	15
Exit angle	90°

The compressor has 15 blades and its rotational speed is 5450 rpm.
Figure 4.1 and Figure 4.2 show a view of the machine examined.

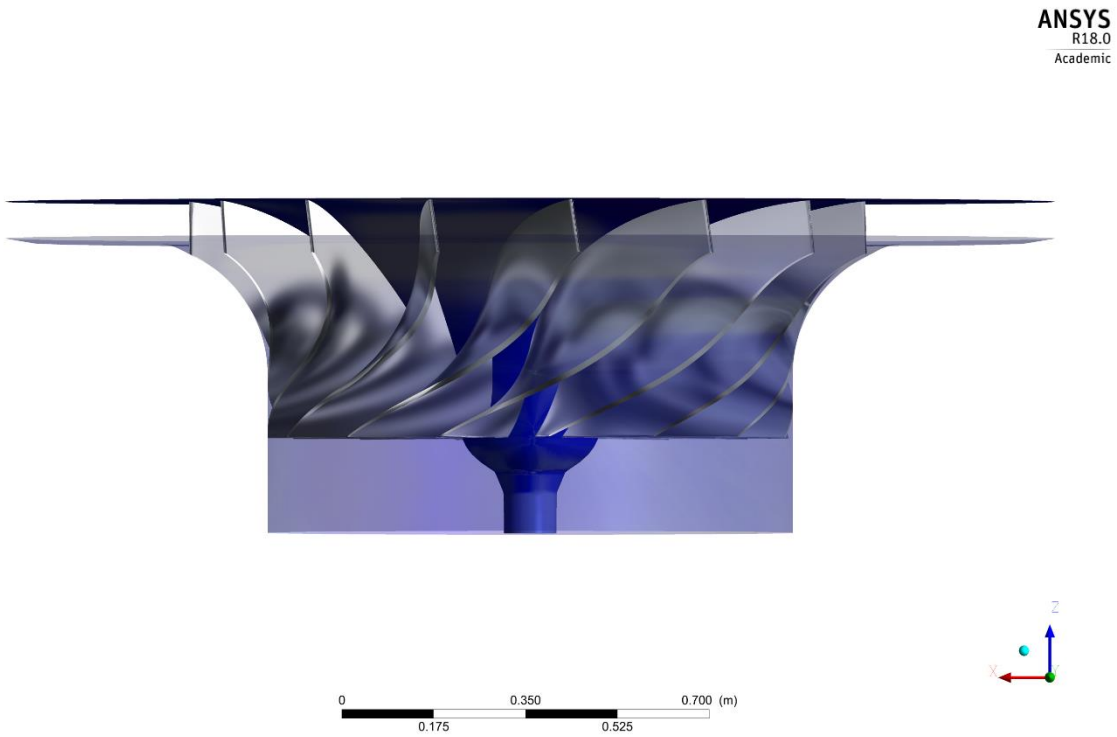

Figure 4.1. *Impeller side view.*

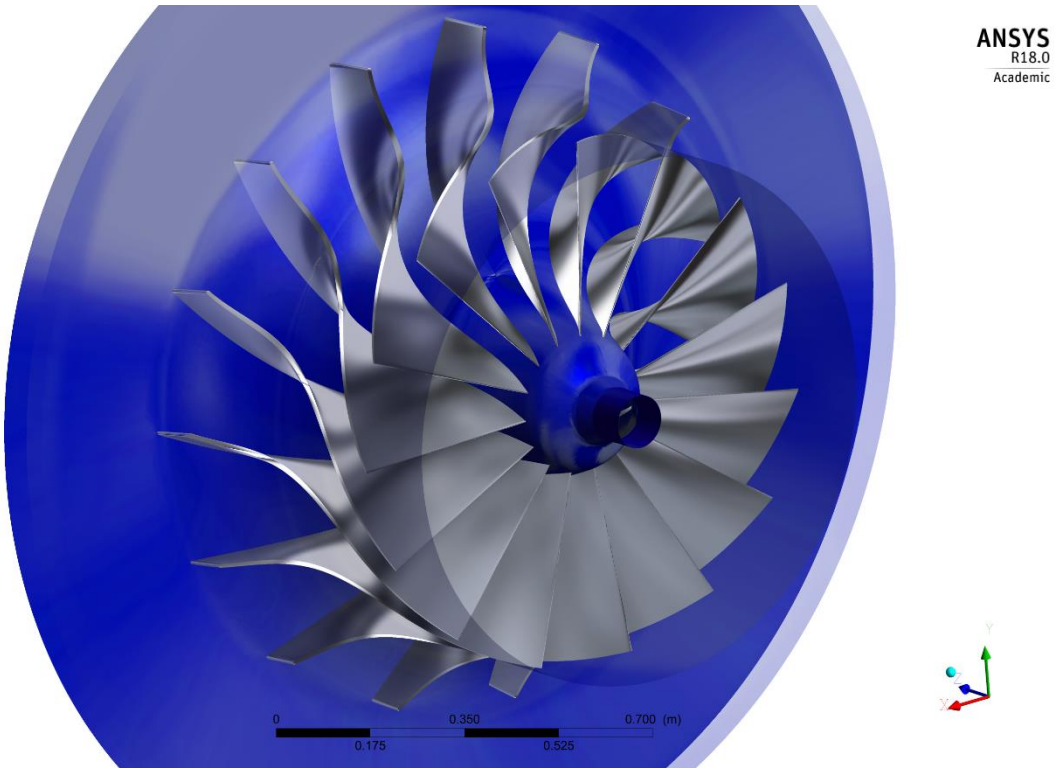

Figure 4.2. *Impeller inlet view.*

4.2 Dry air case set up

The compressor, both in dry and wet compression cases, is tested in design point conditions. As the final wet compression set up is derived from the model with dry air as a working fluid, the dry case is described in the chapter before introducing the more specific settings about the investigation on water injection effects.

4.2.1 Domain

Due to the high computational cost of simulating the behaviour of the whole machine, a 24-degrees sector is tested, taking advantage of the machine symmetry by means of rotational periodic interfaces.

Therefore, the whole domain is composed by the rotating domain, named “R1”, including one blade, and by two stationary domains, “DUCT” for the inlet section and “CHANNEL” for the outlet one. The inlet and outlet section were added in order to get easier convergence and stability of the simulation, as they allow to displace the location where the boundary conditions are applied sufficiently far from the entry of the passage between the blades on one side, and from the wake region downstream the trailing edge on the other.

As it can be easily seen, the model does not include any diffuser blades, as the aim of this work is to investigate the phenomena occurring inside the impeller.

Moreover, to keep the model simple, the gap at the tip of the blade is not considered, as it would be an additional source of turbulence; in this way the stability of the simulation is increased.

Figure 4.3 and 4.4 show two different views of the domain.

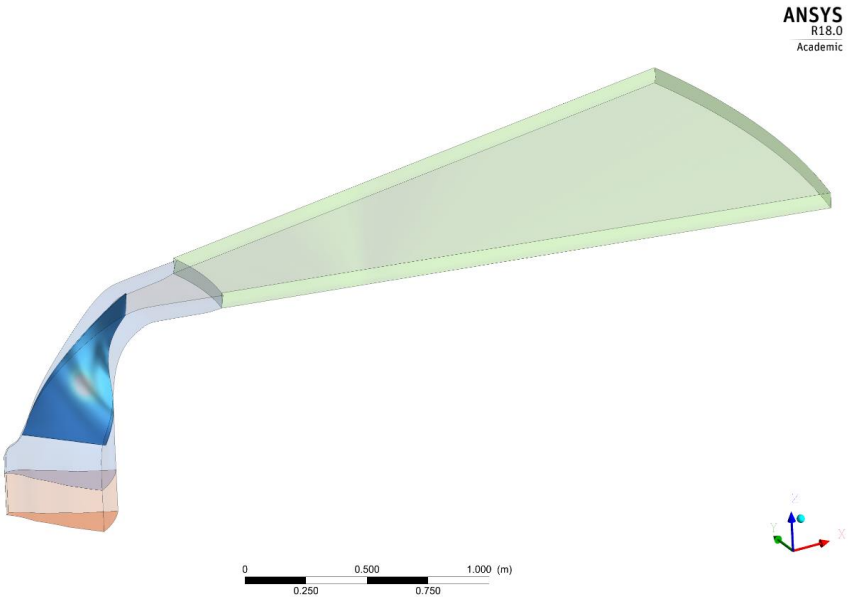

Figure 4.3. *Simulation domain.*

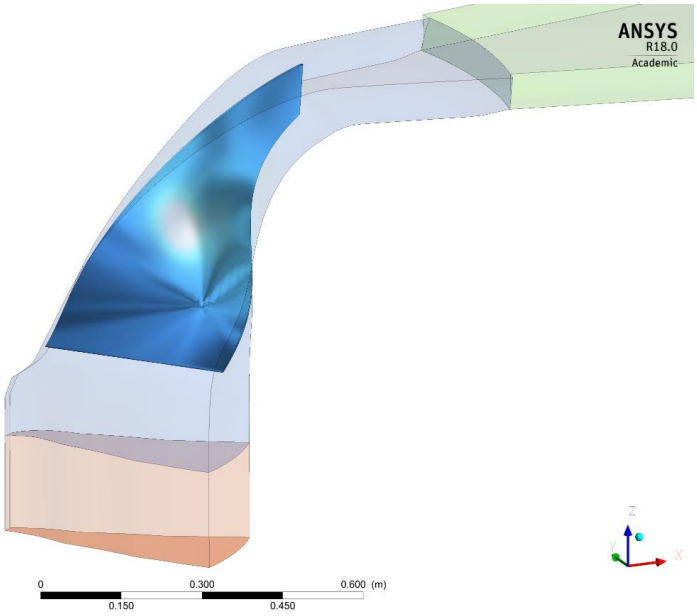

Figure 4.4. *Rotating domain and interfaces.*

4.2.2 Boundary conditions

The design conditions used to test this domain, besides the fixed rotational speed equal to 5450 rpm, are represented by the inlet and outlet boundary conditions. At the inlet total pressure and total temperature values are used, while at the outlet the mass flow rate is set.

4.2.2.1 Inlet and Outlet

The boundary conditions applied at the inlet and at the outlet of the machine are the following:

Table 4.2. *Inlet and outlet boundary conditions.*

Location	Boundary conditions
Inlet	Total pressure = 1 bar Total temperature = 35°C
Outlet	Mass flow rate = 94.1 kg/s

It is worth to say that the mass flow rate value refers to the whole machine; therefore, in the considered domain the value will be 15 times smaller, 6.2733 kg/s.

As a turbulence setting, "Medium (Intensity = 5%)" is chosen.

4.2.2.2 Walls

All the boundaries defined as walls are characterized by Mass and Momentum and Heat Transfer settings. In the present model, Free Slip Walls and Adiabatic options are chosen. The reason of the choice of free slip walls can be found in the Euler's equation to be performed with this model: as in an ideal flow without friction there is no velocity gradient normal to the wall, the velocity near the wall is not influenced and no boundary layer is considered.

4.2.2.3 Interfaces

Several interfaces are present in the model, due to the rotational periodicity of the elements and the connection between the three domains that form the assembly.
The interfaces between the rotating domain R1 and the inlet and outlet section are set up using a Frozen Rotor Frame Change/Mixing Model interface, without any pressure change or mass flow rate additional model being employed.

Periodic interfaces that mark the boundaries of the 24° sector are set as Rotational Periodicity using as Rotation Axis the Z-axis.

4.2.3 Fluid models

The fluid models settings described in this section represent the starting point for the following models and simulations.
Dry air was used as working fluid; therefore, Air Ideal Gas from Material Library is chosen and set as Continuous Fluid.

Heat transfer is described by the Total Energy model, including the Viscous Work Term. In this way, the internal heating by viscosity in the fluid, e. g. the work due to viscous stresses, is taken into account.

As Turbulence model, Shear Stress Transport is chosen. The k-ω based SST model, most commonly used to describe the turbulent flow, accounts for the transport of the turbulent shear stress and gives highly accurate predictions of the onset and the amount of flow separation under adverse pressure gradients [15].

Buoyancy is not considered in this model, as it is negligible compared to centrifugal and aerodynamic forces in a high-speed rotating machine.

4.3 Humid air case set up

As the model is derived from the dry air case, the boundary conditions are unchanged. Few modifications concern the fluid models and are therefore presented in the next paragraph.

4.3.1 Materials

The set up for humid air requires a two-component fluid, whose composition in this case is fixed.
In the Materials section a Variable Composition Mixture has been created, composed by Air Ideal Gas and water vapour (H2O) as shown in Figure 4.5 a).

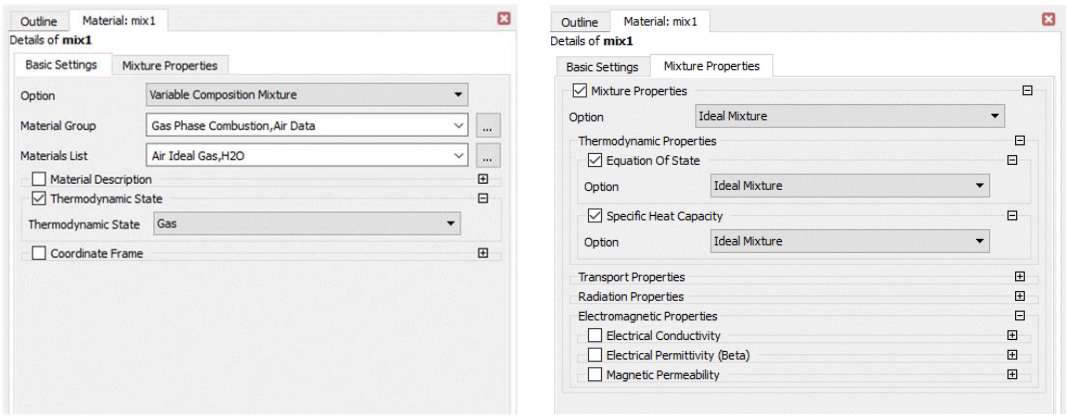

a) b)

Figure 4.5. *Mixture composition a), and properties b).*

A variable composition mixture was chosen instead of creating a Fixed Composition Mixture in order to be able to compare the humid air case with the water injection ones. In fact, this set up is suitable for wet compression [15] , where water droplets evaporation takes place during the process and the vapour mass fraction in the flow changes as mass transfer between the liquid and gas phase occurs.

The mixture properties are defined as Ideal Mixture ones, as reported in Figure 4.5 b).

The percentage mass composition of the two substances in the mixture is defined as Mass Fraction at the inlet of the domain, as shown in Figure 4.6.

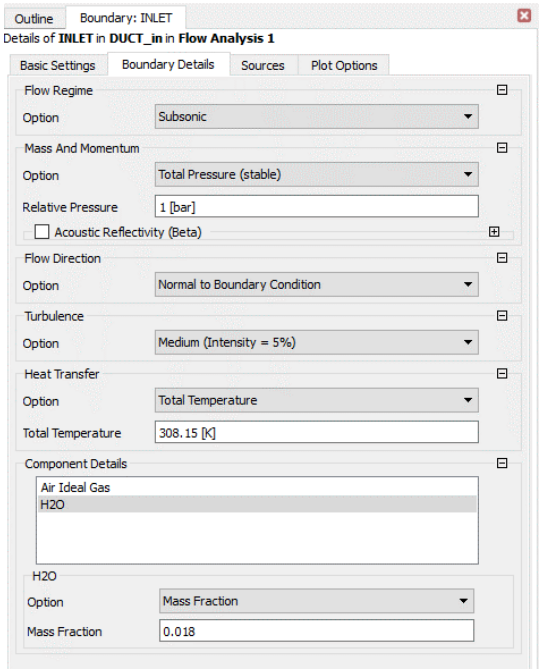

Figure 4.6. *Inlet boundary details.*

The vapour mass fraction value in the mixture derives from the inlet boundary conditions previously presented. In this model the vapour content in humid air is fixed by means of relative humidity; the chosen value is around $\varphi = 50\%$ (51.34%).
This value corresponds to 18.33 g of vapour per each kg of dry air in the psychrometric chart, therefore the vapour mass fraction is set as 0.018.

4.3.2 Fluid models

Then, the mixture is set as Continuous Fluid in the Basic Settings of the domain, and named as Humid Air. This designation will be used in the following to identify the air-water vapour mixture.

The heat transfer and turbulence models are kept the same, except the Viscous Work Term. This option has been disabled from here on, to keep the humid air and the wet compression cases comparable; indeed, the Viscous Work Term disablement guarantees a better stability of the simulations, as the two-phase flow characteristics play a relevant role in increasing the computational effort of the solver.

Buoyancy is not considered, as before.

4.4 Wet compression case set up

The wet compression case set-up derives from the humid air case in many features, and takes into account the injection of water and its evaporation. Boundary conditions are kept the same, including the mass flow rate at the outlet of the domain.
The fluid models and the coupling between the two phases in the flow are presented in the following section. Furthermore, water injection parameters and the investigation mode are described.

4.4.1 Basic settings

The most important feature of the present model is the presence of water as a fluid, and its interaction with the gas phase. Therefore, the first step requires the general definition of the fluid Water.
Water is added to Humid Air as Particle Transport Fluid, choosing from the Material Library the substance H2Ol, liquid water. The Particle Transport Fluid model is chosen as valid as the liquid phase volume fraction is quite low due to the way water injection is performed in the current case [15]. Moreover, it provides a better detail for mass and heat transfer.

The R1 rotating domain is taken as an instance to show the set-up in Figure 4.7 a) and b).

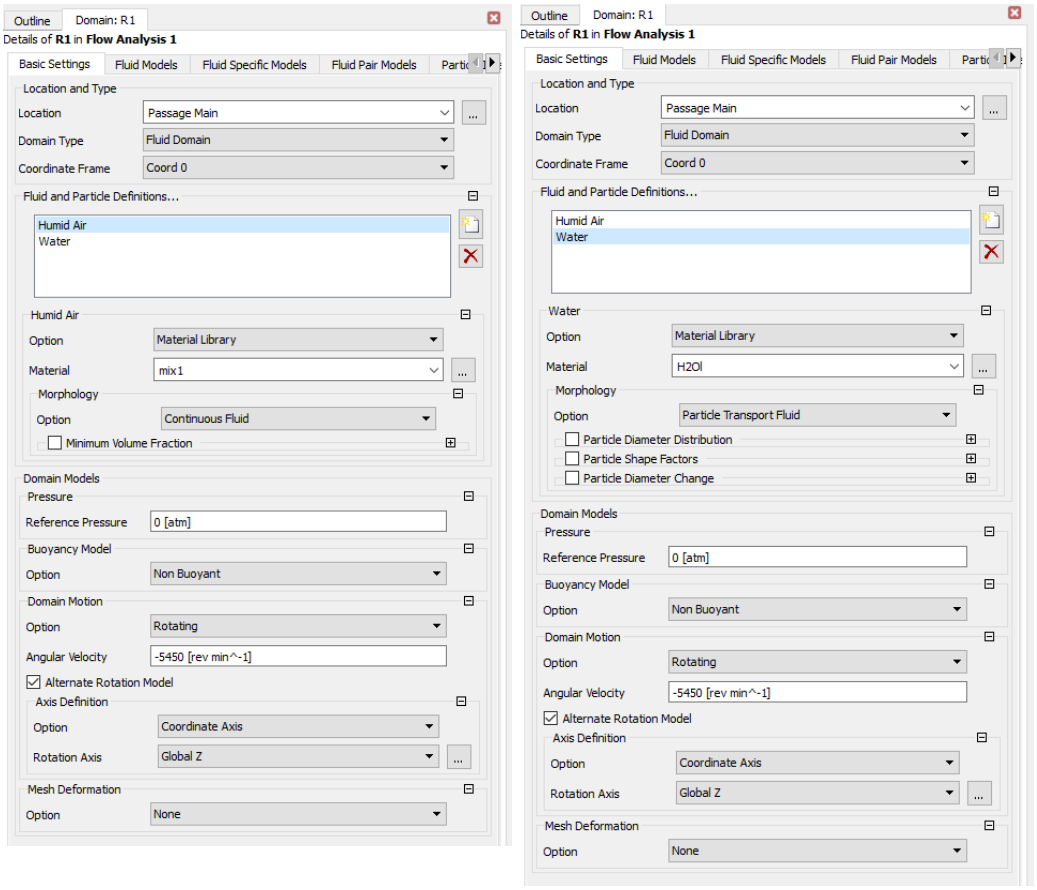

a) b)

Figure 4.7. *Basic settings for Humid Air a), and Water b).*

Once more buoyancy is not taken into account.

4.4.2 Fluid models

In the present case, the models describing the fluids behaviour are set separately for Humid Air and Water. Common settings include Heat Transfer, set as Fluid Dependent, and Turbulence, where Shear Stress Transport is used as in previous models described.

In the Fluid Specific Models tab, the heat transfer model and the components constraint of the mixture are specified.

Total Energy model is employed to describe the heat transfer for Humid Air, without including the Viscous Work Term, as already seen in section 4.3.2.

Regarding the component in the mixture, dry air (Air Ideal Gas) is set as Constraint, as the absolute amount of air mass does not change through the machine, while water vapour (H2O) is described by Transport Equation, as evaporation and mass exchange

between liquid and gas phase occur and the amount of vapour is changing in time and space.
Figure 4.8 a) and b) show the software set up.

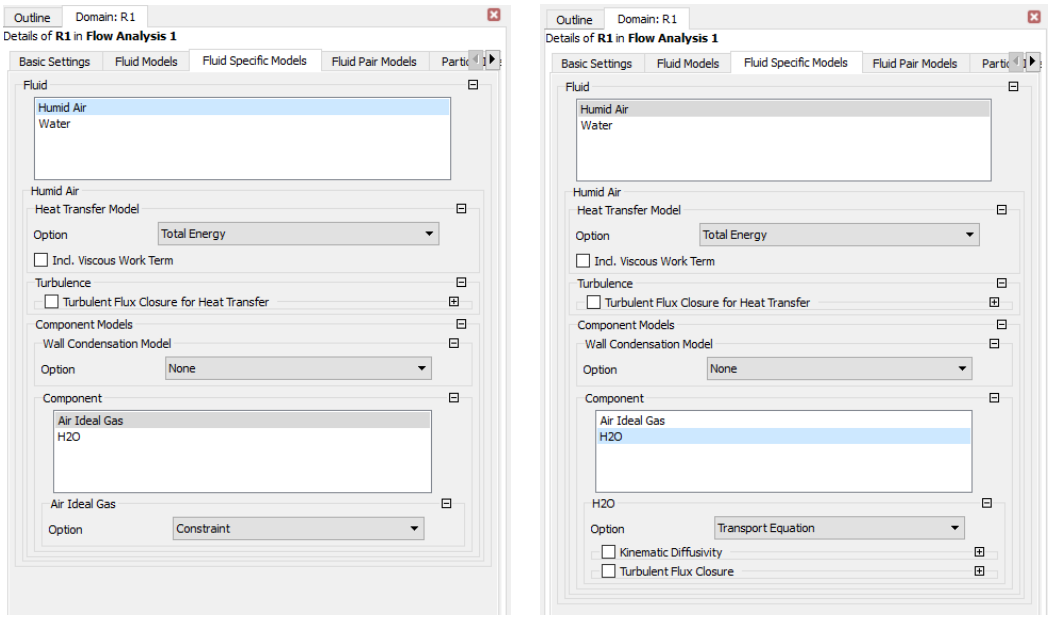

a) b)

Figure 4.8 *Fluid Specific Models for Humid Air, Air Ideal Gas constraint a), and water vapour b).*

Lastly, the Particle Temperature setting governs the liquid phase heat transfer, while no erosion or wall roughness is considered.

4.4.3 Fluid pair

The fluid pair settings describe the interaction between the gas and liquid phases, and allow setting the evaporation model, as presented hereafter.

Particles can be either fully coupled to the continuous fluid or can be one-way coupled. Fully coupled particles exchange momentum with the continuous phase, enabling the continuous flow to affect the particles, and the particles to affect the continuous flow [15]. Therefore, Fully Coupled is chosen as the most suitable option to describe the mutual influence between liquid droplets and the gas flow.
The surface tension coefficient is specified, as 0.0728 N m^{-1}.

Several models, suitable for different applications, different kind of particles, different particle quantities and distributions, can describe the momentum transfer. In the

current model the no slip condition between gas and droplets is applied; to realise this, a drag force coefficient equal to 10^4 is set.

Ranz Marshall model is used to described the heat transfer between the gas flow and the water particles.
Particle Breakup ad Particle Collision are not implemented in this set up.
The coupling between liquid water and water vapour is set by the Liquid Evaporation Model, This option is used to model evaporation of a liquid species in particles to the respective gas phase species in the continuous phase. The model is designed for evaporation of a single species and commonly used for spray dryer and oil combustion applications. However, it can be extended to multi-component evaporation [15].
Figure 4.9 reports the settings presented until now.

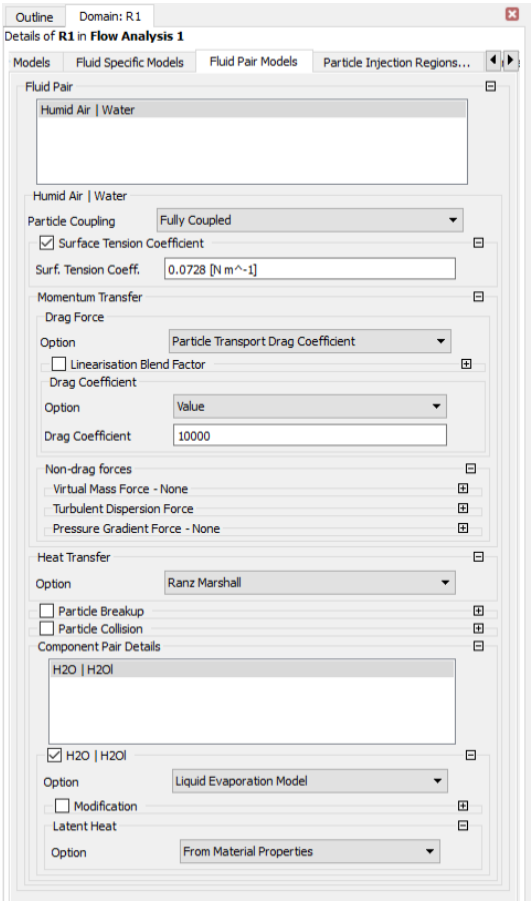

Figure 4.9. *Fluid Pair Models.*

4.4.4 Inlet boundary condition

The boundary conditions at the inlet of the domain are almost the same as presented in 4.2.2.1 and 4.3.1. However, the inlet is chosen as the location where water injection

is performed, therefore a second set of options has to be presented. This set-up can be found in the Fluid Values tab, which allows to define the particle behaviour.

The first element that characterizes the droplets behaviour at the inlet is the velocity of the injected particle. In the model zero slip velocity between the particles and the flow is considered.
The injection position plays an important role in how the droplets are spatially distributed; in order to obtain a uniform spatial distribution, the injection is performed at the centre of each cell face.
As it can be seen in Figure 4.10, the following settings are defined with expressions, as their value has been changed to investigate their influence on the machine behaviour. Before going into detail about the mass of injected water and the droplet size used for the model, it is worth to say that the water temperature, set with an expression, has been defined as a constant value, equal to 30°C.

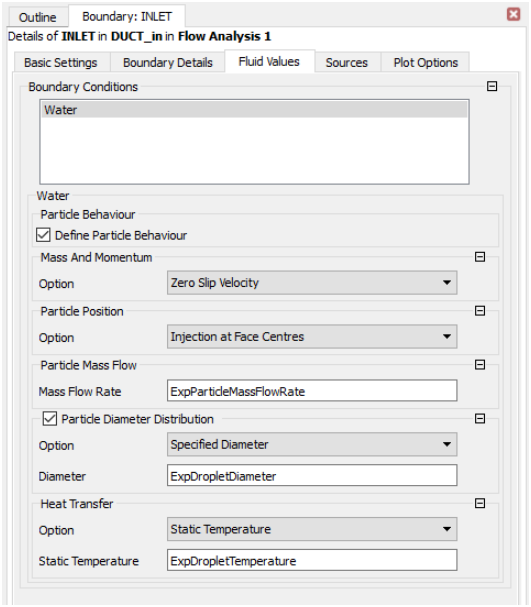

Figure 4.10. *Water injection details.*

4.4.5 Walls boundary condition

As in the dry air case, the walls are set as Free Slip Wall and Adiabatic. Moreover, in the present set-up the interaction of particles with the wall has to be defined. Describing this interaction in a complete and realistic way would require a User Defined model, as particle-wall interactions involve complex physics, especially in the presence of a wall film. A similar work on water film formation in radial turbines has been conducted by Schuster et al. [16] [17].

In the present set up, the interaction is described using a simplified model, where particle sticking to the walls is not taken in account. The Equation Dependent option allows to set two Restitution Coefficients, which describe how the particle is reflected by the wall. These coefficients refer to the parallel and perpendicular direction to the wall.
Both the parallel and the perpendicular coefficient are set equal to 1.0, which means no energy loss is taken into account in the particle velocity components.
A built-in water film formation model can be the target of further work, including droplets spreading and splashing, as investigated by Sun et al. [10] and Zhang et al. [18] in axial compressors.

4.4.6 Water injection

In the present work the injection rate is an important parameter whose influence on the compressor performance has been tested, comparing the results. The injection rate is expressed as a percentage value, in terms of water mass flow rate divided by the gas-phase flow rate.
The values that have been considered in this analysis are the following:

- 0.4% mass of water injected
- 1.4% mass of water injected
- 2.4% mass of water injected

Therefore, as the outlet mass flow rate has been specified as 6.2733 kg/s, the mass of water injected in the domain (one 24° sector) in the three cases respectively is:

- 0.0251 kg/s
- 0.08783 kg/s
- 0.15056 kg/s

Table 4.3 gives a recap of the Particle Mass Flow Rate values.

Table 4.3. *Injected water mass flow rates.*

Injection rate	Water mass flow rate [kg/s]
0.4%	0.02510
1.4%	0.08783
2.4%	0.15056

The second parameter that plays an important role in this investigation is the particles size. The droplets size is set using the particle diameter, on the assumption of a spherical shape of the particle itself.

To study the diameter influence on the evaporation and on the overall behaviour of the compressor, several particle sizes are tested, including a discrete diameter distribution obtained by measured values from the BETE PJ10 nozzle. The investigated diameter values are:

- 5 µm
- 10 µm
- 20 µm
- 50 µm
- BETE PJ10 discrete distribution.

Therefore, in the first four cases, a monodiameter particle size is adopted, in order to investigate the effect of the size and the diameter change as evaporation takes place inside the machine.

In the latter case, the data from experimental measurements are used [19]. From the measurement data, bigger particles, which can be found in very small number, have been neglected, as their contribution to the overall behaviour is irrelevant.
The considered nozzle provides a very fine mist, with very small droplets size; therefore, it is suitable for this application, where small particle diameter is required to get easier evaporation in the machine.
The diameter size distribution, in number and mass, is reported graphically in Figure 4.11.

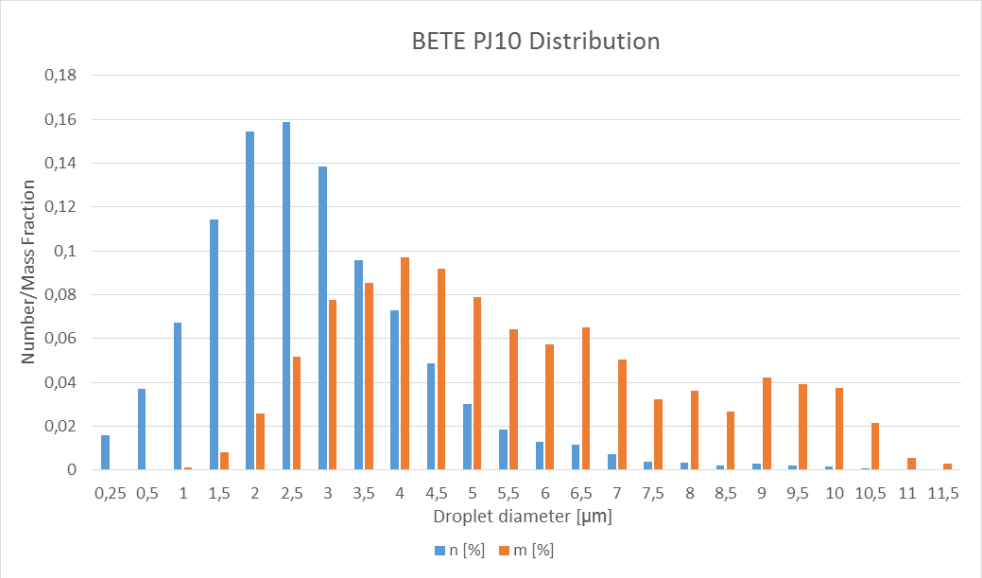

Figure 4.11. *Nozzle droplet distribution in number and mass fraction.*

Table 4.4 shows the values used in the software.

Table 4.4. *Droplets distribution characteristic values.*

Diam	n [%]	m [%]
0.25	0.0157	5.10E-06
0.5	0.0371	9.64E-05
1	0.0671	0.0014
1.5	0.1143	0.0080
2	0.1543	0.0257
2.5	0.1586	0.0515
3	0.1385	0.0778
3.5	0.0957	0.0853
4	0.0728	0.0969
4.5	0.0485	0.0919
5	0.0303	0.0788
5.5	0.0186	0.0644
6	0.0128	0.0575
6.5	0.0114	0.0651
7	0.0071	0.0506
7.5	0.0037	0.0324
8	0.0034	0.0362
8.5	0.0021	0.0268
9	0.0028	0.0424
9.5	0.0022	0.0392
10	0.0018	0.0374
10.5	0.0009	0.0217
11	0.0002	0.0055
11.5	0.0001	0.0032

As it can be easily seen, most of the droplets diameters fall below 5 μm, mainly in the range between 1 and 5 μm. This means that the nozzle creates a very fine fog, with small droplets.

The size distribution in mass shows a shift towards bigger diameters, as the volume (and the mass itself) is a function of the cubic value of the diameter. Indeed, the mass distribution is obtained calculating the volume of the droplet, as

$$V_d = \frac{4}{3}\pi r_d^3 \qquad (20)$$

The mass of the droplets having a specified diameter is calculated multiplying the number n (%) of the particles on the total by the volume and the density of water, assumed constant and equal to 997 kg/m^3:

$$m_i = n_i * V_d * \rho_w \quad [kg] \qquad (21)$$

Where *i* is the index that varies between 1 (d_d=0.25 µm) and 24 (d_d=11.5 µm).
The mass share represented by each category (each diameter size) is obtained dividing each m_i value by the sum of all the mass values obtained before:

$$m_{i\,\%} = \frac{m_i}{\sum_{i=1}^{k} m_i} \qquad (22)$$

On the basis of the above-mentioned parameters, the investigation has been carried out testing the three different injection rates for every particle size, including the BETE nozzle distribution.

4.5 Solver set up

Considering the computational effort required by a two phase flow simulation and the need of stability of the calculation, the solver set up is a crucial point in the model description.
Upwind is chosen as Advection Scheme, to obtain the most robust performance of the solver. Indeed, the physics involved in the calculation are quite demanding and the Upwind scheme is needed to achieve a stable performance of the solver.
For the same reason, the turbulence model equations (Turbulence Numerics) are solved using First Order, which means that the Upwind advection scheme is used in this setting too.
The convergence control is mainly defined by the Timescale Control, where a Physical Timescale is used, setting the value equal to 0.0001 s.
Convergence is reached when the RMS value of the residuals falls below 10^{-4}. However, the simulations have been performed monitoring the value of pressure and temperature at the outlet of the impeller (represented by the interface between the rotating domain R1 and the outlet domain CHANNEL_out), and stopped once these parameters turn constant. This happens in a longer time than the one needed to reach sufficiently small values of the residuals, therefore monitoring the two parameters at the outlet assures also that a converged state is reached.

Further settings concern the particle coupling control, as the particle integrator is completely distinct from the normal CFD solver, and separate control parameters are required.
The most important control is setting the coupling between the flow calculation and the particle integration. Therefore, to control in a better way the particles behaviour, the iteration frequency and the first Iteration are set equal to one. This means that, in terms of flow iterations, the particle integration is carried out every iteration.

Moreover, particle under relaxation factors are set at a low value, equal to 0.1, as particles may introduce a destabilizing influence on the convergence of the hydrodynamic equations, resulting in oscillations, or in severe cases, divergence.

To reduce the computational cost, the particle tracking termination control is enabled. The parameters are the maximum tracking time, distance and number of integration steps after which the particle tracking is stopped, and the minimum diameter size that the particle reaches before being neglected, as it does not play a significant role anymore in the simulation.
All these parameters are set keeping the default values, as shown in Figure 4.11.

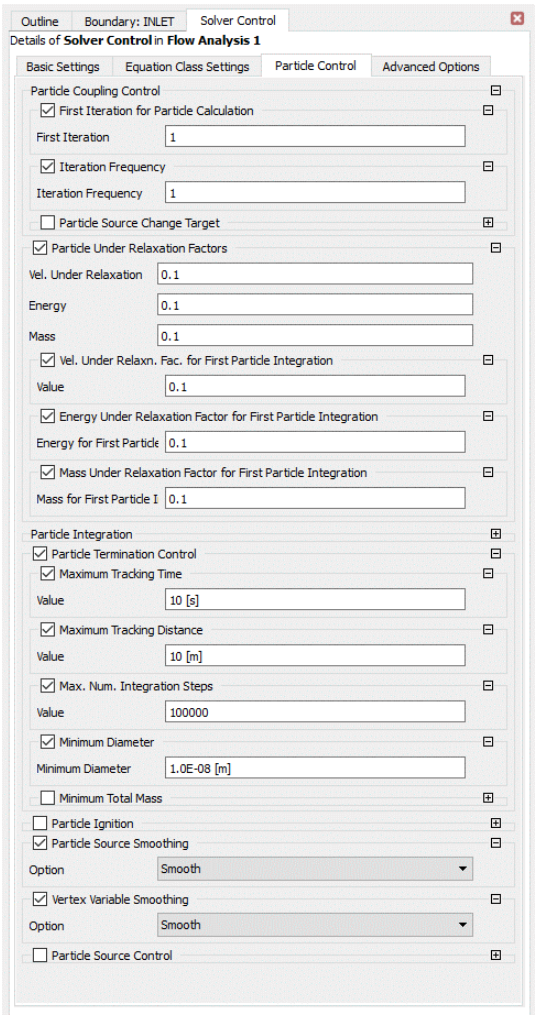

Figure 4.11. *Particle Control settings.*

Chapter 5

Model validation

The model described in the previous chapter has been set following some guidelines in Ansys CFX Modeling Guide, in which the Liquid Evaporation Model is described. Nevertheless, due to the complexity of the case here described, a validation case has been implemented to verify the accuracy of the model.
This validation test is performed comparing the results from 1D calculations and 3D CFD simulations, under the hypothesis of complete evaporation of the droplets in free stream conditions. The 1D calculations have been performed using a MATLAB model.

5.1 1D Model

In the one-dimension case the calculations are built up using MATLAB software, while fluid thermodynamic properties are made available using LibHuAirProp, a library which contains the properties of humid air in a wide range of pressure, temperature and humidity ratio (absolute humidity). Humid air is considered as a real gas.

The model is implemented referring to a 1D case, which means that the thermodynamic parameters change only along one dimension, e.g. the streamwise direction, while the flow is assumed as spatially uniform in the other two dimensions. The aim of the model is to calculate the temperature of the gas-phase, after complete evaporation is achieved; to do so, specific enthalpy is employed.
The calculation considers two different equilibrium states, the first characterized by liquid water droplets in humid air, the second by humid air in different conditions, resulting from the evaporation of all the injected water.
Let us call these two states as Inlet and Outlet, as if they were the inlet and the outlet of a pipe where evaporation takes place. This terminology allows an easier comparison of the results with the ones from the 3D simulation.
At the Inlet, the overall specific enthalpy is obtained by the sum of the specific enthalpy of the gas phase h_g and the specific enthalpy of the liquid phase h_l, weighted by means of the mass fraction of the two phases, as shown hereafter.

$$h_{In} = \frac{m_{HumidAir} * h_g + m_l * h_l}{m_{HumidAir} + m_l} = (1 - y) * h_g + y * h_l \quad \left[\frac{kJ}{kg}\right] \qquad (23)$$

Where $y = \frac{m_l}{m_{HumidAir}+m_l}$ is the liquid mass fraction,

and $1 - y = \frac{m_{HumidAir}}{m_{HumidAir}+m_l}$ corresponds to the gaseous mass fraction.

At the Outlet, as the liquid phase is completely evaporated, the enthalpy is equal to the gas-phase one; at the same time, as no changes in the overall enthalpy occur between the two states, the Outlet value must be the same as the overall value calculated at the Inlet.
Therefore, the following equivalence is valid:

$$h_{In} = h_{Out} \qquad (24)$$

Then, the temperature T at the outlet is calculated from the enthalpy value previously calculated h_{Out}, the pressure p and the liquid mass fraction y. Moreover, the relative humidity ("phi" as reported in the script below) is obtained, using the temperature, pressure and liquid mass fraction values.

Every calculation requires as an input the value of the variables that describe the conditions of the flow at the Inlet. These variables are:

- Pressure
- Temperature of the air
- Mass of dry air, water vapour and liquid water
- Temperature of liquid water

The outputs of the calculation are, as described previously, the enthalpy, the temperature and the relative humidity at the Outlet.

The script built in this numerical model is shown below.

```
clc
clear all
addpath('LibHuAir_Xiw')
%
% Begin Input Section
%
Inlet.p = 1.0;      % bar
Inlet.T = 60      % °C
Inlet.mg = 1.0;     % kg Dry Air
Inlet.mv = 0;     % kg Steam
Inlet.ml = 0.001    % kg Liquid water
Inlet.Tl = 30.0;    % °C
```

```
%
% End Input Section
%
Inlet.m = Inlet.mg + Inlet.mv + Inlet.ml;    % kg Mixture
Inlet.mHUAir = Inlet.mv + Inlet.mg;          % kg Humid Air
(without liquid)
Inlet.x = Inlet.mv/Inlet.mHUAir;             % kg Steam in kg Humid
Air
Inlet.y = Inlet.ml/Inlet.m;                  % kg liquid Water in
kg Mixture
Inlet.hg = h_pTXiw_HuAir(Inlet.p,Inlet.T,Inlet.x);  % kJ/kg
Inlet.hl = h_pTXiw_HuAir(Inlet.p,10.,1.0);          % kJ/kg
%
Outlet.h = (Inlet.mHUAir * Inlet.hg + Inlet.ml * Inlet.hl) / ...
    (Inlet.mHUAir + Inlet.ml);
Outlet.T = T_phXiw_HuAir(Inlet.p,Outlet.h,Inlet.y);  % °C
Outlet.phi = phi_pTXiw_HuAir(Inlet.p,Outlet.T,Inlet.y);
%
% Print results to command line
%
Outlet
%
```

5.2 3D CFD Model

A parallel calculation is performed using the software CFX, in a three-dimensional case where a 1° sector of a pipe is considered. This choice reduces the computational effort, taking advantage of the rotational periodicity of the domain considered.

The domain is shown in Figure 5.1.

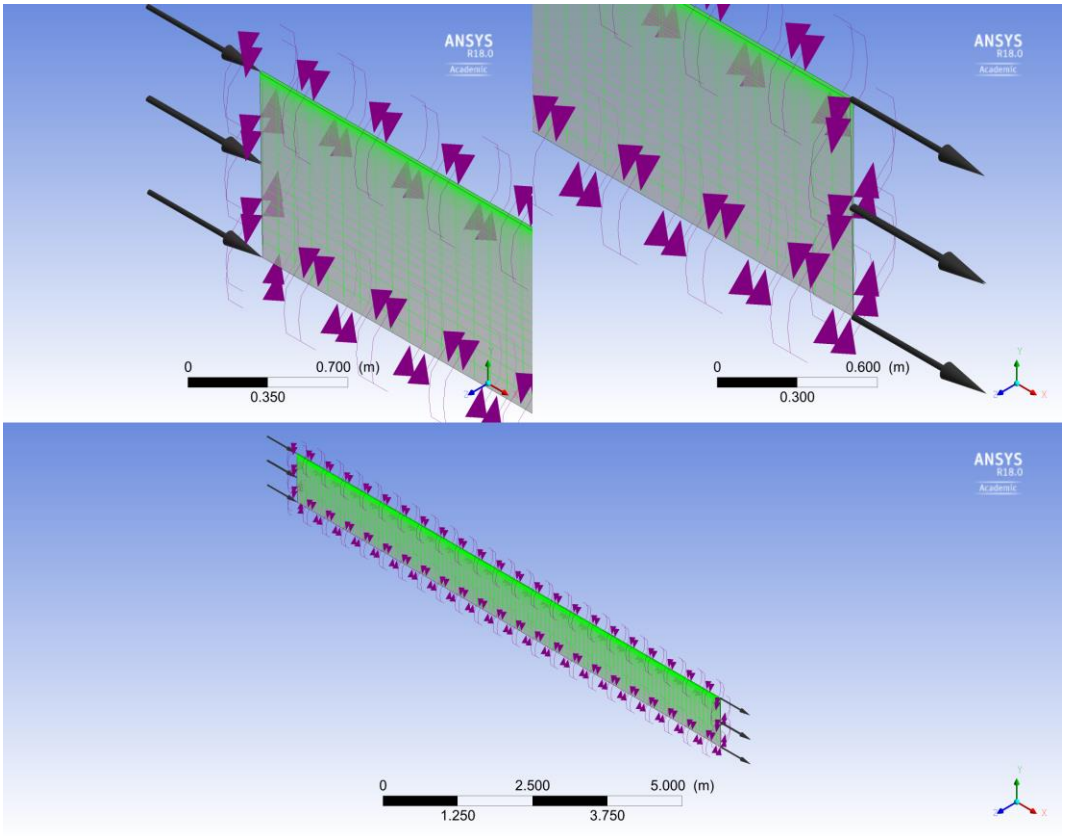

Figure 5.1. *Validation case: inlet, outlet and whole domain*

In the model, the same settings described in Chapter 4 are used, to assess the validity of it.
However, it is meaningful to explain how the inlet parameters are defined in CFX-Pre, as the whole validation is conducted changing some of those values to test different inlet conditions. These parameters are the air temperature and the injected water mass flow rate.

The boundary conditions at the inlet are described by the air mass flow rate, set with an expression equal to 1 kg/s, and the air temperature, whose value is changed through the validation. The flow direction is set as Normal to Boundary Condition, and for turbulence, Medium intensity (5%) is used, as shown in Figure 5.2.
Moreover, as in the 1D model, the vapour mass fraction at the inlet is assumed equal to zero.

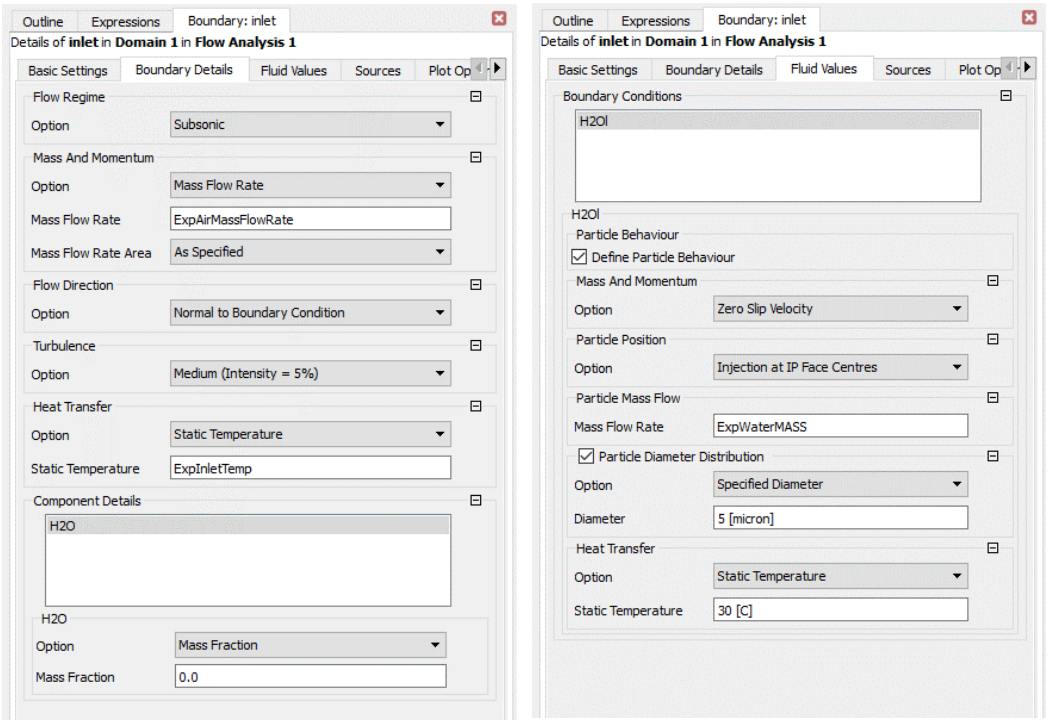

a) b)

Figure 5.2. *Inlet boundary conditions: Boundary Details a) and Fluid Values b)*

The particle (liquid water) behaviour is defined in the Fluid Models tab. In the same way as in the compressor model, injection is performed with zero slip velocity between the flow and the droplets, in a spatially uniform way (Injection at IP Face Centres).
The particle size is chosen equal to 5 micrometre, and water temperature is set at 30°C, as previously done.
The expressions values used to define air temperature and water mass flow rate are changed to assess the model validity, and will be described at a later stage.

At the outlet, Average Static Pressure equal to 1 bar is used as boundary condition, with pressure averaging over the whole outlet.

The wall of the pipe is considered as Free Slip Wall, to be in agreement with the 1D free-stream calculation model, and with the compressor model used for the present work.

As pointed out before, all the remainder settings (the fluid properties, the turbulence and heat transfer models, the solver parameters etc.) are the same as in the compressor wet model. Therefore, an ideal mixture is considered as working fluid, using the Variable Composition Mixture option as done in the model previously described.

5.3 Investigated conditions

The present validation is based on nine different tested conditions, obtained changing the temperature at the inlet and the water mass flow rate. Indeed, the accuracy of the model is mainly influenced by these parameters, as higher amount of water and lower inlet temperature - and therefore lower temperature difference between the gas and the liquid phase - can lead to a bigger error.

The values employed for this validation are shown in Table 5.1, where the amount of water is expressed as a fraction of the air mass flow rate; however, as the air mass flow rate is set equal to 1 kg/s, the water fraction can be considered also as a mass flow rate value (kg/s).

Table 5.1. *Input parameters value.*

Air temperature	Water injected
80°C	0.001
60°C	0.005
40°C	0.01

5.4 Validation results

The results obtained from the simulations show a good agreement between the two models, despite a small error, which can be assumed as not relevant for the current work.

The trend extrapolated from the results confirms the expectations, as higher injection rate and lower temperature difference lead to a bigger difference between the 3D and the 1D case, slightly overestimating the temperature of the fluid after complete evaporation has occurred, in the 3D case.

Figure 5.3 reports as interpolated data the 1D results, while 3D CFX ones are plotted as single points.

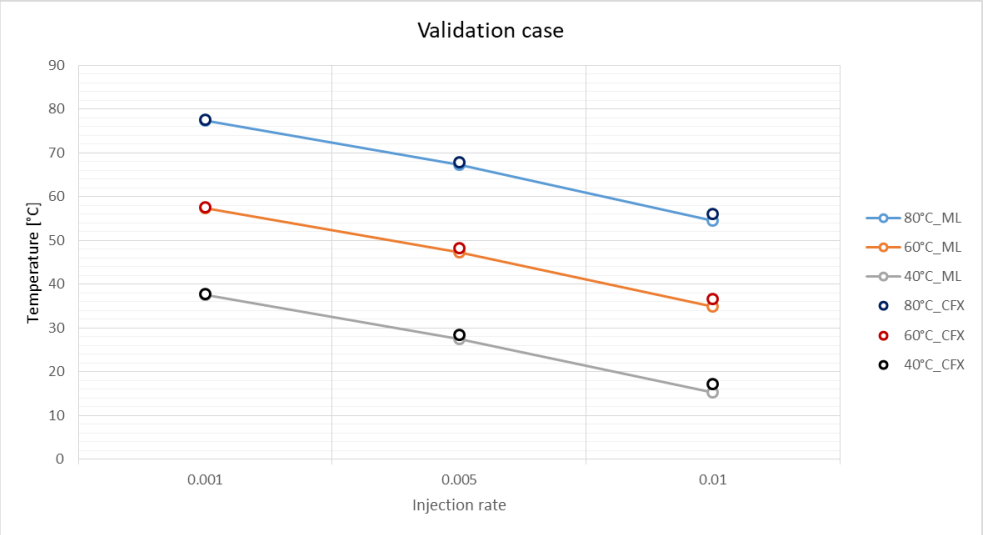

Figure 5.3. *Result comparison between one-dimensional and 3D calculations.*

The values of the temperature at the outlet are shown, in °C, in Table 5.2 a) and b).

Table 5.2 *Result comparison between one-dimensional a) and 3D calculations b).*

a)

1D case	**Injection rate**		
Temperature	**0.001**	**0.005**	**0.01**
80°C	77,42	67,19	54,61
60°C	57,45	47,36	34,95
40°C	37,49	27,53	15,29

b)

3D case	**Injection rate**		
Temperature	**0.001**	**0.005**	**0.01**
80°C	77,56	67,92	56,08
60°C	57,61	48,18	36,58
40°C	37,68	28,45	17,10

The difference between the two models is mainly due to the gas properties employed in the calculation; indeed, the 3D model considers ideal properties for humid air (Ideal Mixture, see above), while the 1D model uses real gas properties, as a function of pressure and temperature, which are available from the LibHuAirProp library.

As expected, the difference in the results becomes more significant when the inlet temperature decreases and when the water amount introduced is bigger. However, as the use of real gas properties in the CFX model requires time and is a cumbersome process, the error deriving from this validation case can be taken as acceptable. Moreover, it is worth to notice that the CFX model slightly overestimates the temperature at the outlet, therefore the error goes in a conservative direction.

The present validation of the model allows to go back to the compressor investigation. Mesh creation and related observations are described in the next chapter.

Chapter 6

Mesh creation and numerical simulation requirements

6.1 Introduction

The aim of the present model is to perform an Eulerian calculation, therefore friction at the walls in the domain is not considered. This choice leads to the creation of a different grid, specifically designed for the wet compression process examined, whose characteristics are explained in the following sections.

The domain used in the model consists of three parts:

- the inlet section, named “DUCT_in”;
- the blade domain, named “R1”;
- the outlet section, named “CHANNEL_out”.

The first two parts are created together using TurboGrid, and then characterised in a different way (stationary and rotating part) in CFX-Pre as described previously. On the other hand, the outlet section has been created with ICEM.
As pointed out in the CFX-Pre characterization, a 24°-sector is considered in the model, taking advantage of the rotational periodicity of the machine; therefore, only one blade is present in the domain.

6.2 Inlet and impeller mesh

The rotating domain R1 mesh is made using TurboGrid, and a short inlet section is added in the same project, as an extension of the geometry available.
Therefore, starting from the geometry data in Workbench, a TurboGrid project is implemented.

6.2.1 Mesh data

The creation of the mesh is achieved setting several parameters that describe the properties of the grid.

The first group of settings is implemented in the Mesh Size tab, where the general size of the mesh and the boundary layer refinement are set.

In the current model, the mesh size is defined by means of a Global Size Factor, whose value is set equal to 1.5. In this way a higher number of nodes and element is used, compared to the default value set by the software.
Moreover, the Boundary Layer Refinement Control allows to choose the size of the cells in the boundary layer, more precisely the first one closer to the wall, using two different methods. It is possible to set an absolute value of the first cell height, or to use a value proportional to the mesh size. In the present model, First Element Offset is chosen, using a cell height equal to 0.2 cm. As in a frictionless model there is no velocity gradient in the direction normal to the wall, the boundary layer does not exist; therefore, a finer mesh structure near the walls is not needed. Using the chosen value, no boundary layer velocity profile is solved.

In the same table the Inlet section can be enabled and an additional tab becomes available to define the characteristics of the grid.
The Inlet tab allows to set the characteristics of the mesh for the added section; the chosen Mesh Type is H-Grid, and its definition is achieved by using a Target Expansion Rate equal to 1.2.
The added part can be seen in Figure 6.1.

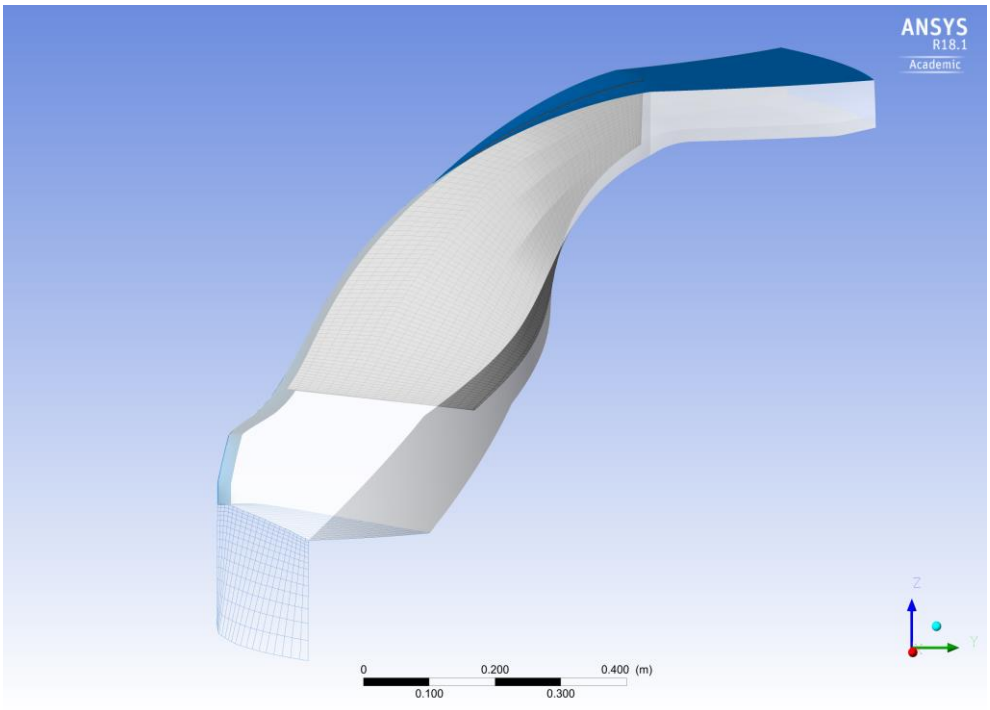

Figure 6.1. *Inlet section addition.*

The second set is defined in the Passage tab, where the characteristics of the mesh in the spanwise direction can be chosen using different methods.
The Element Count and Size method is used, to set the number of elements along the blade span, and the number of them whose size is constant.
In addition, the size of the element next to the wall can be set, defining the width of the first cell close to the hub and to the shroud on the two sides of the blade.
The chosen values are shown in Figure 6.2.

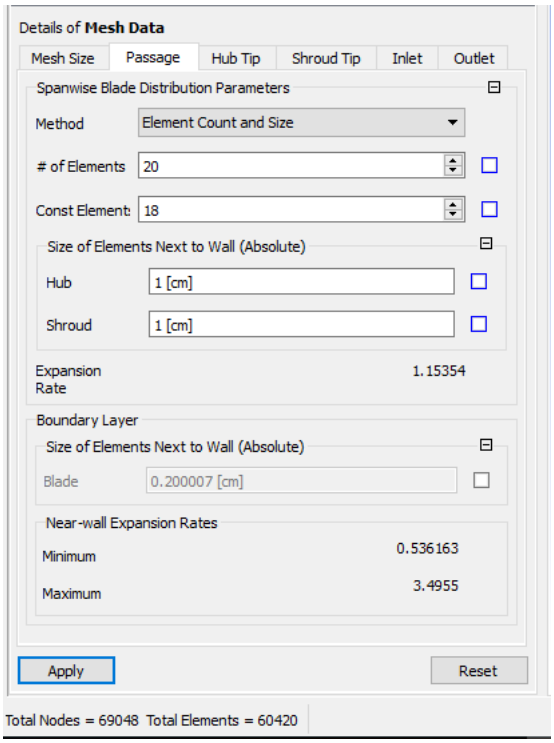

Figure 6.2. *Spanwise distribution parameters.*

6.2.2 Layers, leading edge and trailing edge

The mesh obtained with the settings described above is a relatively small size mesh, with 69048 nodes and 60420 elements.
In order to get a good transition between the hub and the shroud layers, i.e. to guide the mesh creation in a better way, two intermediate layers are used. Indeed, due to the twisted shape of the blade, one layer is not sufficient to obtain a smooth transition along the spanwise direction.
Figure 6.3 shows the layers and the mesh obtained on the high pressure side of the blade.

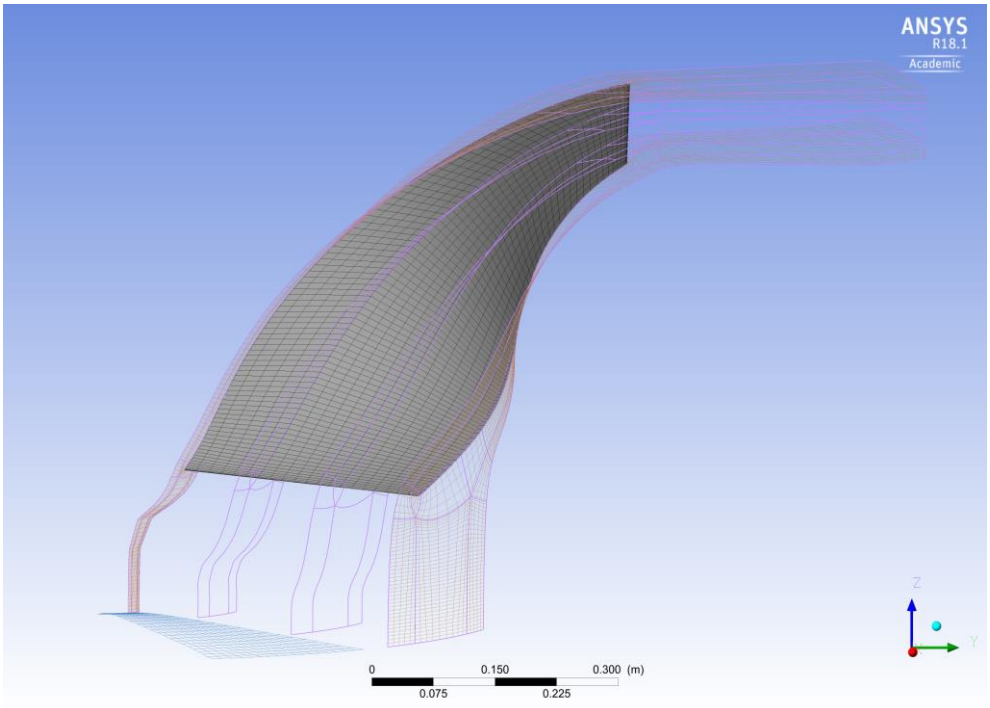

Figure 6.3. *Blade mesh and layers.*

The grid structure obtained at the intermediate upper layer location is shown in Figure 6.4 and Figure 6.5, in which also the shroud mesh lines are included.

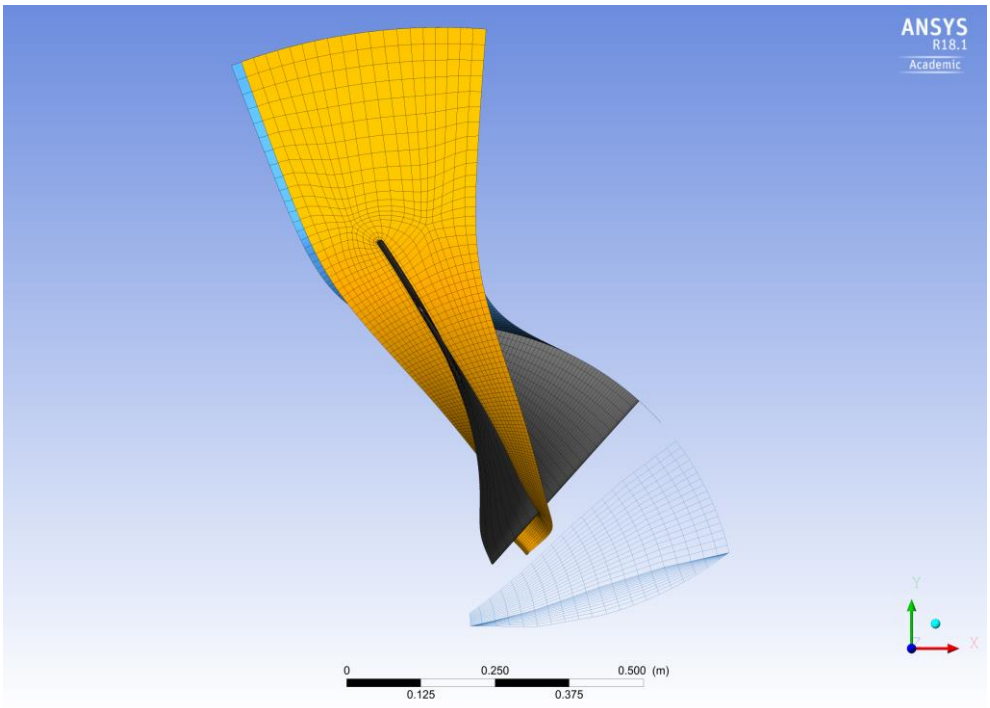

Figure 6.4. *Layer mesh, upper view.*

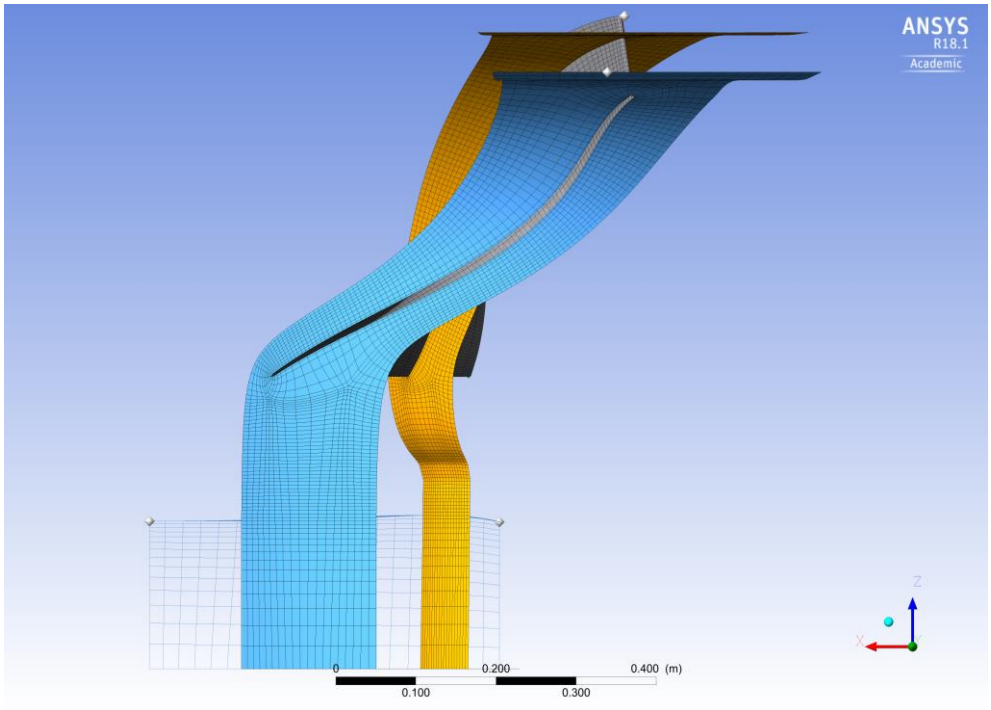

Figure 6.5. *Layer and shroud mesh, side view.*

The inlet mesh can be easily seen from the two pictures above, added as an extension of the inlet surface, whose original position is visible in Figure 6.5, where the solid grey points are located.

As the boundary layer is not solved in the model, and the first cell size is set using a value bigger than the one needed to solve the velocity profile in that position, no refinement near to the wall is considered. Nevertheless, it may be useful to show the grid structure in the proximity of the leading edge and trailing edge.
A zoomed view can be observed in Figure 6.6 and Figure 6.7.

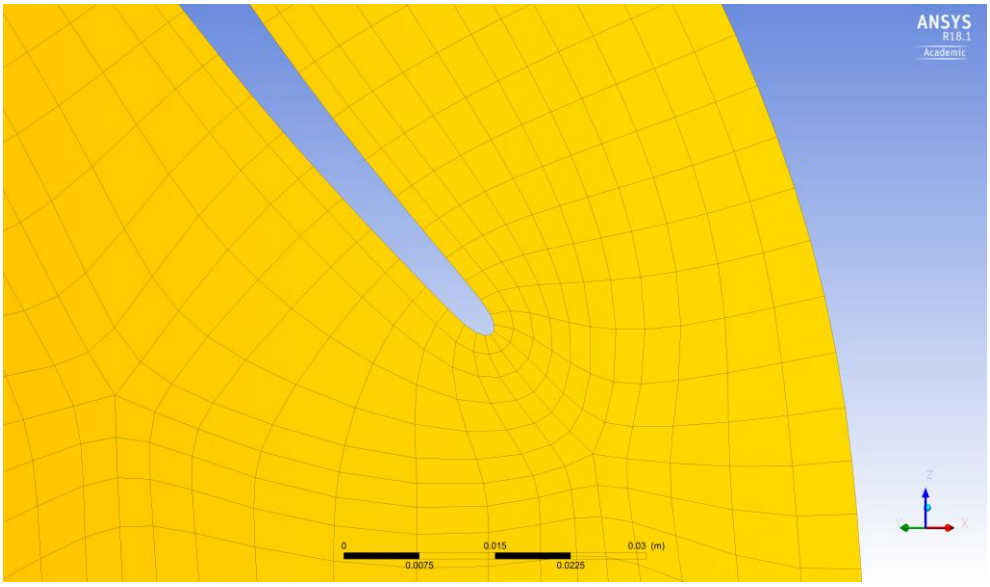

Figure 6.6. *Leading edge.*

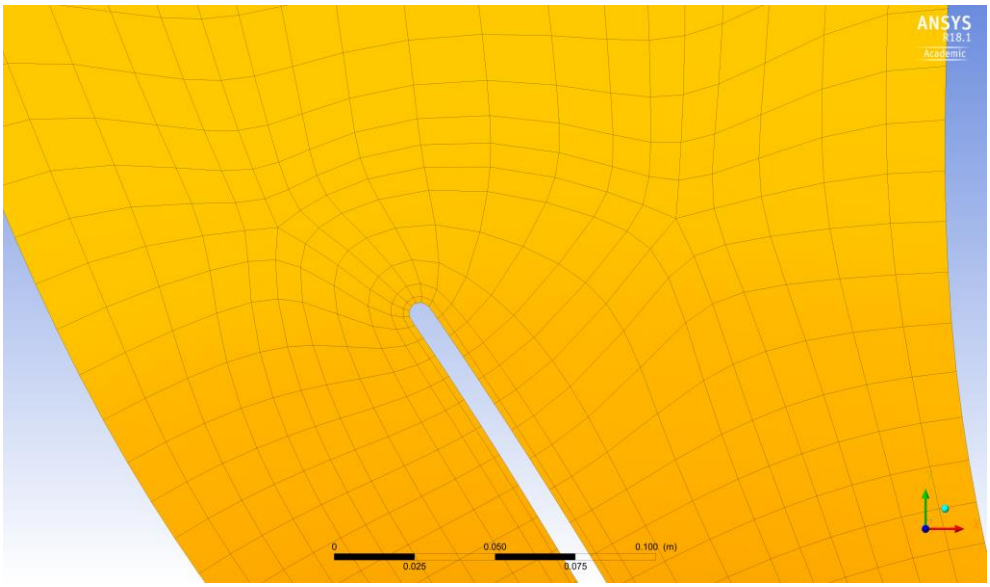

Figure 6.7. *Trailing edge.*

6.2.3 Mesh quality

The quality of the mesh in TurboGrid can be checked using the Mesh Analysis drop-down tool, where the Mesh Statistics are available. The quality parameters are shown in Figure 6.8, reporting also the values observed in the current grid.

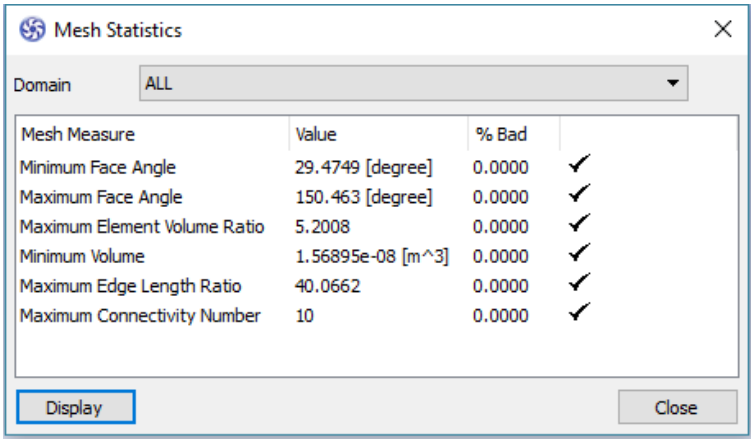

Figure 6.8. *Mesh quality statistics.*

The present grid shows a good quality, as the minimum and maximum angle lie in a good range, almost 30° and 150° respectively. These values are good if compared to the ones that are usually adopted as limit values in creating a grid in ICEM (20° and 160°); moreover, they lie inside the limits set by TurboGrid itself, as shown in Table 6.1.

Table 6.1. *Mesh Limits.*

Mesh Measure Limit	Value
Maximum face angle	165°
Minimum face angle	15°
Connectivity number	12
Element volume ratio	20
Minimum volume	0 m^3

6.3 Outlet mesh

The outlet section “CHANNEL_out” of the mesh is created using ICEM, in order to achieve a bigger distance between the wake zone after the trailing edge and the surface where the outlet boundary condition is applied in CFX-Pre.

Therefore, creating this additional section, the outlet surface is moved far from the impeller blade. The length of the domain in the radial direction is chosen as twice the external diameter of the impeller, while in the angular dimension it covers a 24° sector, as already said for the TurboGrid mesh.

6.3.1 Mesh creation

Starting from the outlet of the impeller domain, the surface has been copied and shifted in the radial direction, and then used as a reference for the outer surface. The outer surface has been created using the Surface of Revolution tool, in order to cover the whole 24° sector, as in the outer region the circumferential length of the arc increases.

After creating the basic geometry with curves and surfaces, the blocking step has been carried out, associating the edges and vertices to form a single block.
In the Pre-mesh Params tool, the mesh is built up using a uniform distribution of the nodes along all the edges, as no boundary layer refinement is needed. The resulting grid consists of 27300 nodes and 31248 elements; it is shown in Figure 6.9.

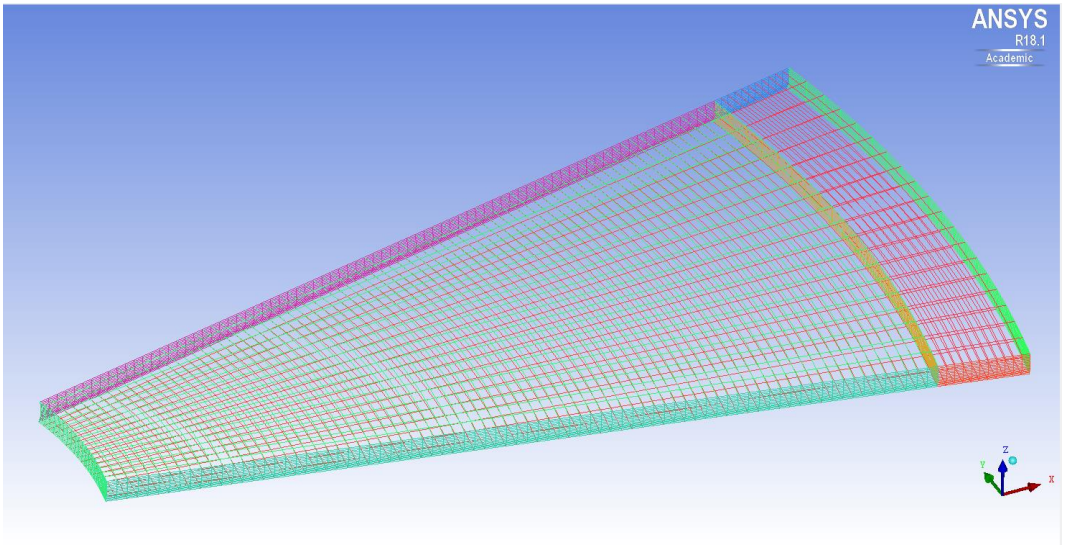

Figure 6.9. *Outlet section mesh, upper view.*

The outer section, visible in the picture, is part of the same block and therefore part of the same domain, and has no specific relevance in the whole model.

6.3.2 Mesh quality

The shape of the domain and the simple structure of the mesh guarantees a good mesh quality, as all the elements have a nearly parallelepiped shape.
The quality of the mesh is checked in ICEM using the Edit Mesh > Display Mesh Quality tool, taking into account as quality parameters the Minimum and Maximum Angle and the Quality one.

The minimum angle lies between 63 and 90 degrees, while the maximum angle is below 117 degrees, as shown in Figure 6.10 and Figure 6.11:

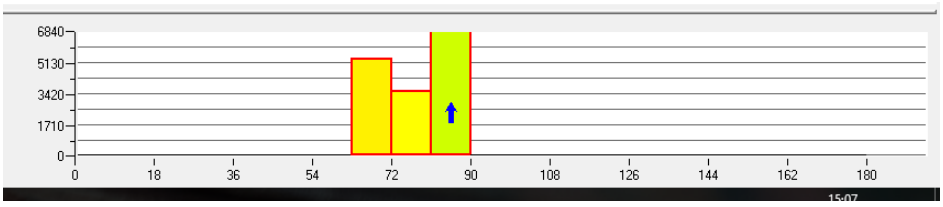

Figure 6.10. *Mesh quality: Minimum angle.*

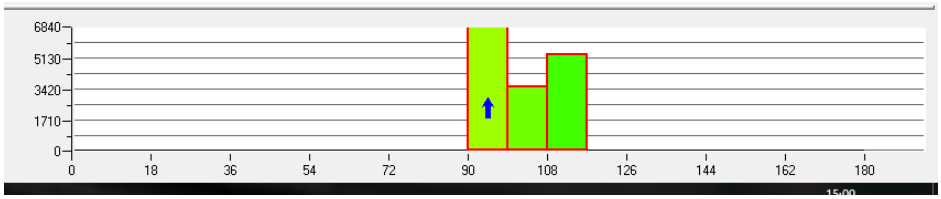

Figure 6.11. *Mesh quality: Maximum angle.*

Those values guarantee a good mesh quality, as pointed out by the Quality parameter in Figure 6.12.

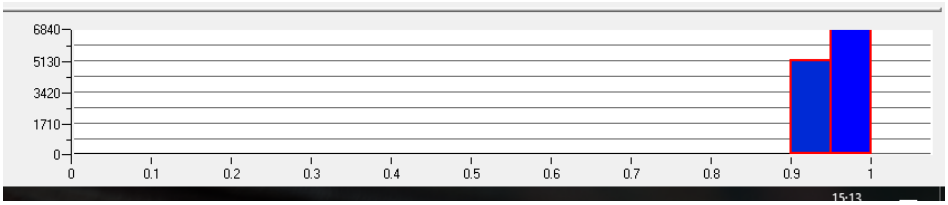

Figure 6.12. *Quality parameter.*

6.4 Advantages and observations

The grid described above has been built up in accordance with the flow field and the characteristics of the model implemented in CFX-Pre. The presence of a two-phase flow, with droplets evaporation, and the physics involved in the model are highly demanding and require a considerable computational effort.
The mesh and the model itself allow to get a lower computational cost and a higher stability of the solver in the calculations, making possible to perform several simulations. In this way, different droplet sizes and injection rates have been tested and a wider set of investigations is carried out.

As previously pointed out, the investigation is carried out performing an Eulerian calculation, without including friction in the machine. This means that the velocity profile near the wall is uniform, and there is no gradient in the region and no boundary layer exists. Due to this aspect the mesh is created with a different approach, using a lower number of nodes, as no grid refinement with smaller cells is required close to the walls. Moreover, as shown in section 6.2.1, the mesh in the region nearby the leading edge and the trailing edge is quite simple, and no further edge split refinement is applied. This would have been necessary with smaller cells in the boundary layer, to obtain a better mesh quality by means of lowering the aspect ratio and get a better shape of the elements in those regions.

This choice gives to the model a strong stability, and reduces the computational time. On the other hand, the use of this grid and the model itself may result in a loss of

information about the real behaviour of the machine. In other words, the frictionless simplifying assumption determines a different flow field close to the blade, where a lower velocity would increase the residence time of the particle in the domain, even if in a thin region.
However, as the scope of this work is to understand how water evaporation influences the overall performance of the machine, the grid employed guarantees a good reliability.
Moreover, the comparison between the wet cases and the dry one is carried out using the same grid and settings; the results are analysed in relative terms, taking the Humid Air model as a reference and pointing out the differences with the use of relative values.

To give a better overview about the grid influence, a comparison with a finer grid, employed in a non-frictionless model, is carried out in the next paragraph.

6.5 Grid comparison

6.5.1 Grid description

In a compressor model where friction at the walls is considered, the flow field needs to be covered by the grid in a suitable way. Therefore, as previously mentioned, the gradient of velocity in the boundary layer requires a finer grid structure near the walls, in order to calculate in an accurate way the flow field in that region. The mesh is created with local refinement, to satisfy this accuracy in the calculation.
In addition, the leading edge and trailing edge regions, due to the sharp shape of the blade, require further refinement to obtain a better cell shape, lowering the aspect ratio. An example of the grid appearance in the trailing edge region is given in Figure 6.13.

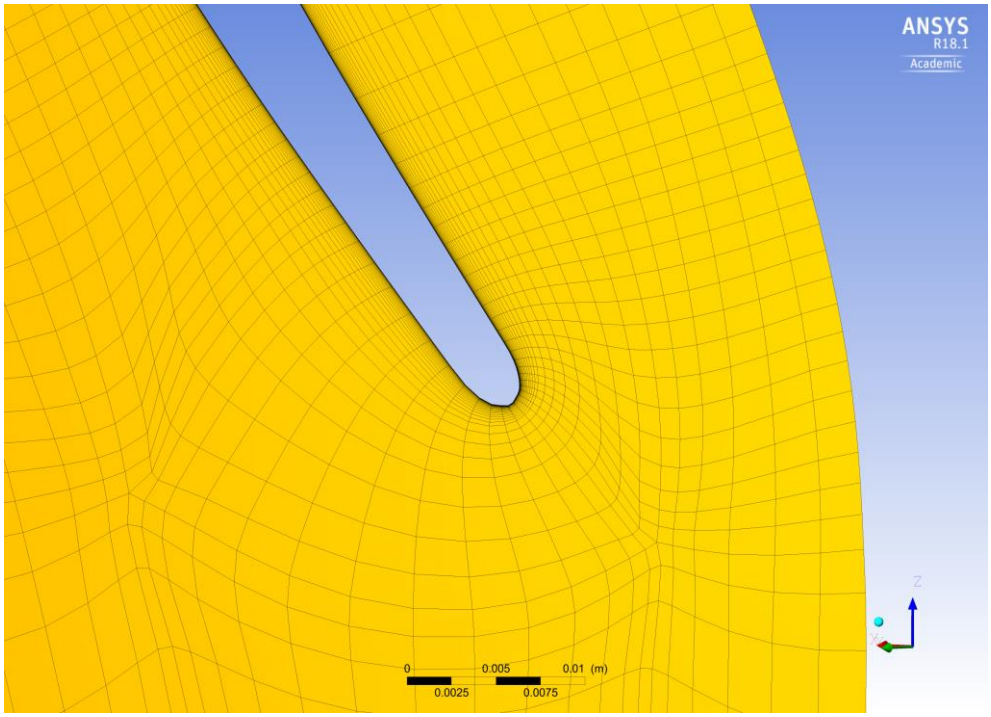

Figure 6.13. *Mesh refinement: blade leading edge.*

The mesh obtained is composed by 2.025 million nodes, and 1.955 million elements. Moreover, at the tip of the blade, a tight gap (2.6 mm) is considered.

6.5.2 Model setup

The comparison is carried out considering the dry case, using dry air as working fluid. The setup used is the same described in section 4.2, for both cases. Heat transfer is implemented using Total Energy, including the Viscous Work Term; Shear Stress Transport is used for turbulence modelling.
In the Solver Control settings, a 0.0005 s physical timescale is used.

The domain is composed by the same sections previously described; only the mesh of the rotating domain R1 is changed, using the 2.025 million nodes and the 70 thousand nodes grids. Hereafter the two cases will be called as 2025k and 70k respectively.

6.5.3 Comparison

The two grids are compared referring to overall values that describe the performance of the machine: outlet pressure, outlet temperature, pressure and temperature ratios, torque and power required by the compressor are the parameters taken into exam.

The outlet pressure value shows a difference between the two grids, as plotted in Figure 6.14; the relative change observed in the 70k grid case is around +7.85%. Pressure is the parameter which shows the biggest difference.

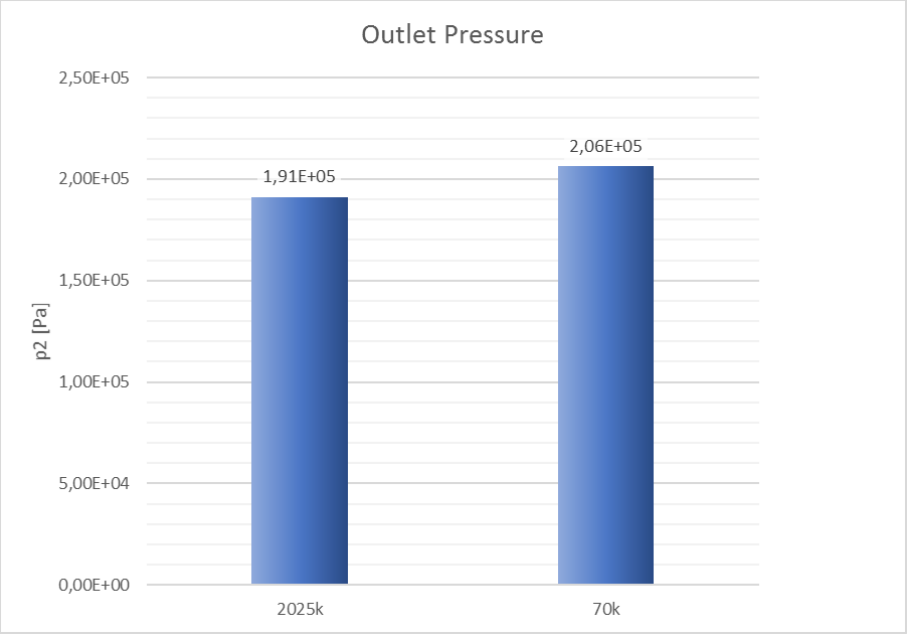

Figure 6.14. *Outlet pressure comparison.*

The temperature at the outlet shows a smaller difference comparing the two cases, as its relative change is around +1.17%. The change in temperature occurs in an unexpected way, as for a frictionless model the contribution to heat generation inside the machine given by friction is not taken into account, and no increase would be expected. Figure 6.15 shows the values obtained.

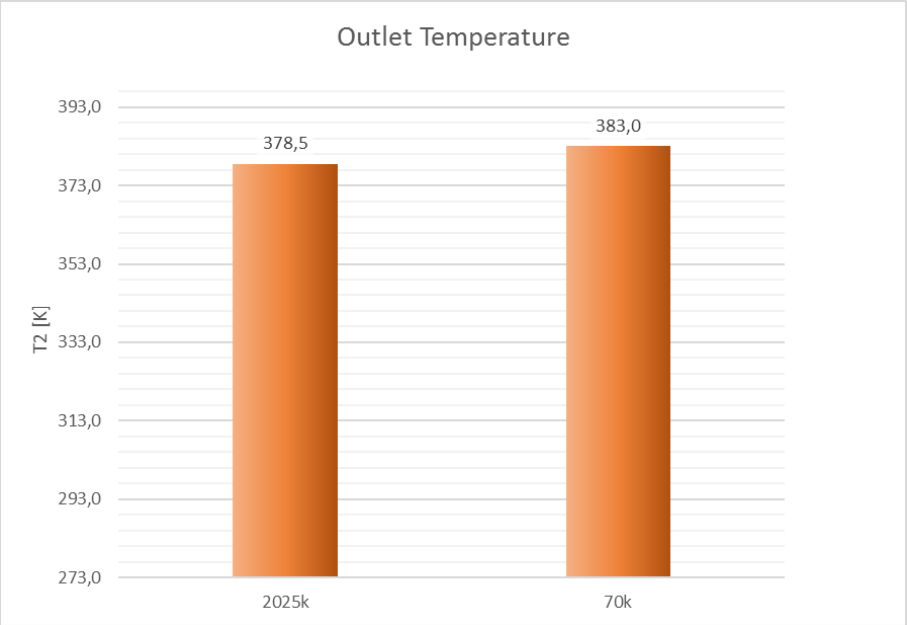

Figure 6.15. *Outlet temperature comparison.*

The pressure and temperature variation can be understood in a better way looking at the ratios between the values at the inlet and the outlet of the impeller. The values are plotted in Figure 6.16, and show the same change described above.

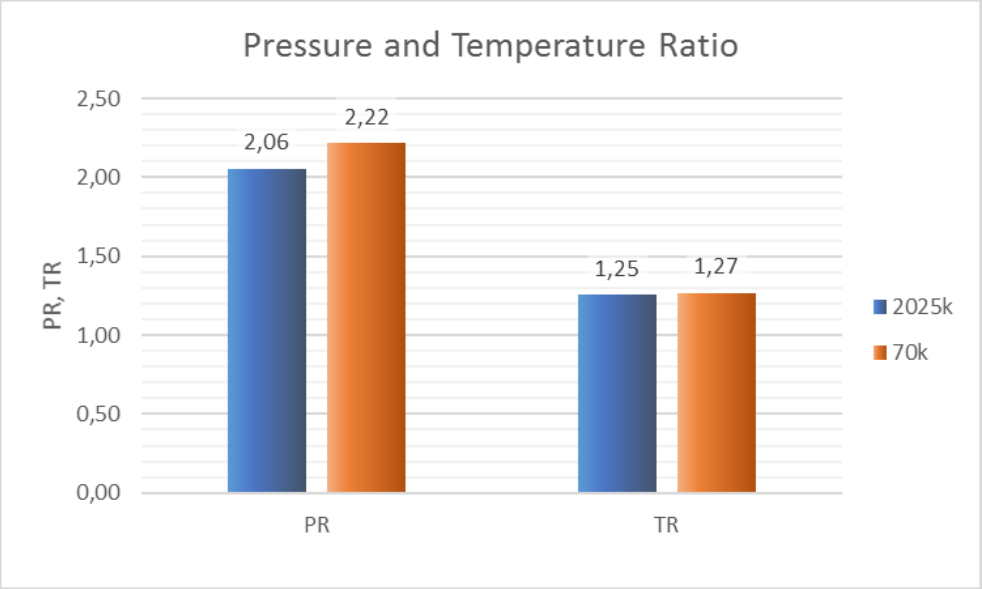

Figure 6.16. *Pressure and Temperature ratio comparison.*

Lastly, torque and power values are plotted together in Figure 6.17 a) and b), as power is calculated starting from the torque itself. The percentage variation of both parameters is around 2.3%; the use of the 70k grid leads to overestimate the power consumption, even if only slightly.

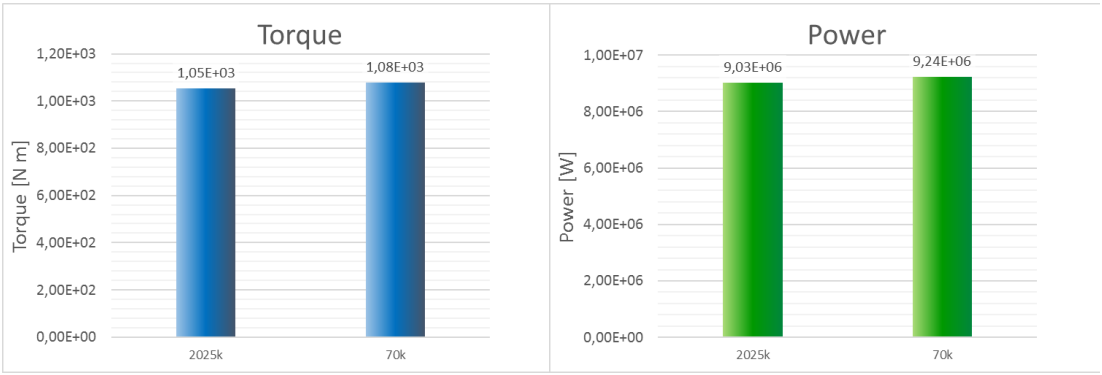

a) b)

Figure 6.17. *Comparison of torque a) and power b) observed using two different grids.*

As previously said, the differences observed between the smaller grid and the 2025k one do not affect the validity of the investigation about wet compression, as the focus is on the effects of water injected compared to the dry case, rather than on the absolute values obtained.

Chapter 7

Results

The results of the simulations performed with the set of conditions described in 4.4.6 are reported in this chapter. The wet compression process is compared with the humid air one, and a general comparison between the different wet conditions is carried out. Three different injection rates have been tested, and five different droplet size setups have been used, obtaining 15 simulations that describe the behaviour of the machine and the effects of water injection on the process depending on these parameters.
The diameter size and the injection rate influence in the monodiameter distribution cases is described first, for a better understanding before analysing the nozzle droplets distribution one.
In addition, the investigation is broadened describing how evaporation occurs inside the impeller and analysing how the mean droplet diameter, pressure and temperature vary through the stage. Lastly, the injection rate influence on local variation of these parameters is presented.

7.1 Monodiameter droplet distribution

The performance of the compressor is described by means of overall parameters, such as:

- Evaporated water
- Static pressure at the impeller outlet
- Static temperature at the impeller outlet
- Pressure and temperature ratio
- Power consumption
- Efficiency and polytropic index

Therefore, the influence of the droplets size and the amount of water injected is assessed referring to this set of variables.
It is relevant to notice how the investigated parameters are free to vary, as the boundary conditions used for the model include pressure and temperature at the inlet, and mass flow rate at the outlet.

7.1.1 Evaporated water

The amount of water evaporated plays an essential role in understanding how the parameters described in the following vary.

The evaporated water is calculated from the mass flow rate value at the inlet of the domain and at the impeller outlet using the Function Calculator; as this tool provides the value of the gas-phase mass flow, the difference observed between inlet and outlet of the impeller is due to water vapour generated by droplets evaporation.

The amount of water evaporated is expressed as an absolute value in Table 7.1, in kg/s.

Table 7.1. *Evaporated water [kg/s] depending on diameter and injection rate.*

Diameter	Injection rate		
	0.4%	1.4%	2.4%
5 µm	0,0228	0,0672	0,0944
10 µm	0,0084	0,0272	0,0398
20 µm	0,0023	0,0076	0,0095
50 µm	0,0009	0,0002	0,0010

The trend that emerges from the values shows, as expected, a higher amount of water evaporated with higher injection rate. At the same time, smaller diameters enhance evaporation and a bigger mass of water participates in the phase change, as made distinctly clear in Figure 7.1.

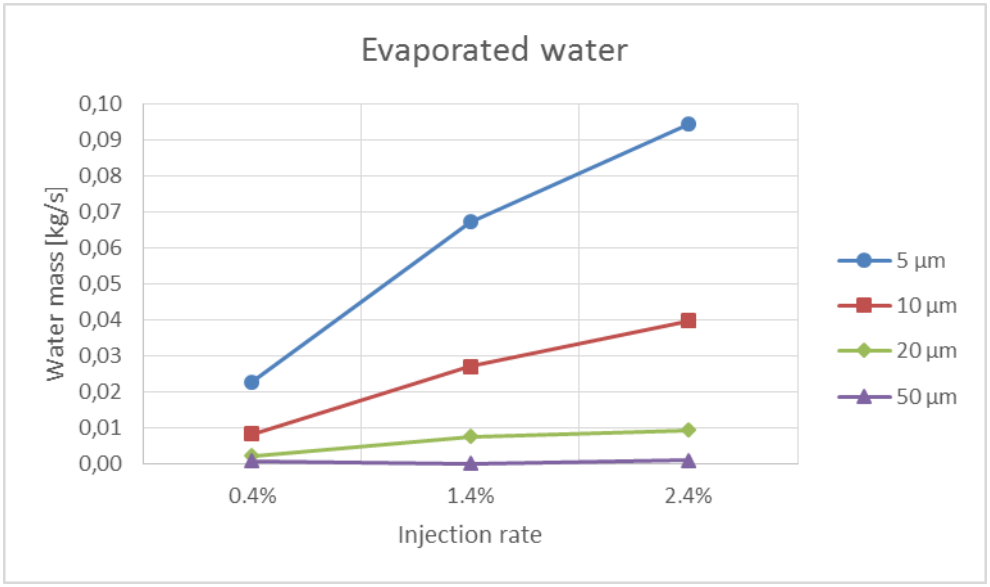

Figure 7.1. *Injection rate influence on evaporated water.*

The diameter influence is even more evident in Figure 7.2, where the data are grouped according to the injection rate.

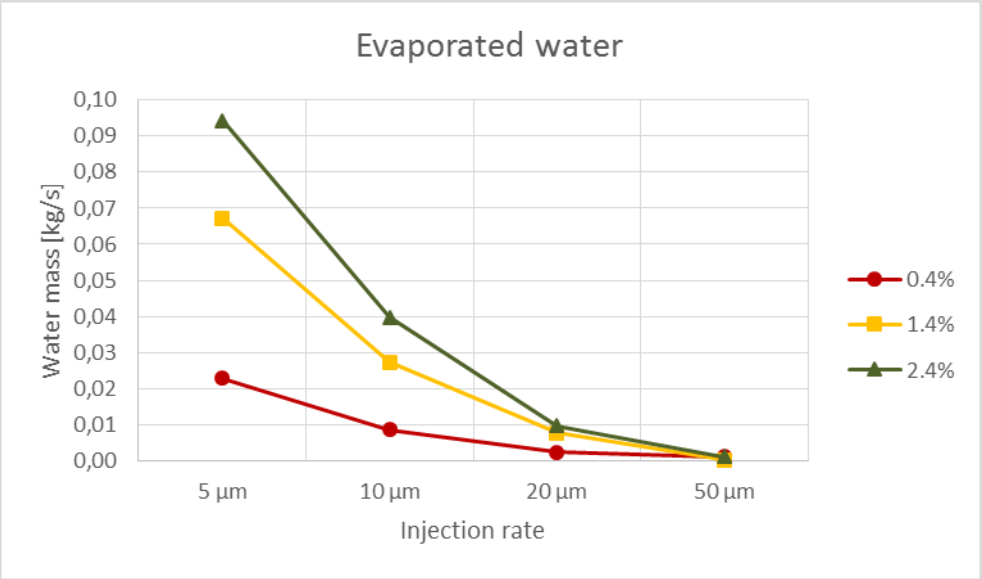

Figure 7.2. *Droplet diameter influence on evaporated water.*

As it can be noticed the effectiveness of increasing the injection rate is higher using smaller diameter vales, such as 5 and 10 micrometre.
Evaporation is strongly reduced with 20 µm droplets and becomes null considering 50 micrometre particles.

Moreover, the diagram in Figure 7.1 shows a smaller improvement shifting from the 1.4 to the 2.4% injection rate case, than the one observed in the 0.4-1.4% comparison. The trend shown by 1.4 and 2.4% injection rate simulations can be further investigated, calculating the percentage of water evaporated on the whole amount injected in the machine. Therefore, the values in Table 7.1 are divided by the respective water mass flow rate used (0.0251, 0.0873 and 0.15056 kg/s) and the percentage values in Table 7.2 are obtained.

Table 7.2. *Share of evaporated water on the total injected amount.*

Diameter	Injection rate		
	0.4%	1.4%	2.4%
5 µm	90,88%	76,51%	62,71%
10 µm	33,59%	30,93%	26,41%
20 µm	9,28%	8,62%	6,32%
50 µm	3,75%	0,24%	0,67%

Then, the reduced improvement is not only due to the fact that the increase of water injected is smaller (1.7 times from 1.4 to 2.4%, while 3.5 times from 0.4 and 1.4%),

but also to the smaller amount of evaporated water, i.e. the share of phase-changing water becomes smaller as the injection rate is increased. This is true in all the cases, except the 50 micrometre one, where the difference, however, is low.

Figure 7.3 describes the decrease in evaporation efficiency as a function of the injection rate (and diameter).

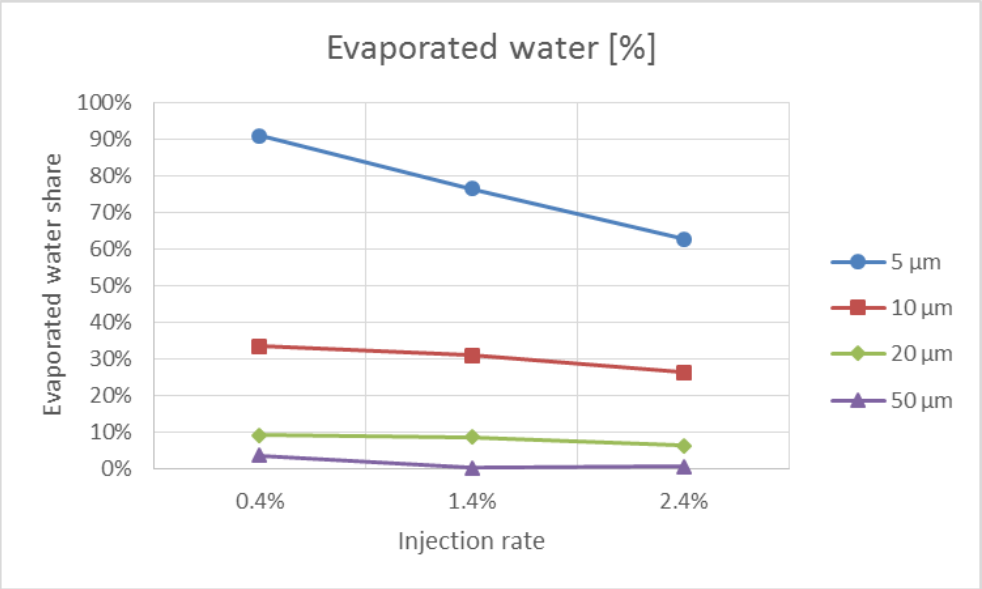

Figure 7.3. *Diameter and injection rate influence on evaporated water share.*

7.1.2 Outlet pressure

The pressure value at the outlet is obtained using a mass flow average function, and is strongly influenced by the injection rate and the droplets size.
Comparing the wet cases with the humid air one, an increase in pressure is generally observed.
Higher injection rate entails higher pressure at the outlet of the stage, showing a quite linear growth with respect to the tested values. The reason can be found in the bigger amount of water evaporated observed as the injection rate is increased, even though the share on the overall amount is lower.

The diameter size plays a very important role, as smaller droplets allow to obtain easier evaporation and a stronger effect on the compression process. As can be easily seen in Figure 7.4 the result show a clear trend, where the pressure increase becomes higher as the diameter decreases.

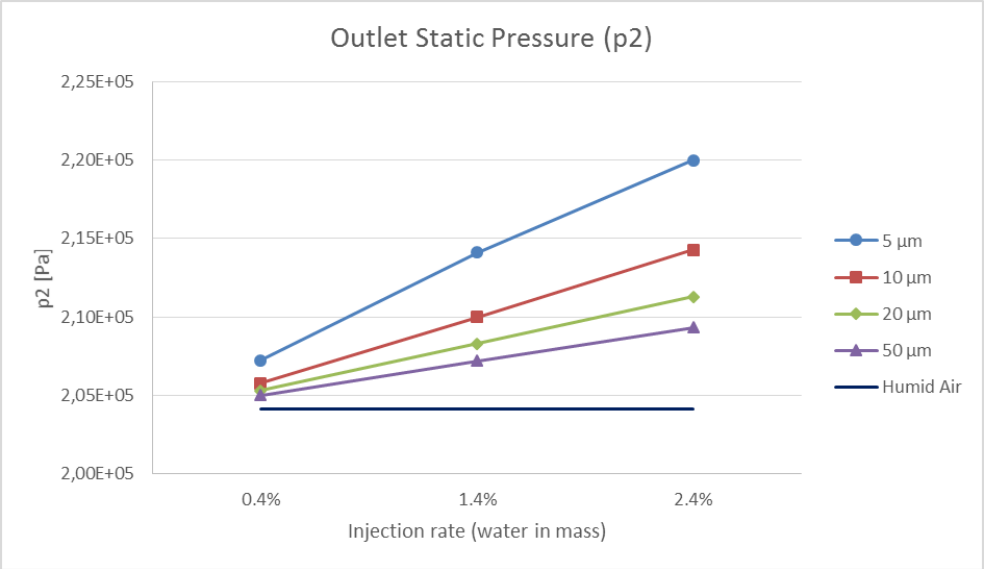

Figure 7.4. *Injection rate and droplet diameter influence on the outlet pressure.*

Starting from the 50 µm droplets, the effect is clear compared to the dry case, while smaller diameters as 20 and 10 µm lead to stronger and stronger effect, in combination with increased injection rate; the 5 µm droplets produce the highest increase.
The injection of 2.4% water mass can lead to an increase in percentage value up to 7.75%, with the smaller diameter.
The pressure values are reported in Table 7.3.

Table 7.3. *Outlet pressure [Pa] for wet cases and humid air compression.*

Diameter	Injection rate		
	0.4%	1.4%	2.4%
5 µm	2,072E+05	2,141E+05	2,200E+05
10 µm	2,058E+05	2,100E+05	2,143E+05
20 µm	2,053E+05	2,083E+05	2,113E+05
50 µm	2,050E+05	2,072E+05	2,093E+05
Humid Air	2,04E+05	2,04E+05	2,04E+05

7.1.3 Outlet temperature

The most important effect of wet compression is to lower the temperature of the fluid, using evaporation as cooling method. The evaporation influence is evident analysing the set of data obtained, as the greater cooling effect is reached with the smallest diameter and highest injection rate.
Figure 7.5 shows a strong impact of the droplets diameter on the temperature, as 5 and 10 µm allow to lower the value considerably, up to 35 K, as it occurs using the highest

injection rate. On the other side, the use of a bigger droplets size is not effective in lowering the temperature: the 20 micrometre droplets have only a small effect on the outlet temperature, while considering the 50 micrometre ones the benefit is negligible.

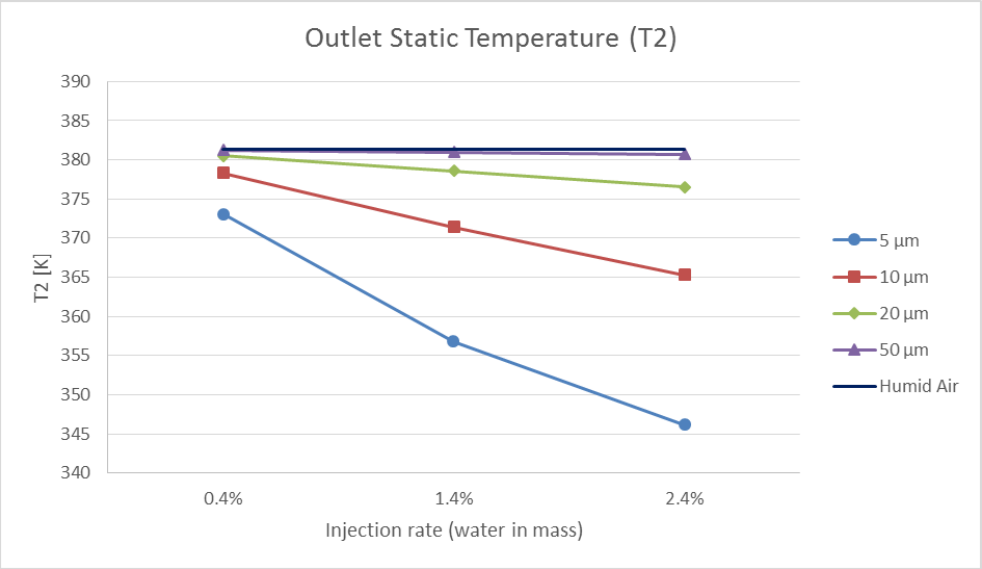

Figure 7.5. *Injection rate and diameter influence on the outlet temperature T_2.*

This behaviour is closely related to the amount of water evaporated inside the impeller. In the 5 micrometre case it can be observed how the increase of the injection rate leads to a decrease of the temperature, although with a lower effectiveness than in the 2.4% case. This can also be related to the evaporation, as the water injected in the 2.4% simulation is evaporated in a lower percentage of the total amount, compared to the 0.4 and 1.4% cases.
The share of evaporated water mass is more stable analysing the 20 and 10 micrometre cases, as shown by the temperature linear decrease in Figure 7.5.

Table 7.4 reports the temperature values obtained in the investigation.

Table 7.4. *Outlet temperature [K] for wet cases and humid air compression.*

Diameter	Injection rate		
	0.4%	1.4%	2.4%
5 µm	373,04	356,70	346,17
10 µm	378,33	371,43	365,28
20 µm	380,54	378,57	376,53
50 µm	381,23	380,97	380,69
Humid Air	381,33	381,33	381,33

7.1.4 Pressure and temperature ratio

The effect of wet compression on the pressure and temperature can be described in a clear way employing the ratio between inlet and outlet values. The inlet conditions do not change significantly, however a non-dimensional parameter can highlight in a better way the difference between the various investigated conditions.
The pressure ratio values are shown in Table 7.5.

Table 7.5. *Pressure ratio for wet cases and humid air compression.*

Diameter	Injection rate		
	0.4%	1.4%	2.4%
5 µm	2,23	2,30	2,36
10 µm	2,21	2,26	2,30
20 µm	2,21	2,24	2,27
50 µm	2,21	2,23	2,25
Humid Air	2,20	2,20	2,20

It can be easily seen that the lower injection rate has almost no effect on the ratio, with a small change only in the 5 micrometre case. Higher amount of water increase the pressure ratio, and stronger effect occurs with smaller diameters, as already explained in section 7.1.1.

Considering the temperature ratio, this behaviour is even more evident, as the 50 and 20-micrometre cases do not show any change, while smaller droplets sizes and higher injection rates can lead to a decrease up to 9% (2.4% injection rate, 5 µm diameter).
Table 7.6 provides the values obtained for an easier comparison. The ratio is calculated using temperature vales in Kelvin.

Table 7.6. *Temperature ratio for wet cases and humid air compression.*

Diameter	Injection rate		
	0.4%	1.4%	2.4%
5 µm	1,24	1,18	1,15
10 µm	1,25	1,23	1,21
20 µm	1,26	1,25	1,25
50 µm	1,26	1,26	1,26
Humid Air	1,26	1,26	1,26

7.1.5 Power consumption

The main aim of wet compression process is to reduce the compressor power consumption, by means of lowering the temperature rise through the stage. The effect of water injection is described in the present and next section, in order to give a thorough analysis about the machine behaviour.

The power consumption in this model shows an unexpected behaviour, which apparently does not follow the trend seen in the section 7.1.2 and 7.1.3. The obtained results are plotted in Figure 7.6 and Figure 7.7.

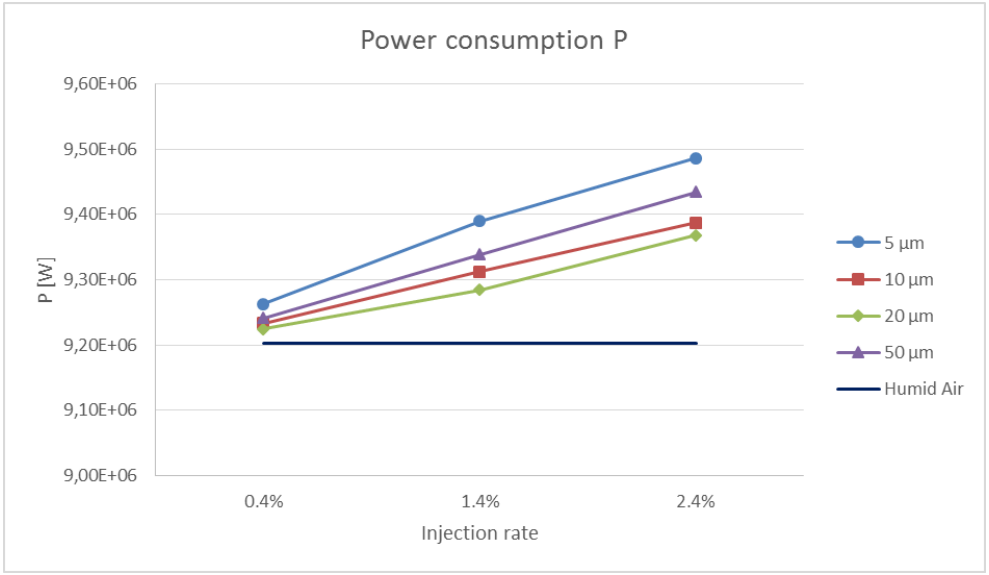

Figure 7.6. *Injection rate influence on the compressor power consumption.*

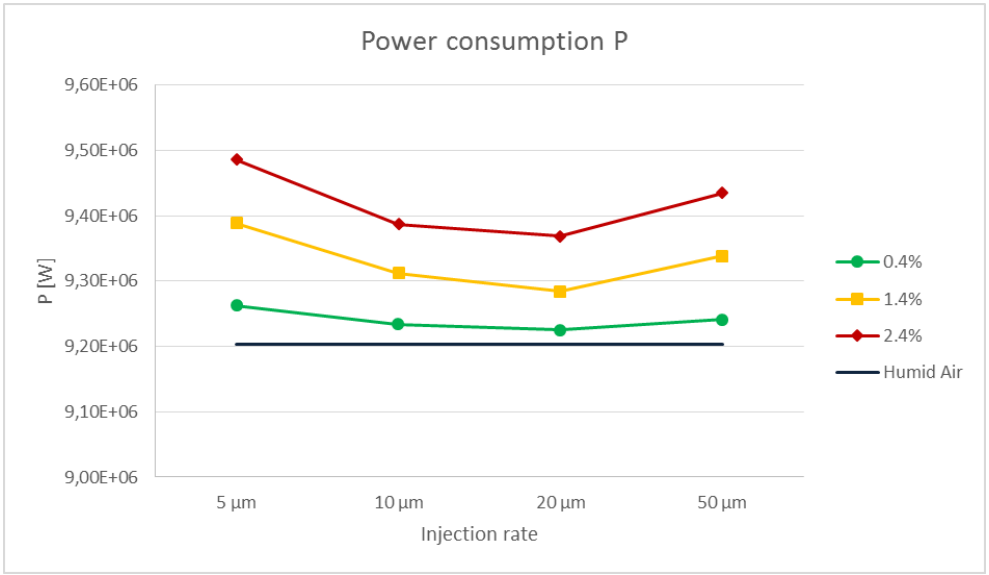

Figure 7.7. *Droplet diameter influence on the compressor power consumption.*

It can be noticed from Figure 7.6 that, in contrast with what could be expected, the power demand of the compressor is increased in all the wet cases compared to the humid air one. Nevertheless, it must be considered that the current boundary conditions allow the pressure at the outlet to vary from case to case; therefore, different "performances" are compared in this diagram.
However, some meaningful observations can be made, while the analysis of the real improvement achieved in the process is discussed in the next section of the chapter.

The diameter size influences the power needed by the compressor in a different way compared to the pressure and the temperature. The smallest diameter droplets generate a higher power demand, while the 10- and 20-micrometre droplets lead to a lower value of the power required. The biggest diameter, i.e. 50 μm, shows a higher power demand than the 10 and 20 micrometre case, and at the same time a lower consumption compared to the 5 micrometre case.
This behaviour can be analysed taking into account the amount of evaporated water, and the additional drag that the particles cause passing through the domain.
The evaporation inside the impeller adds water vapour to the flow, therefore a higher mass fraction of vapour can be found in the mixture; water vapour, whose density is lower than the dry air one, increases the volume of the compressed fluid and a higher power is required to compress it.
On the other hand, the beneficial effect of evaporation must be taken into account: as the temperature is lowered, the density of the mixture is increased, and the process comes closer to an isothermal process, although the temperature rise still occurs inside the machine.
Therefore, these two aspects combine and the overall effect will prove to be beneficial to the process.

At the same time, while evaporation takes place, the particles are accelerated and carried through the stage by the gas-phase.
The presence of the particles, in turn, affects the flow in a way that depends on their size, as smaller particles can follow the flow more easily, while bigger particles, due to their mass and inertia, follow different paths and cause additional friction in the flow. Therefore, additional losses are generated, and more power is required.

Then, the particle size influence on the power consumption can be described starting from the previous statements. To investigate more in detail the influence of the density on the specific work of the compressor, the volumetric flow rate and the pressure variation through the stage are taken into account.

The compressor specific work is defined as:

$$w = \int_{in}^{out} v\, dp \qquad (25)$$

The power of the compressor can be expressed as proportionally consistent with the product of the mass flow rate, the specific work and the inverse of the efficiency, on the assumption of a constant mass flow rate:

$$P \sim \dot{m} \cdot \frac{1}{\eta} \cdot w \qquad (26)$$

In the present case, the gas-phase mass flow rate changes as long as evaporation occurs, therefore a different relation can be written, introducing the expression of the specific work previously described:

$$P \sim \frac{1}{\eta} \int_{in}^{out} \dot{m}\, v\, dp \sim \frac{1}{\eta} \int_{in}^{out} \dot{V}\, dp \qquad (27)$$

From this, the volumetric flow rate and the pressure values through the stage have been collected and plotted for each droplet diameter in a $p - \dot{V}$ diagram, and the area under the curve, which represents the integral shown above, is calculated.

Figure 7.8 shows the curves obtained in the pressure-volumetric flow rate diagram, while the area values are shown in Figure 7.9. The data refer to the 1.4% injection rate case.

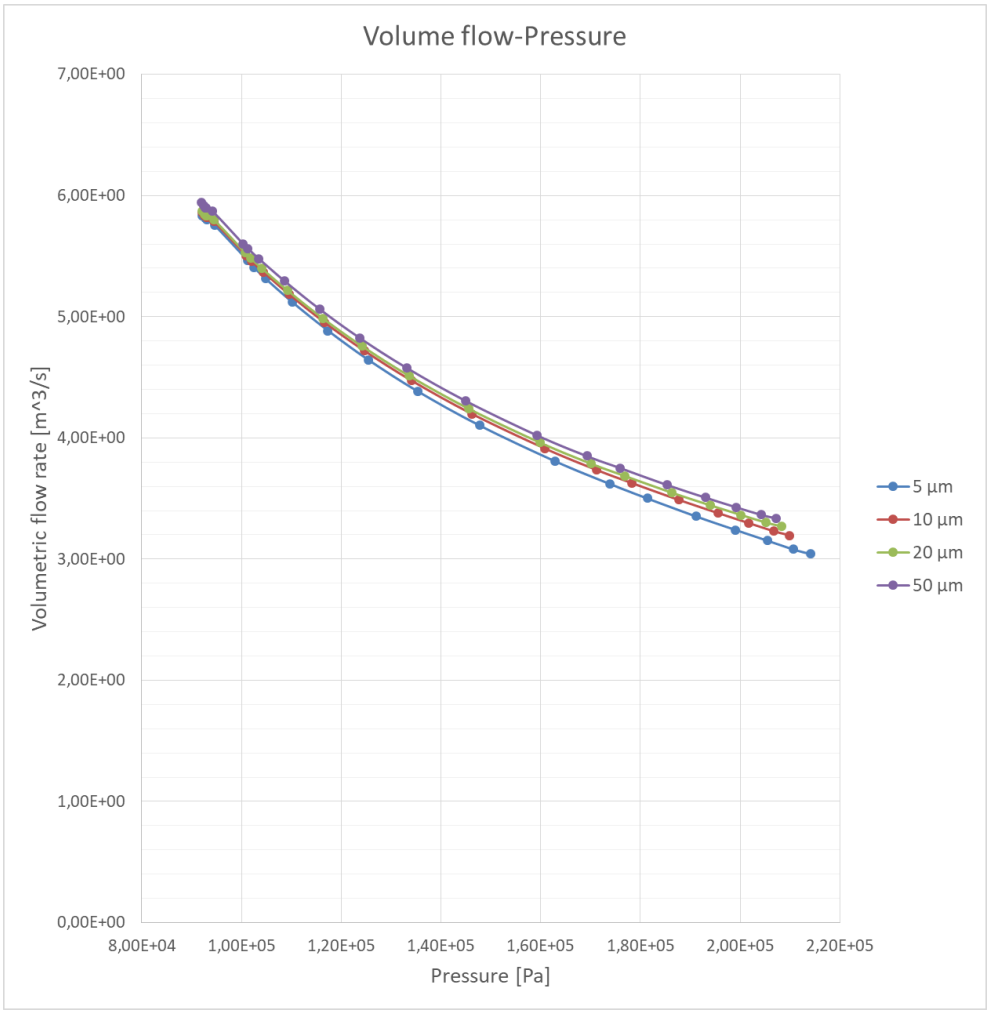

Figure 7.8. *Compression curves in volume flow – pressure diagram.*

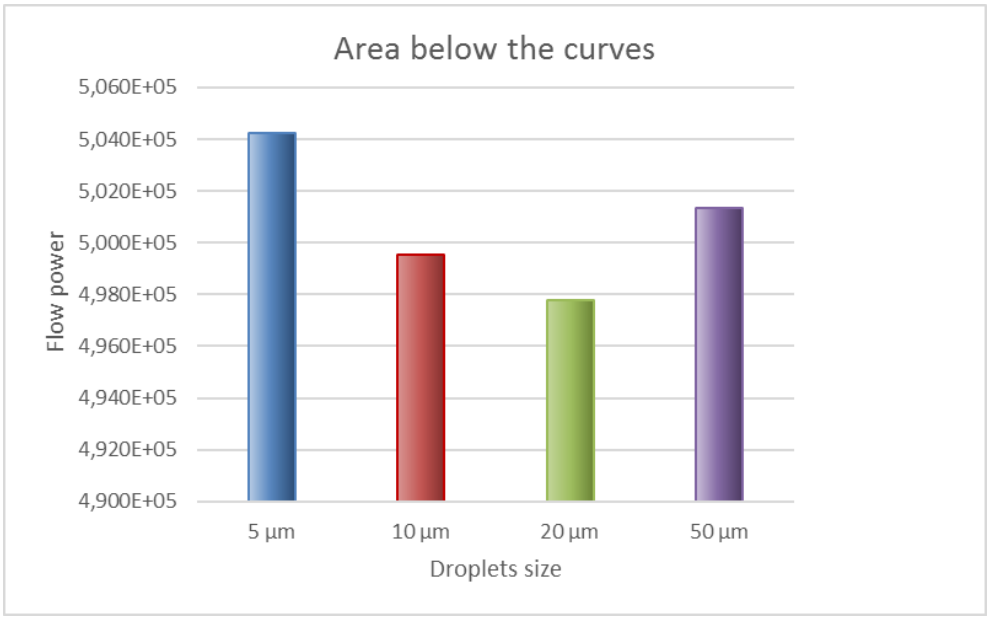

Figure 7.9. *Droplet diameter influence on power*

The results obtained in Figure 7.9 are in accordance with the behaviour observed in the power consumption diagram. A lower value in the 20 and 10-micrometre cases is shown, while the 5-micrometre droplets give the highest demand. The 50-micrometre case is characterized by a value that lies between the 10-micrometre and 5-micrometre case, which may seem incongruous; several aspects must be considered to give deeper understanding of this behaviour.

The first aspect to analyse is related to the boundary conditions of the model, where the mass flow rate at the outlet of the whole domain is set and takes into account only the gas-phase. This means that, if more evaporation occurs in the machine, more water vapour is generated and less air is introduced at the inlet, to comply with the outlet boundary conditions. Therefore, as in the 50-micrometre case almost no evaporation happens (less than 1% of water is evaporated in the considered case in Figure 7.8 and 7.9) a greater amount of air in introduced in the domain, as it can be seen from Table 7.7, which compares the inlet mass flow rate in the 10, 20 and 50 µm cases.

Table 7.7. *Droplet diameter influence on the inlet mass flow rate.*

Diameter [µm]	Inlet Mass Flow Rate [kg/s]
5	6.1853
10	6.1854
20	6.1904
50	6.2530

It is evident that, comparing these values to the amount of water evaporated shown in Table 7.1 and 7.2, the inlet mass flow rate increases as the evaporation becomes smaller. At the same time, it can be noticed how the 5, 10 and 20 micrometre cases are characterized by similar values, and the influence of this mass flow rate change phenomenon on the power is negligible.

The second point concerns the pressure value obtained at the impeller outlet and the thermodynamic variables that determine its value; this analysis allows to give an explanation for the higher power demand in the 5 micrometre case compared to the 10 and 20 ones.
As water droplets evaporation occur, the temperature rise in the compressor is reduced, and so is the outlet temperature. This leads to a lower local speed of sound; hence, the Mach number at the outlet is increased and the effect of this increase consists in a variation of the pressure value, as a higher Mach number value entails a higher pressure.

Therefore, due to different percentage of evaporated water in the four cases, the temperature at the outlet changes case by case and therefore the Mach number varies too. This leads to a comparison between different conditions, which at first sight do not allow to get a clear understanding about the power reduction (or increase) obtained with wet compression, as the compared simulations refer to different Mach conditions.

Then, further investigation about the Mach number influence on the pressure is carried out, starting from one case of the previously described above. It is worth to remind that the compressor rotational speed is kept constant in the present work.
Therefore, to obtain a Mach number at the outlet close to the one observed in the dry case, the rotating speed is changed. The chosen value depends on the condition that occur at the impeller outlet in the case considered. As evaporation effect is stronger using 5 micrometre droplets, this diameter size and 1.4% injection rate are chosen.
The chosen value for the rotating speed is 5285 rpm, which means nearly 97% of the original one.
The choice is made considering the ratio between the local speed of sound at the impeller outlet in the humid air (no water injection) and in the 5-micrometre cases, and multiplying this value for the 5450 rpm speed.
The results show a lower Mach number at the impeller outlet, with a value closer to the humid air case one, and a strong effect on the pressure.
Figure 7.10 shows in a clear way the effect of evaporation on the Mach number and therefore on the pressure, comparing the humid air and the 5 micrometre-original speed cases.
Moreover, the modified rotating speed decreases the Mach number at the outlet, generating a strong pressure reduction, reaching a slightly lower value than in the dry case one.

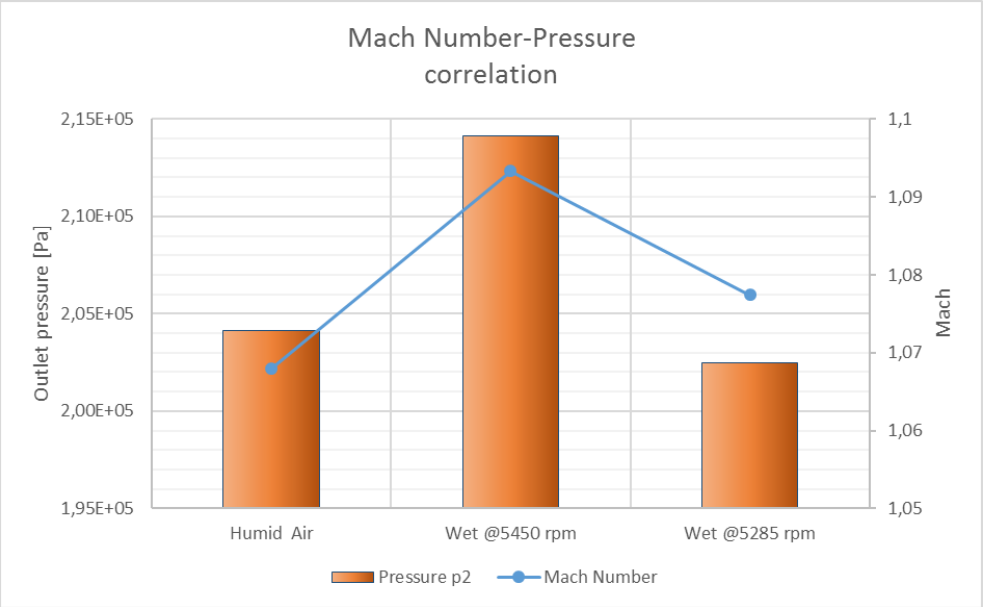

Figure 7.10. *Pressure - Mach number correlation.*

This different set up allows to give some statement about the power required by the compressor comparing similar Mach number conditions.

Table 7.8. *Power consumption and rotating speed.*

Case	Rotational speed	Power [MW]
Humid air	5450 rpm	9.203
Wet compression, 5 µm	5450 rpm	9.389
Wet compression, 5 µm	5285 rpm	8.683

It is worth to remind that the power is calculated multiplying the torque on the blade, the number of blades and the angular velocity; therefore, the power depends on the rotational speed. Bearing in mind this fact, the comparison between the values in Table 7.10 needs some more comments about, as the second and third case refer to different rotational speed.

The power required by the compressor rotating at 5285 rpm shows a reduction, compared to the humid air case, equal to 5.65%. This value has to be considered taking into account that the reduction of the rotational speed, which is nearly -3%, causes an intrinsic decrease of the same quantity.
Nevertheless, the general reduction of the power consumption is bigger than the effect introduced by the new adopted rotating speed. Beneficial effects of water injection are therefore proven, and the present analysis shows further development of this topic, performing simulations with similar outlet conditions - and therefore comparable

between each other - to achieve improved understanding about the influence of various parameters on the performance of the machine.

7.1.6 Isothermal efficiency and polytropic index

The analysis on the compressor performance is supplemented by two more parameters, the isothermal efficiency and the polytropic index. Both of them provide further information about the thermodynamic process and the cooling effect obtained with water injection, taking as a reference the ideal isothermal process and comparing the several cases to the dry one.

The choice of these parameters derives from the fact that the use of the polytropic efficiency is not suitable, as the cooling effect provided by the evaporation overcomes the definition of the efficiency itself: the isentropic work of wet compression is less or equal to the isentropic work of dry air compression, which means that the equivalent adiabatic efficiency value will be above 1.0 [4].

7.1.6.1 Isothermal efficiency

The isothermal efficiency is calculated from the ratio of the specific work in isothermal conditions and the specific work obtained by the simulations; as described in Chapter 3.3.2, its value depends on the temperature at the inlet and on the pressure values at the inlet and at the outlet of the impeller.

This allows to evaluate in a clear way the effect of water injection on the process, as both pressure and temperature are shown to be affected by evaporation, and it makes possible to compare different conditions and simulations.

The calculated values are shown in Table 7.9.

Table 7.9. *Isothermal efficiency for wet cases and humid air compression.*

Diameter	Injection rate		
	0.4%	1.4%	2.4%
5 µm	71,35%	73,00%	74,14%
10 µm	70,75%	71,35%	71,92%
20 µm	70,54%	70,67%	70,82%
50 µm	70,48%	70,56%	70,54%
Humid Air	70,50%	70,50%	70,50%

The analysis can be conducted taking into consideration first of all the value obtained for the dry case, equal to 70.5%: this means that the specific work of the compressor in an isothermal process would be 30% smaller compared to the one obtained from the

model. In other words, the obtained value of the specific work is nearly 42% higher than the isothermal one, as results from the inverse of the efficiency.
The comparison between the dry and the 50 and 20 micrometre cases shows almost no improvement in the process, mainly because almost no evaporation occurs in the 50 µm case and only a small amount of water is evaporated in the 20 µm one.
Taking into account the 10 micrometre case, the evaporation effect starts to show some improvement, especially with the 1.4 and 2.4% injection rate; in the latter case the efficiency is increased of 1.42%, which means that the specific work is slightly decreased (~2%).
The higher improvement is achieved in the 5 µm case, where an absolute increase of efficiency up to 2.64% is obtained. The 74.14% efficiency value corresponds to a ratio between the real and the isothermal specific work equal to 1.349.
Comparing this value with the dry one (1.418), this means that a 4.9% reduction of the compressor work is obtained, as shown by the following expression:

$$\Delta w = \frac{\frac{1}{\eta_{iso(5\ \mu m)}} - \frac{1}{\eta_{iso(dry)}}}{\frac{1}{\eta_{iso(dry)}}} = -0.0491$$

The effect of the injection rate and droplets size is shown in the diagram in Figure 7.11 and Figure 7.12: the increase of efficiency is clear, as the diameter decreases and the injection rate is increased.

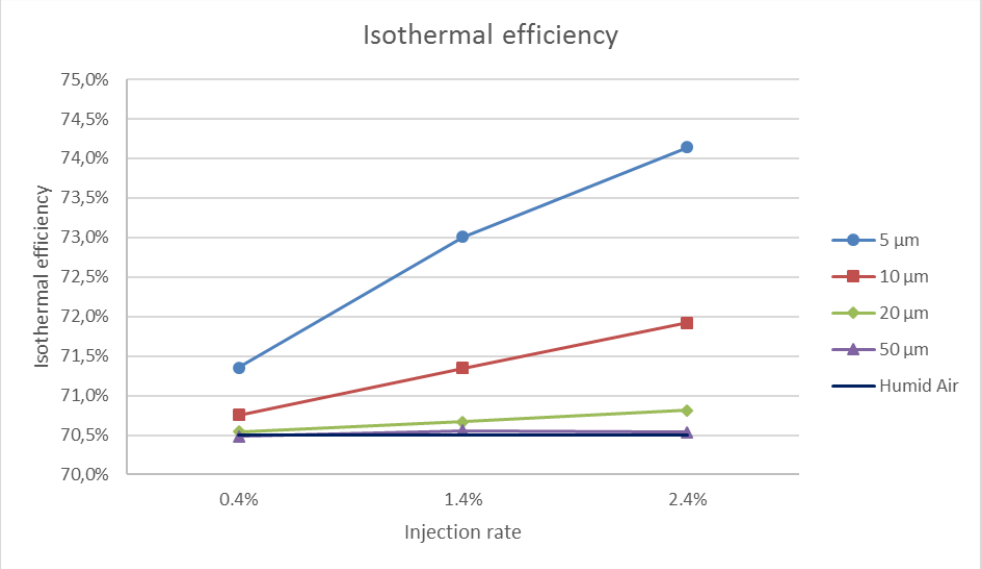

Figure 7.11. *Injection rate influence on the isothermal efficiency.*

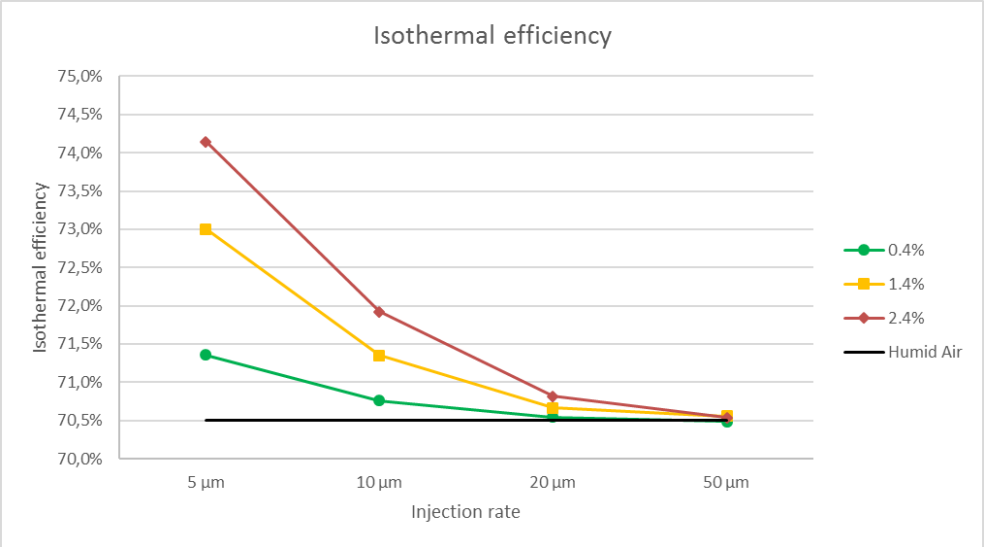

Figure 7.12. *Droplet diameter influence on the isothermal efficiency.*

The efficiency value depends strongly on the amount of evaporated water, which affects the temperature at the outlet and the pressure, from what has been previously discussed.

The correlation is shown in Figure 7.13, where the efficiency is plotted as a function of the evaporated water mass flow rate. The data plotted show a linear trend, as they are distributed along the red dashed straight line.

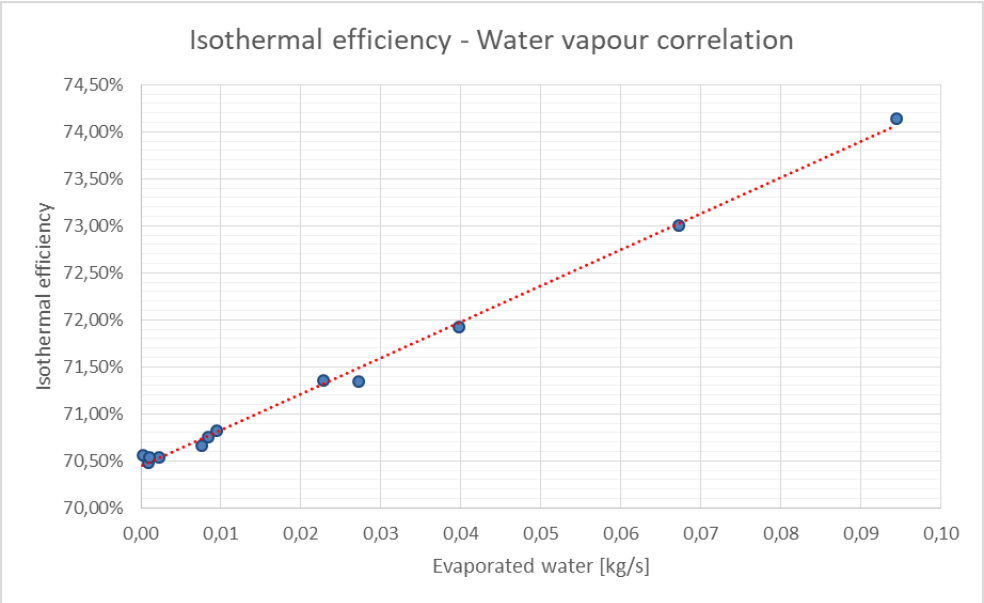

Figure 7.13. *Isothermal efficiency and water vapour correlation.*

This analysis allows to give a statement about the reduction of power obtained with water injection, and encompasses the pressure, temperature and power consumption trends outlined in the previous sections.

7.1.6.2 Polytropic index

The polytropic index is used in the analysis of the machine performance in a similar way as the isothermal efficiency. As pointed out by Zheng et al. [4], the use of the polytropic efficiency in a wet compression process can lead to anomalous findings, such as values above 1, which do not have a real meaning, considering the standard use of this parameter. Then, isothermal efficiency was introduced as a meaningful way to evaluate the beneficial effect of water injection.

The polytropic index is employed here as a complementary parameter to analyse the cooling effect provided by the evaporation of droplets, as in an isothermal process its value is equal to 1.

Once more, the value calculated in the humid air case is taken as a reference for all the cases, as without any cooling effect its value, equal to 1.423, is the highest observed.

The calculated values are shown in Figure 7.14 and Figure 7.15.

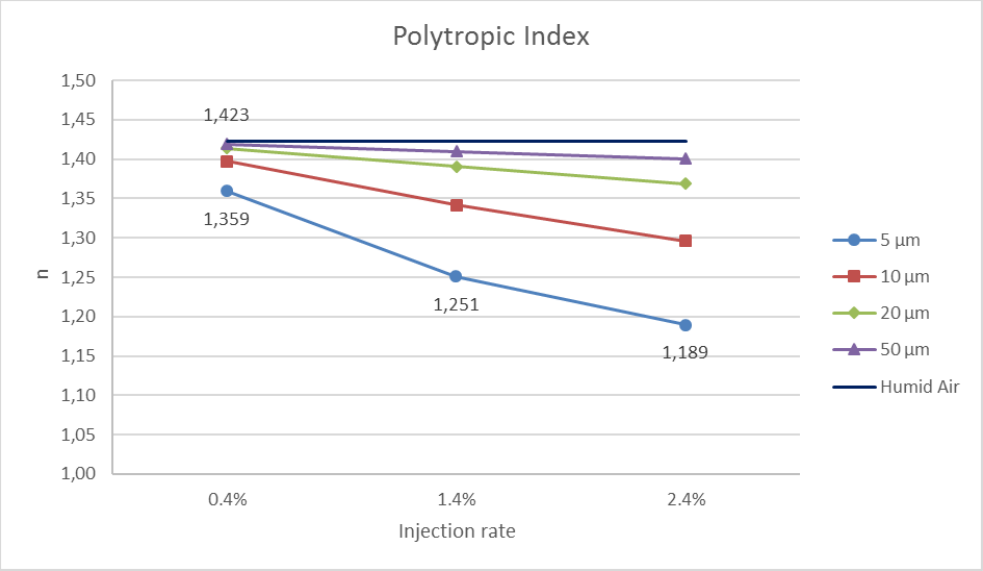

Figure 7.14. *Injection rate influence on the polytropic index.*

Figure 7.14 shows a similar trend to what has been observed analysing the outlet temperature variation. The decrease of the polytropic index is bigger when smaller droplets and higher amount of injected water are used, as they provide more mass evaporation and therefore a better cooling effect. At the same time more water vapour increases the pressure at the outlet of the impeller. Hence, the evaporation effect consists in a decrease of the temperature ratio and an increase of the pressure ratio;

these are the parameters that influence the polytropic index, as shown in Chapter 3.3.3. In fact, both variations of these ratios contribute in the same way to decrease the index analysed.

$$n = \frac{ln\frac{p_2}{p_1}}{ln\frac{p_2}{p_1} - ln\frac{T_2}{T_1}} \qquad (28)$$

The same data lines are plotted in Figure 7.15 according to the injection rate, and show in a similar way the stronger reduction effect in the 5 and 10 µm cases, with an increased amount of water injected in the machine.

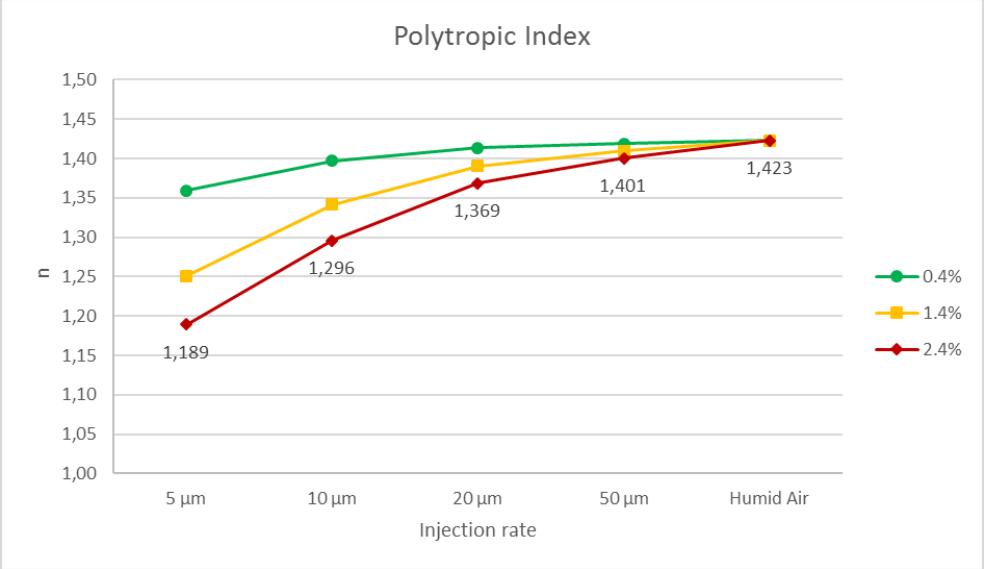

Figure 7.15. *Droplet diameter influence on the polytropic index.*

In the same way as shown in Figure 7.13 with the isothermal efficiency, it is interesting to plot the values of the polytropic index to highlight the correlation with the amount of evaporated water in the process. The points in Figure 7.16 seem to follow approximately a linear trend, as observed in the isothermal efficiency diagram.

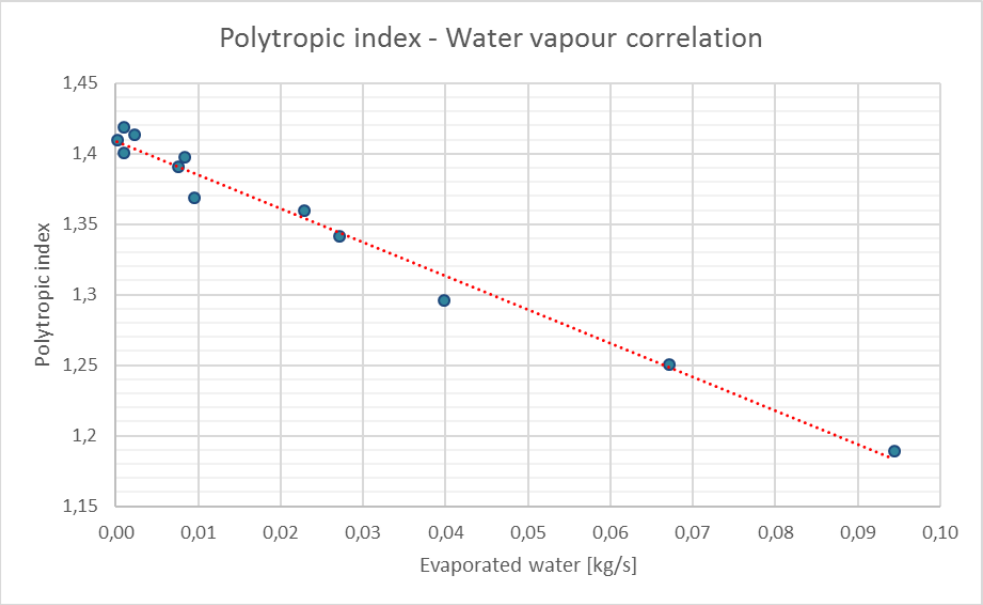

Figure 7.16. *Polytropic index and water vapour correlation.*

7.2 Nozzle droplets distribution

After discussing the effects of monodiameter droplets injection, it is interesting to analyse the behaviour of the machine comparing the previous trends with the one observed using the nozzle particle distribution described in section 4.4.6. The same parameters are used to evaluate the effect of the discrete diameter distribution. The results are shown using BETE as a designation, from the company's name of the nozzle taken as study case.

7.2.1 Evaporated water

The first aspect to be analysed is the amount of evaporated water inside the impeller. It is relevant, even more than in the cases previously described, to investigate the reason of the overall effect observed.

The use of a discrete particle size distribution leads to a combination of the effects of smaller and bigger particles, whose behaviour is different as shown in the previous investigation. It is important to keep in mind that the droplets size distribution ranges between 0 and 11 μm. Hence, the results of the nozzle simulation are always compared with the 5 and 10 μm cases, taken as a reference.

The data about the mass of evaporated water show that the nozzle distribution has a behaviour similar to the 5 μm case. As it can be seen in Table 7.10, the evaporated mass values lie between the 5 and 10 μm ones; however, the values are quite close to the 5 μm ones.

Table 7.10. *Evaporated water [kg/s], comparison between nozzle and monodiameter cases.*

Diameter	Injection rate		
	0.4%	**1.4%**	**2.4%**
5 µm	0,0228	0,0672	0,0944
10 µm	0,0084	0,0272	0,0398
20 µm	0,0023	0,0076	0,0095
50 µm	0,0009	0,0002	0,0010
BETE	0,0194	0,0604	0,0896

A better view is given in Figure 7.17 and Figure 7.18, where the nozzle results are plotted and can be easily compared with the monodiameter cases.

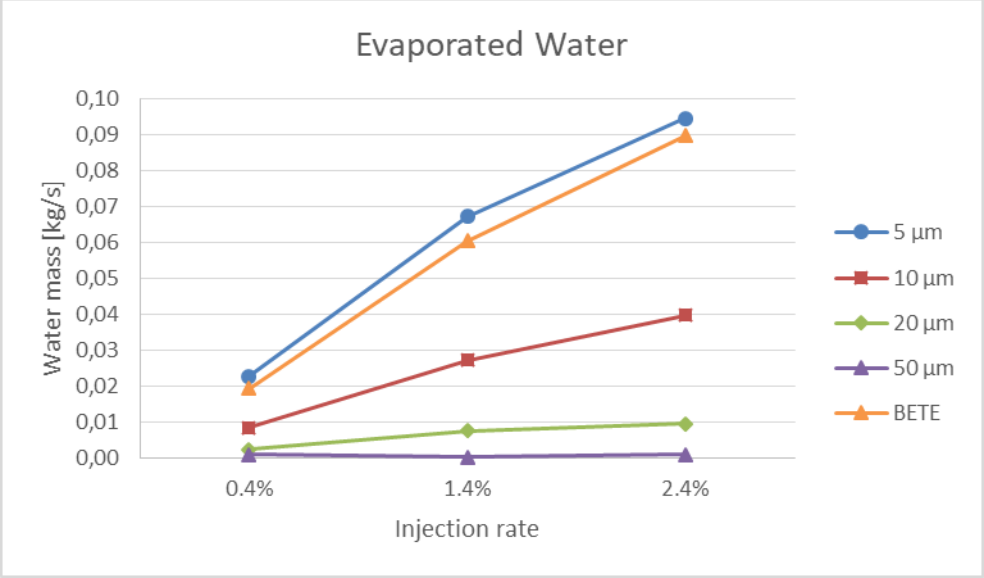

Figure 7.17. *Injection rate influence on evaporated water, including the nozzle case.*

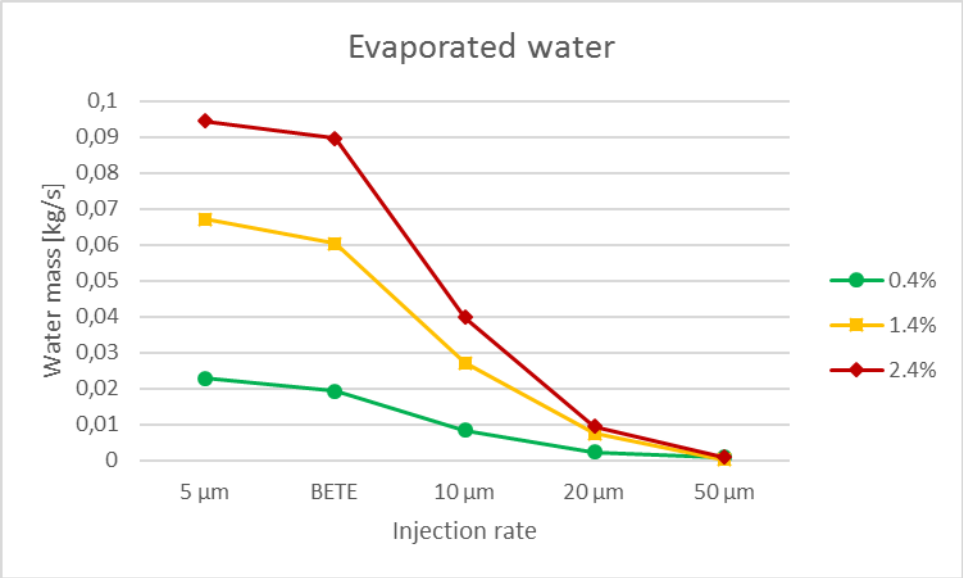

Figure 7.18. *Droplet diameter influence on evaporated water, including the nozzle case.*

In a similar way, the percentage of water evaporated on the whole injected amount shows that the nozzle distribution enhances evaporation, as the medium droplet size is small and a great share of water participates in the phase change. Table 7.11 contains all the data.

Table 7.11. *Share of evaporated water on the total injected amount, nozzle case comparison.*

Diameter	**Injection rate**		
	0.4%	**1.4%**	**2.4%**
5 µm	90,88%	76,51%	62,71%
10 µm	33,59%	30,93%	26,41%
20 µm	9,28%	8,62%	6,32%
50 µm	3,75%	0,24%	0,67%
BETE	77,25%	68,79%	59,52%

The nozzle values are lower than the 5 µm ones, but still closer than the 10 µm ones; this means that the effect of smaller particles prevails, but at the same time the relatively bigger droplets, whose evaporation is more difficult because of their lower surface-volume ratio, have an impact on the overall effect. It can be observed, keeping in mind the mass distribution in Figure 4.11 that the bigger particles, whose number is quite small, give an important contribution in terms of mass.

The influence of the injection rate can also be observed: a higher quantity of injected water determines a lower evaporation percentage, but at the same time the difference between 5 µm and BETE case decreases. Considering that only the smaller droplets

participate completely in the evaporation process, while bigger ones give only a small contribution, the decrease may be due to the fact that with more water injection, a higher amount of water makes evaporation more difficult, therefore middle-size particles (5-7 μm) participate less efficiently in the phase change. Thus, the overall effect becomes closer to the 5 micrometre one.
The trends are plotted in Figure 7.19.

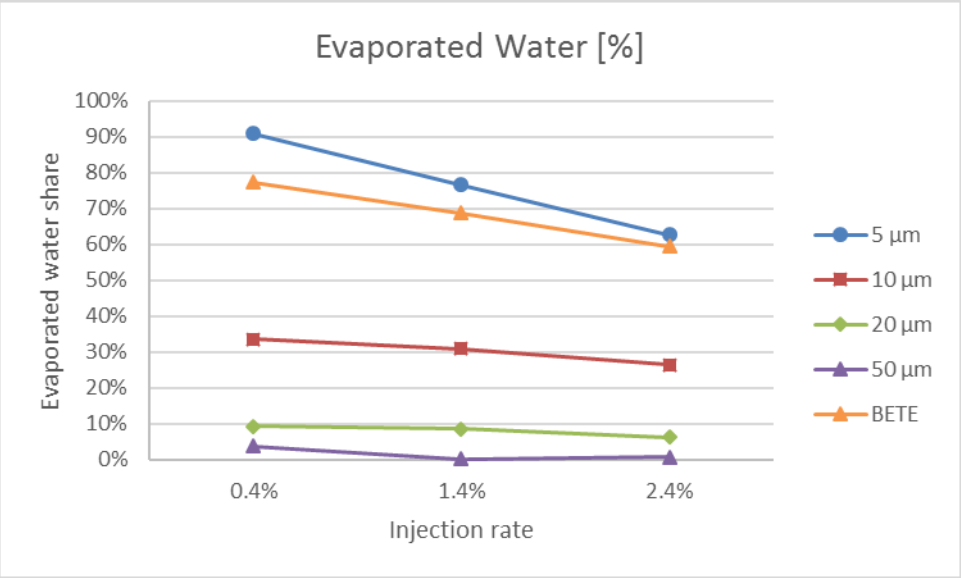

Figure 7.19. *Diameter and injection rate influence on evaporated water share, including the nozzle case.*

7.2.2 Outlet pressure

The evaporation of droplets inside the machine has an effect, with the present set up, on the outlet pressure. As seen before, a smaller droplet size leads to a stronger influence, increasing the pressure after the impeller. The trend is confirmed also in the nozzle distribution case, where as shown by Table 7.12, the values look very close to the 5 μm ones.

Table 7.12. *Outlet pressure [Pa], comparison between nozzle and monodiameter cases.*

Diameter	**Injection rate**		
	0.4%	**1.4%**	**2.4%**
5 μm	2,072E+05	2,141E+05	2,200E+05
10 μm	2,058E+05	2,100E+05	2,143E+05
20 μm	2,053E+05	2,083E+05	2,113E+05
50 μm	2,050E+05	2,072E+05	2,093E+05
BETE	2,073E+05	2,143E+05	2,204E+05

It is worth to notice that the pressure values lie slightly above, probably because of the contribution given by the left side of the droplets spectrum, where particles below 5 µm are found; however, their impact is limited and the overall effect is almost the same observed with 5 µm diameter droplets, as it can be seen in Figure 7.20.

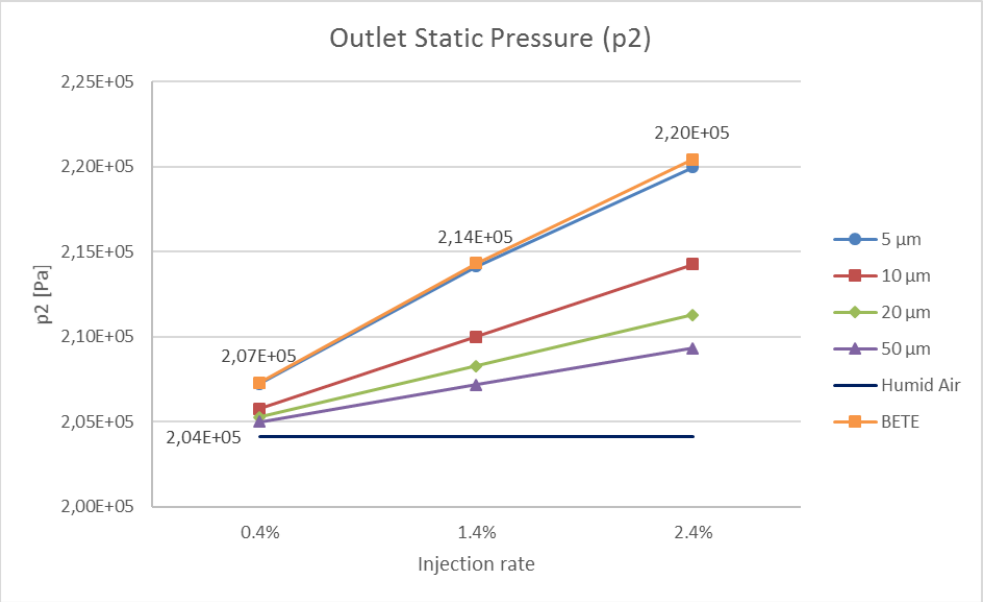

Figure 7.20. *Injection rate and droplet diameter influence on the outlet pressure, including the nozzle case.*

The pressure increase, taking the humid air case as a reference, is around 8% (7.97%) considering the 2.4% injection rate.

7.2.3 Outlet temperature

The effect of water injection on the outlet temperature is closely related to the amount of evaporated water inside the machine. The trend discussed in section 7.1.3 showed this close link and it allows to explain the results obtained using the BETE droplets distribution. Indeed, in section 7.2.1 it has been highlighted that the amount of evaporated water using this distribution is similar to the values observed in the 5 µm case, but lower; this means that a lower cooling effect is present, as less water mass - and latent heat – participate in the process.

The lower cooling effect is evident in Figure 7.21, where the BETE points lie above the 5 µm ones, and therefore the observed outlet temperature is higher.

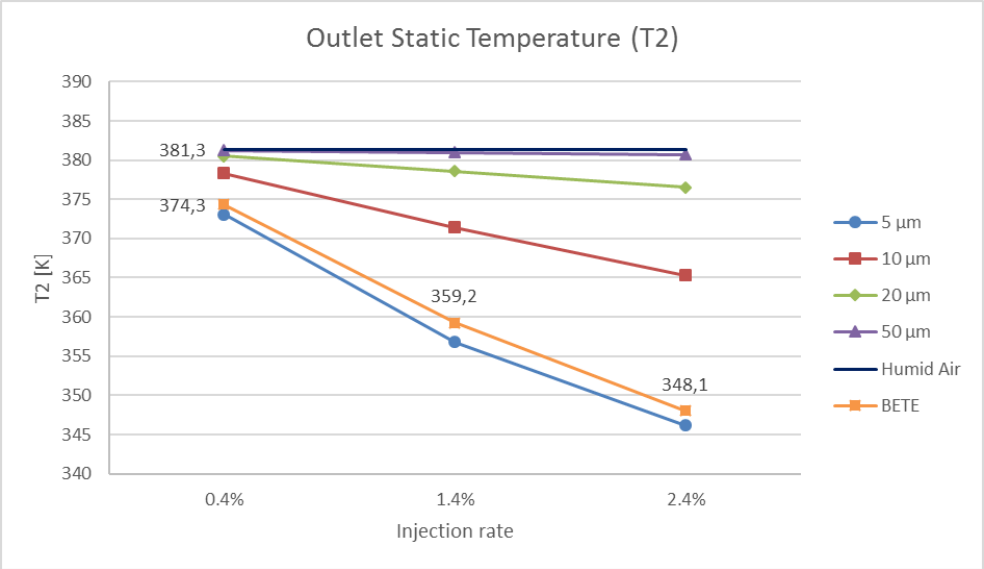

Figure 7.21. *Injection rate and diameter influence on the outlet temperature T_2, including the nozzle case.*

The data labels in the diagram report the values of the current case and the reference value from the humid air simulation. Table 7.13 shows the full set of results.

Table 7.13. *Outlet temperature [K], comparison between nozzle and monodiameter cases.*

Diameter	Injection rate		
	0.4%	1.4%	2.4%
5 µm	373,04	356,70	346,17
10 µm	378,33	371,43	365,28
20 µm	380,54	378,57	376,53
50 µm	381,23	380,97	380,69
BETE	374,30	359,24	348,06

Taking the case with the highest injection rate, the decrease in temperature at the impeller outlet, compared to the humid air calculation, is -8.72%, while in the 5 µm case the variation of T_2 was - 9.22%.

7.2.4 Pressure and temperature ratio

The data presented so far can be also shown, as in section 7.1.4, using a non-dimensional ratio between the inlet and outlet values of pressure and temperature. The values in Table 7.14 and Table 7.15 give a clear idea about how close are the values of the first and last case.

Table 7.14. *Pressure ratio, comparison between nozzle and monodiameter cases.*

Diameter	Injection rate		
	0.4%	**1.4%**	**2.4%**
5 μm	2,23	2,30	2,36
10 μm	2,21	2,26	2,30
20 μm	2,21	2,24	2,27
50 μm	2,21	2,23	2,25
BETE	2,23	2,30	2,36

Table 7.15. *Temperature ratio, comparison between nozzle and monodiameter cases.*

Diameter	Injection rate		
	0.4%	**1.4%**	**2.4%**
5 μm	1,24	1,18	1,15
10 μm	1,25	1,23	1,21
20 μm	1,26	1,25	1,25
50 μm	1,26	1,26	1,26
BETE	1,24	1,19	1,15

The relative variations in terms of pressure and temperature ratio are almost identical to the percentage values already described in the two previous sections.

7.2.5 Power

The power consumption is characterized by a trend that is similar to the pressure one, as the BETE results lie slightly above the 5 micrometre case, with a growing need of power as the injection rate increases. Figure 7.22 gives the full view of the results.

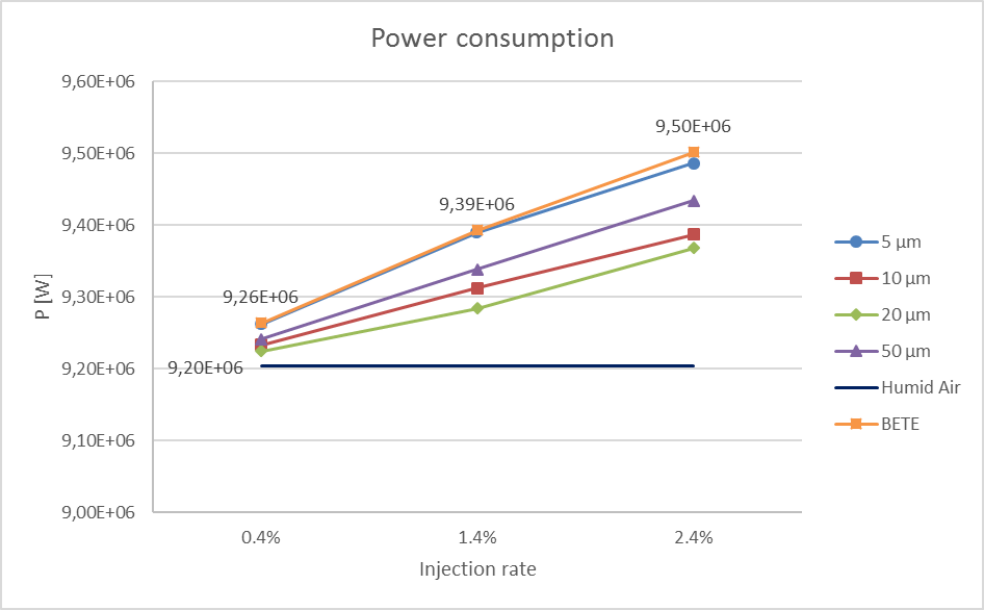

Figure 7.22. *Injection rate and diameter influence on power consumption, including the nozzle case.*

To analyse the behaviour of the nozzle case it is important to keep in mind what has been already said about the model boundary conditions and about their influence on the power variation in different cases: the mass flow rate constraint at the impeller outlet allows the outlet pressure to vary in the different cases, as a consequence of the different amount of water vapour in the flow.
Hence, when the amount of evaporated water is bigger, also the power is increased, but this trend is influenced by the model, as different performances are being compared.

However, some comments about the BETE distribution can be made, first of all about the factors that contribute to the similarity between the 5 µm and nozzle cases.
The first aspect to be checked is the air intake in the two cases, to avoid incompatible comparisons as in the 50 µm case discussed above. The values of the mass flow rate at the inlet are almost the same for the two cases, 6,1853 kg/s in the 5 µm simulation and 6,1850 kg/s in the nozzle one, considering the 1.4% injection rate case. Hence, the two performances are comparable.

The power consumption looks higher in these cases because of the higher evaporation and higher presence of water vapour in the flow; as its density is lower than the dry air

one, the volume of the flow is increased and more power is required to handle it. As both cases have a similar amount of evaporated water, as shown in Table 7.10, the link between power, pressure and water vapour is confirmed.
On the other hand, the cooling effect influences the density and has a strong influence on the Mach number and pressure, as discussed in section 7.1.5.

The reason of the higher power consumption in the nozzle calculation needs to be analysed more in detail. The slightly lower water vapour content in the flow provides a lower cooling effect, and therefore the compressor performance improvement is slightly smaller. But, on the other side, a lower water vapour mass fraction should lower the power consumption, as the volume of the flow is lower and less effort is needed by the compressor to handle the mass flow rate. The overall effect shows an increased power consumption, therefore the first factor prevails.
A better idea about the improvement in the process is given in the next section, where the isothermal efficiency is evaluated.

Table 7.16 contains the values obtained in all the cases investigated.

Table 7.16. *Power consumption [W], comparison between nozzle and monodiameter cases.*

Diameter	Injection rate		
	0.4%	1.4%	2.4%
5 μm	9,263E+06	9,389E+06	9,486E+06
10 μm	9,234E+06	9,312E+06	9,387E+06
20 μm	9,225E+06	9,284E+06	9,368E+06
50 μm	9,241E+06	9,338E+06	9,434E+06
BETE	9,263E+06	9,393E+06	9,501E+06

7.2.6 Isothermal efficiency and polytropic index

The performance improvement can be easily assessed having a look at the efficiency calculated taking as a reference an isothermal process characterized by the same pressure ratio and inlet temperature. In Figure 7.23 the improvement in the process is clear, and also its magnitude: water injection using the BETE distribution allows to achieve an increase in efficiency similar to the 5 μm one.

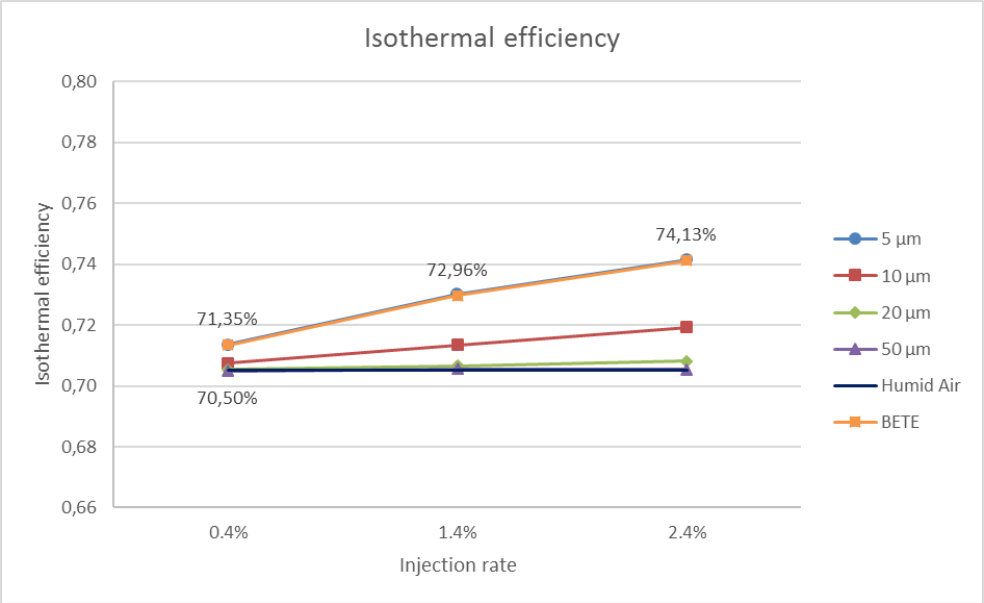

Figure 7.23. *Injection rate and diameter influence on the isothermal efficiency, including the nozzle case.*

The values shown in the data labels in Figure 7.23 are also reported in Table 7.17.
The efficiency values obtained without water injection is 70.5%.
Only a small difference is shown between the BETE and 5 micrometre case, related to the slightly different amount of evaporated water.

Table 7.17. *Isothermal efficiency, comparison between nozzle and monodiameter cases.*

Diameter	Injection rate		
	0.4%	1.4%	2.4%
5 µm	71,35%	73,00%	74,14%
10 µm	70,75%	71,35%	71,92%
20 µm	70,54%	70,67%	70,82%
50 µm	70,48%	70,56%	70,54%
BETE	71,35%	72,96%	74,13%

The reduction of the work of the compressor is almost identical to the one calculated for the 5 micrometre simulation, around 4.9% with the highest injection rate. This value can be considered in accordance with Abdelwahab‘s investigation [13] using a numerical method based on both droplet evaporation and compressor mean-line calculations, where injection ratios up to 3% led to a reduction of the compressor work up to 5%.
The calculated values for the three different injection rates are shown in Table 7.18.

Table 7.18. *Reduction of compressor work, depending on the injection rate.*

	Injection rate		
	0.4%	**1.4%**	**2.4%**
Work reduction [%]	-1,191	-3,371	-4,897

The polytropic index shows a trend similar to the one that characterizes the outlet temperature values, with a significant reduction in the simulations where smaller droplets and higher injection rates are employed.

As it can be seen in Figure 7.24, the nozzle distribution values are located just above the 5 micrometre case ones, therefore the performance not as good as in that case, but the values are quite close, as shown in Table 7.19.

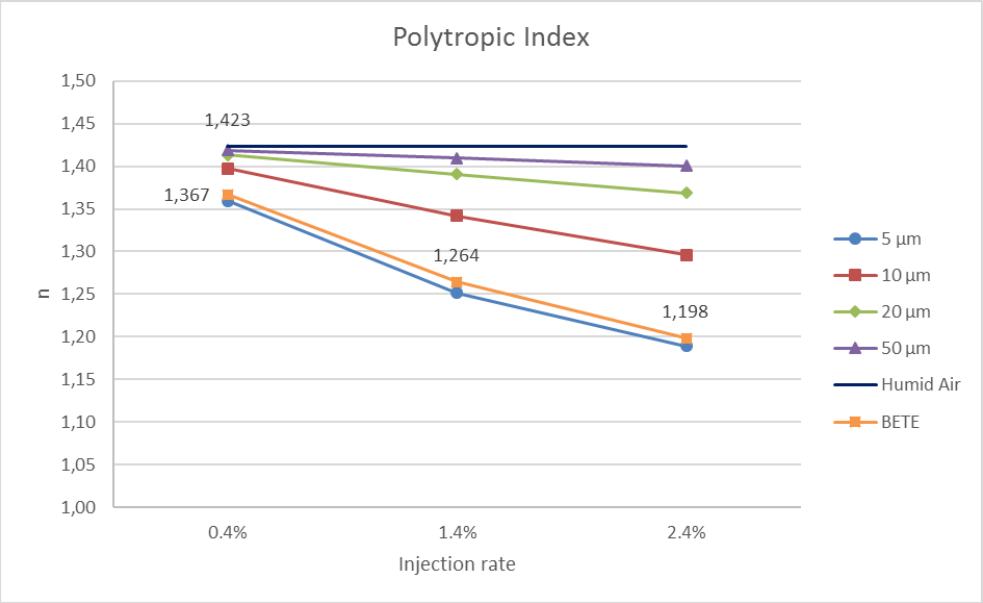

Figure 7.24. *Injection rate and diameter influence on the polytropic index, including the nozzle case.*

The reason of this trend lies in the outlet pressure and temperature values obtained in the simulations: on one side the pressure is almost identical in both the 5 micrometre and BETE cases, on the other side the temperature values are different, as shown in section 7.2.3. Thus, the temperature effect prevails on the pressure, and the resulting polytropic index value follows the temperature trend.

Table 7.19. *Polytropic index, comparison between nozzle and monodiameter cases*.

Diameter	Injection rate		
	0.4%	1.4%	2.4%
5 μm	1,359	1,251	1,189
10 μm	1,397	1,342	1,296
20 μm	1,414	1,391	1,369
50 μm	1,419	1,410	1,401
BETE	1,367	1,264	1,198

7.3 Through the impeller analysis

The scope of the investigation consists not only in the evaluation of the improvement in terms of machine performance, but it also aims at giving more knowledge about the process inside the impeller. Water evaporation, of course, is the main focus of the following analysis.

The 10 μm and BETE distributions, using 1.4% injection rate, are taken as representative cases.

7.3.1 Analysis method

In this section of the investigation the parameters described are analysed through the stage, using mean values calculated in different positions inside the rotating R1 domain. The described parameters are calculated using a Mass Flow Average function. A set of surfaces is implemented through the stage considering the locus of points located in a specified streamwise position. In other words, all the points that form the surface share the same distance from the outlet and the inlet, along the streamwise direction.

The surfaces are implemented using the variable available in CFX-Post, Streamwise Location, whose value is varied from 0 to 1 across the impeller with a step equal to 0.05 in order to obtain 24 consecutive surfaces. Each surface is identified by a number, in the range 00-100. Figure 7.25 gives a clear view of the set of surfaces used.

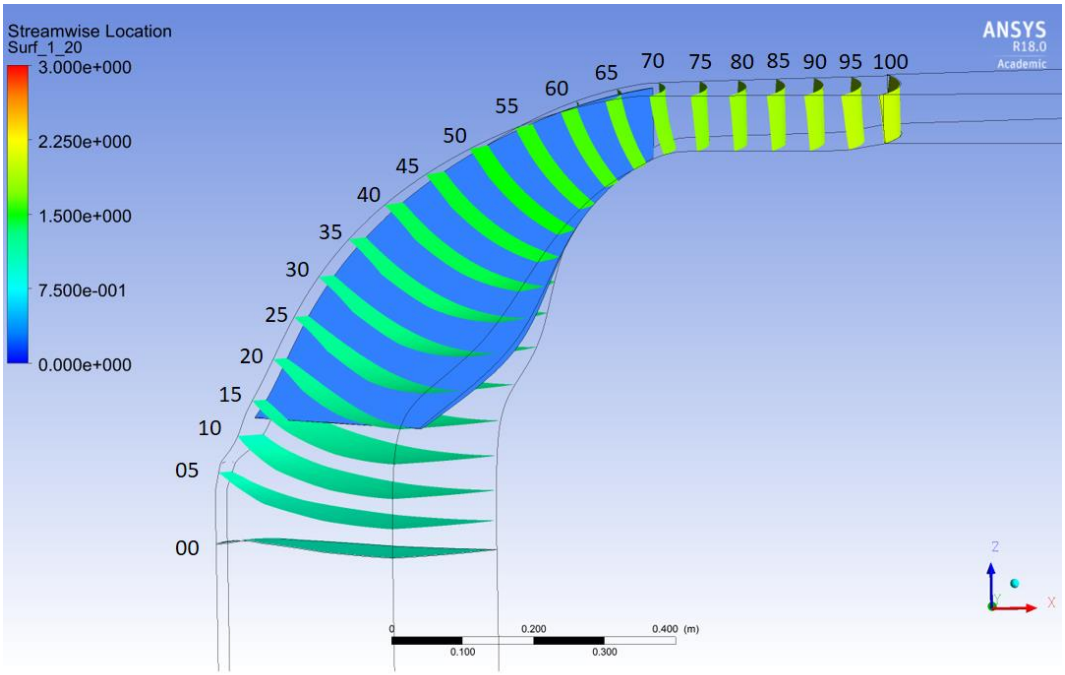

Figure 7.25. *Impeller analysis, surfaces set.*

It is relevant to comment some meaningful surfaces that have a key position in the analysis. Besides the 00 and 100 surfaces, which represent inlet and outlet of the domain, the surfaces No. 15 and 20 share part of the leading edge, while the trailing edge is located in proximity of surface No. 65 and 70.
These surfaces will be useful to understand which positions are related to the impeller and which ones correspond to the upstream and downstream parts of the domain.

7.3.2 Mean droplet diameter

The most interesting parameter to be analysed through the impeller is the droplet diameter. Its change along the streamwise direction is meaningful to describe how the evaporation takes place. The Sauter mean diameter has been chosen to describe the size of the different particles with a representative parameter, and asses the changes that occur inside the machine. This parameter is strictly related to evaporation and to the vapour mass fraction.

Two different particle distributions, the 10 μm monodiameter one and the nozzle distribution, are considered to illustrate in a thorough way the behaviour of the droplets.
Keeping in mind the meaning of the surfaces No. 15-20 and n. 65-70, the diameter change can be seen in Figure 7.26 and 7.27 for both distributions.

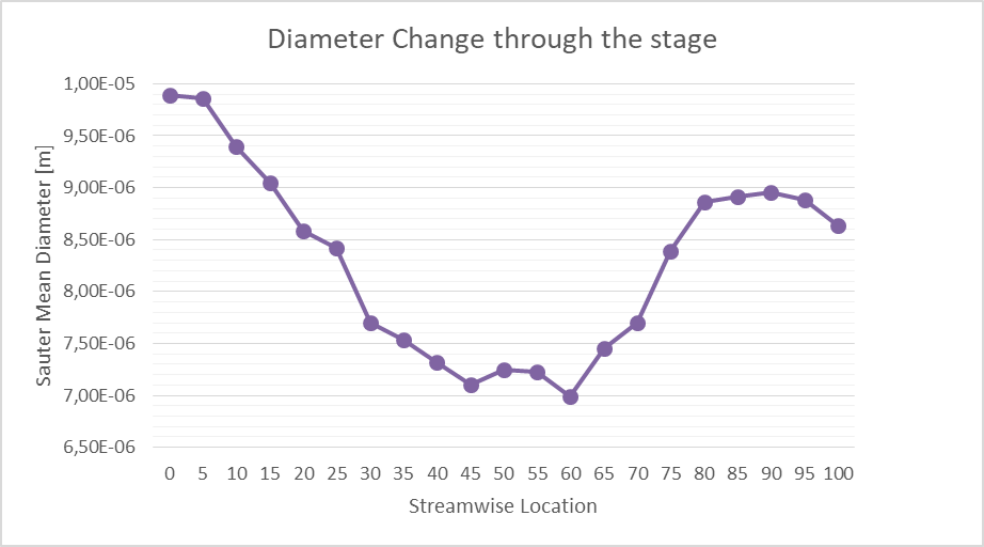

Figure 7.26. *Sauter Mean Diameter change considering the 10 µm uniform droplet distribution.*

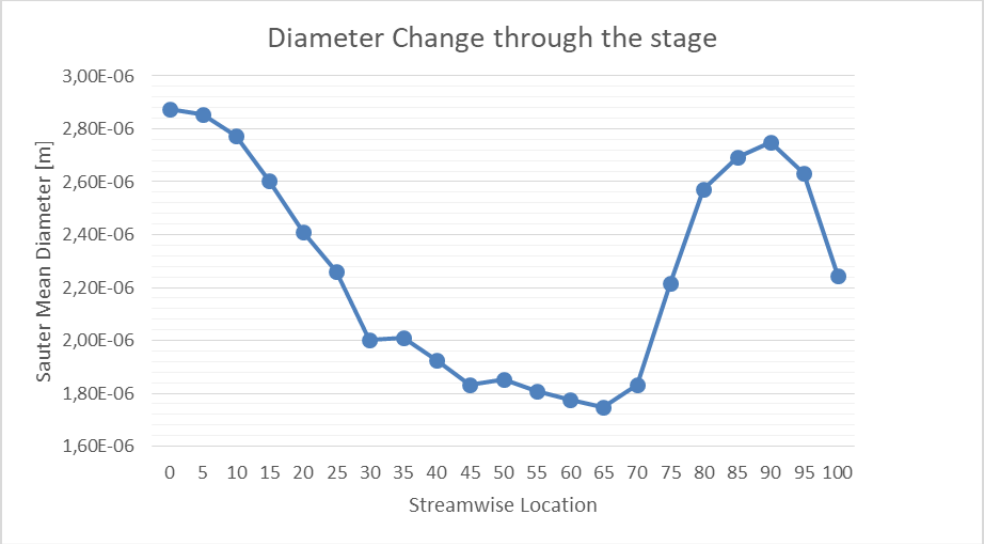

Figure 7.27. *Sauter Mean Diameter change considering the nozzle droplet distribution.*

Both distributions show, in different diameter ranges, the same trend. The evaporation starts in the inlet section with a small diameter variation, and continues inside the blades with a strong decrease of the mean diameter in the first half of the passage; then, the diameter change becomes less significant in the second part, reaching the minimum at surfaces No. 60-65.

The following locations show a rapid increase of the mean particle size, reaching a maximum value at surface No. 90 and then decreasing again downstream.

The reason of this unexpected trend is not completely clear. The decrease of the diameter looks reasonable in the inlet and impeller region, but the cause of the increase after the trailing edge has no physical explanation.

The region downstream the trailing edge is characterized by turbulence, additional pressure increase and a small increase of temperature. These conditions should enhance evaporation and the droplets should become smaller, accordingly.

The first aspect to check is the correlation with evaporation, to understand if the vapour mass fraction increases as expected through all the domain. As shown in Figure 7.28 and 7.29 the vapour mass fraction increases smoothly across the impeller, which means that evaporation occurs in the whole stage without any anomaly. In addition, evaporation occurs in an equivalent way inside the passage and downstream the trailing edge; therefore, an additional diameter decrease should occur also in the latter region, e. g. between the surfaces No. 70 and No. 100.

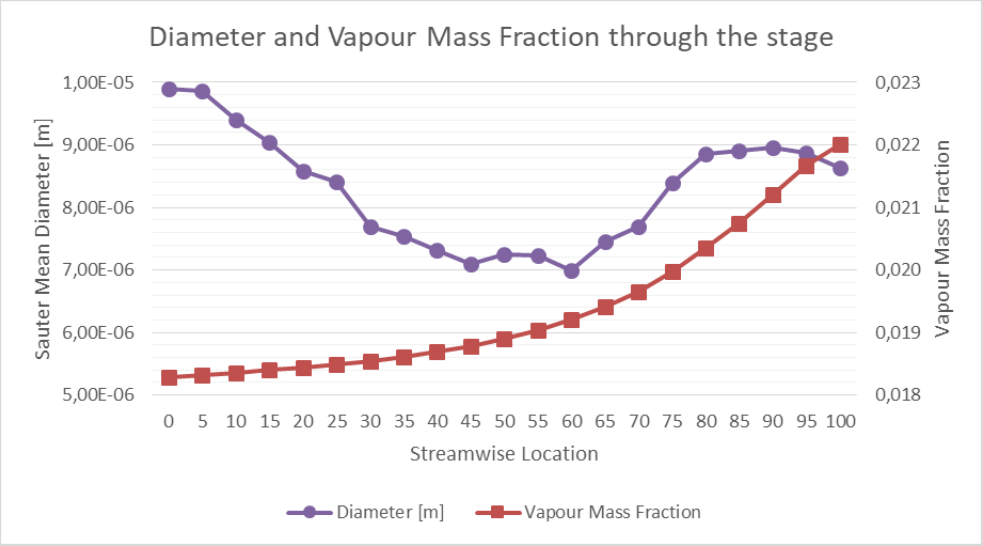

Figure 7.28. *Sauter mean diameter and vapour mass fraction through the impeller, 10 µm droplet distribution.*

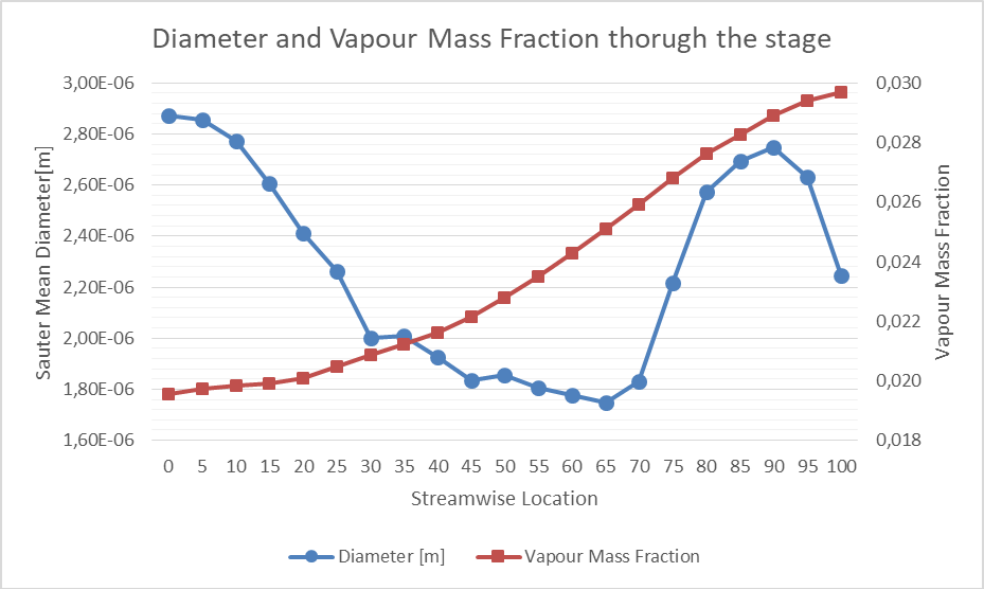

Figure 7.29. *Sauter mean diameter and vapour mass fraction through the impeller, nozzle droplet distribution.*

Although no physical explanation can be found, considering the model and the way in which the droplets parameters are calculated, some comments can be made.
Taking the BETE case as a reference, it should be considered that the Sauter Mean Diameter is calculated on the number of droplets still present in the liquid state, and that those particles whose diameter falls below 10^{-8} m (0.01 micrometre) are not considered anymore by the model.
This means that once the particle is almost completely evaporated, it is not taken in account anymore, and the Sauter Diameter is calculated on the remaining droplets. Thus, as many particles evaporate (many of them have a small size, in the nozzle distribution) completely, the mean diameter can increase due to the fact that these particles are not lowering its value anymore with their contribution. Analysing Figure 7.29, it may be said that many particles evaporate inside the impeller, before surface n. 70, as also shown by the vapour mass fraction value that increases significantly until the mentioned surface. Therefore, these particles are not considered anymore and only those which did not evaporate are used by the software to determine the mean diameter.

On the other hand, it should be observed that the same trend is found in the uniform distribution case, where this “effect” is less significant, as the particles at the inlet have all the same size and the size variation will occur in a more uniform way; it is unlikely to have, on one hand, a number of particles that evaporate completely, and on the other

a similar amount of droplets that do not evaporate and determine the increase the mean diameter after the trailing edge.
The scope of further work could be the analysis of the particles spectrum, implementing a method to characterize the full distribution, in addition to the use of its mean diameter.

7.3.3 Vapour mass fraction, pressure and temperature

The through-the-stage analysis is carried out examining not only the diameter change, but also the parameters that are affected by the evaporation of water inside the machine, such as pressure and temperature.

It is interesting to highlight the difference between a wet compression process and the dry one, where humid air is employed (hence, the designation “humid” in the following paragraphs) and no water injection is performed.
Figure 7.30 and 7.31 show how pressure increases through the domain in the dry case compared to the wet cases, 10 μm and nozzle distributions respectively.
In the first graph, the difference starts to be relevant in the second part of the passage, and the gap is evident after surface n. 65, e.g. in the region downstream the trailing edge.
A similar behaviour is found in the nozzle distribution case, but the higher pressure increase is evident from the first part of the impeller passage, and gets bigger downstream. As already pointed out in section 7.2, the smaller particles in the distribution guarantee a stronger effect, as their evaporation is easier and their contribution higher.

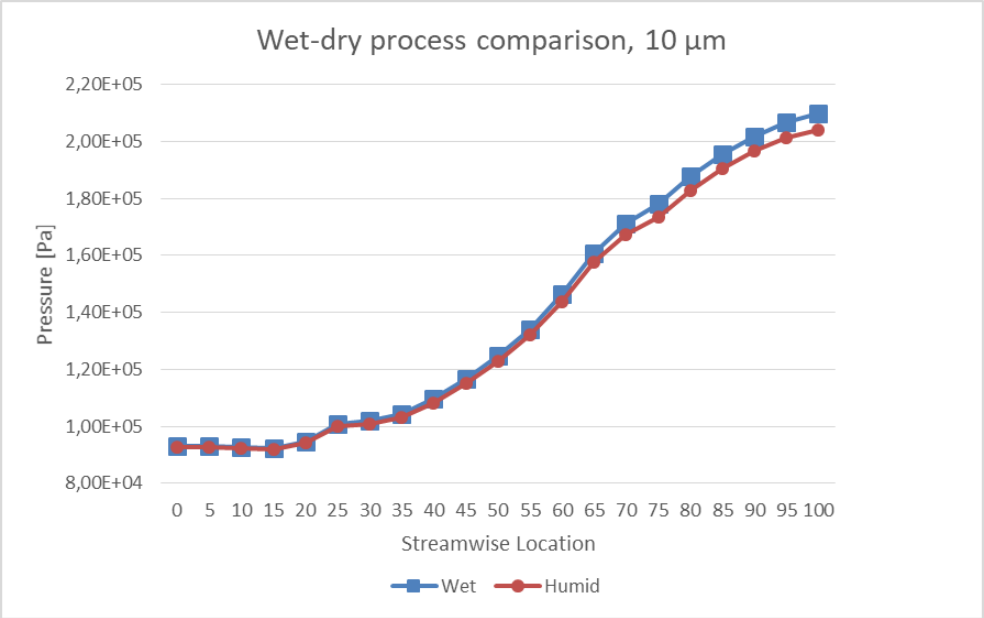

Figure 7.30. *Pressure rise through the stage, 10 µm droplets injection and dry compression comparison.*

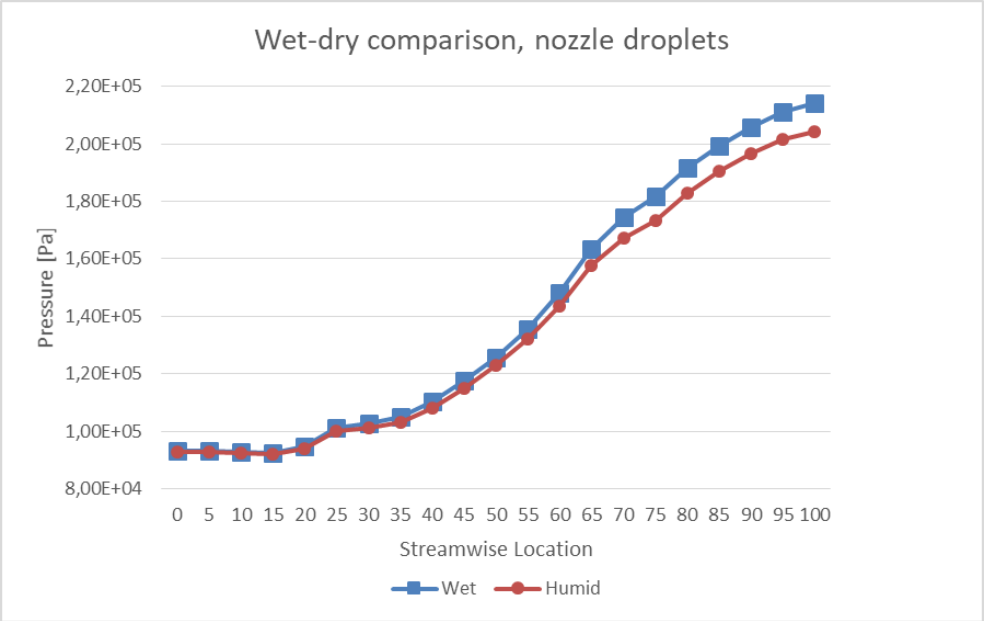

Figure 7.31. *Pressure rise through the stage, nozzle injection and dry compression comparison.*

It is interesting to notice that the droplets evaporate mainly inside the impeller and after they leave the blade passage, while at the inlet no effect is present, which is in accordance with this wet compression method, where evaporation is needed inside the machine.

The two cases show a common trend in terms of pressure, but their different deviation from the dry curve may be explained having a look at the vapour mass fraction curve in Figure 7.32 and 7.33.

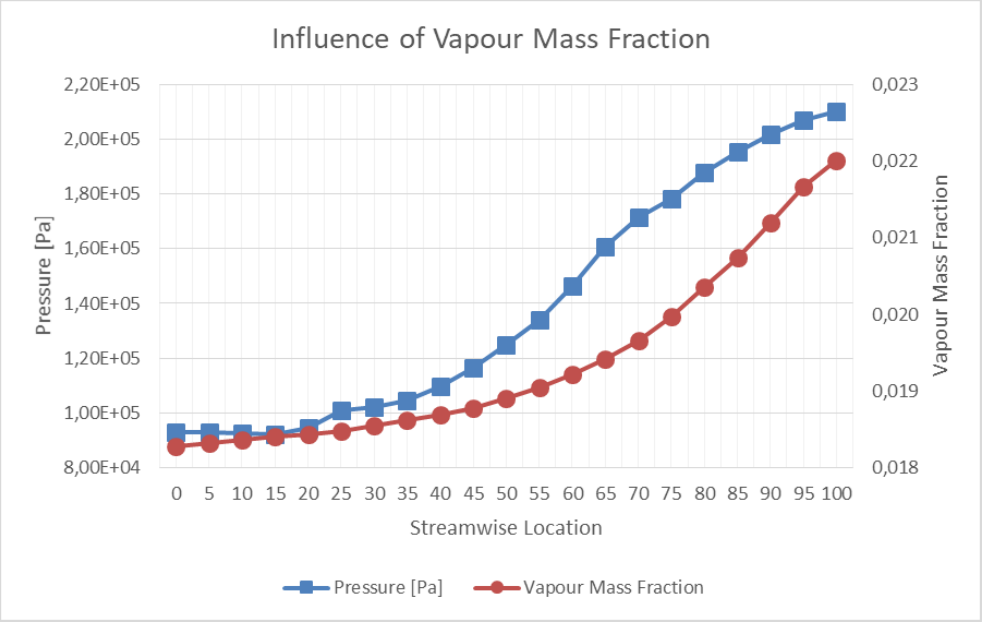

Figure 7.32. *Pressure and vapour mass fraction through the impeller, 10 μm distribution.*

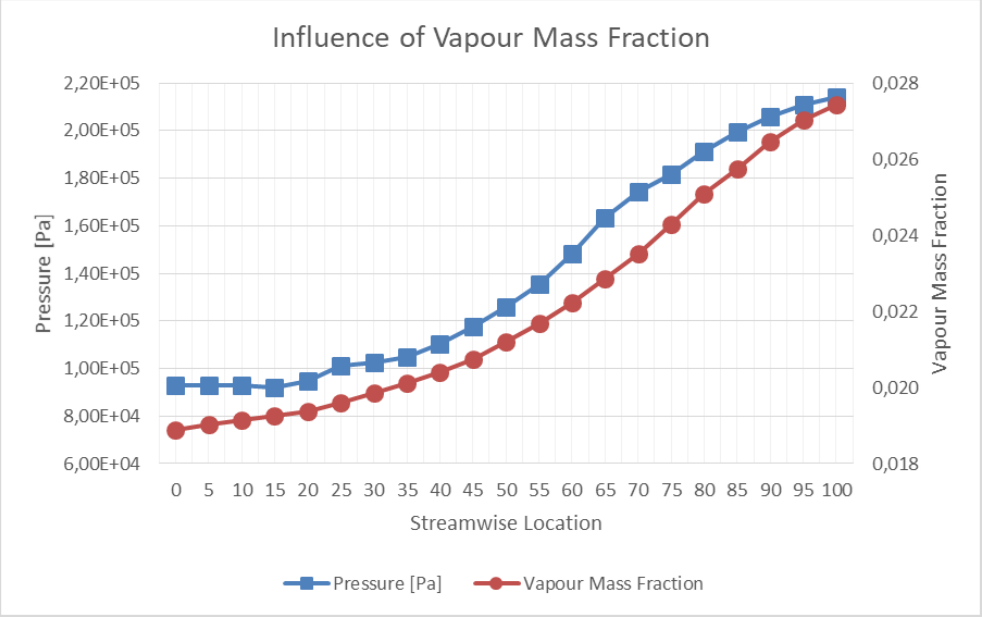

Figure 7.33. *Pressure and vapour mass fraction through the impeller, nozzle distribution.*

In the 10 micrometre case the evaporation takes place slowly in the first half of the path, as the slope of the water vapour line is small, while in the second part the slope becomes bigger and more evaporation occurs, especially after the trailing edge. The nozzle distribution, on the other hand, shows bigger evaporation since the first

positions inside the passage and then keeps increasing downstream. Therefore, the particle distribution does not only influence the overall performance of the machine, but also the position where evaporation happens with higher velocity: smaller particles enhance evaporation in the early locations inside the rotating domain, providing cooling at the beginning of the process rather than in later positions.

The difference is clear if the temperature profile is analysed and compared in the two cases, as shown in Figure 7.34 and 7.35. In the nozzle simulation the cooling effect is provided from the first points at the inlet of the R1 domain, and the deviation from the dry process becomes apparent starting from the blade edge and increases downstream as the droplets phase change goes on.

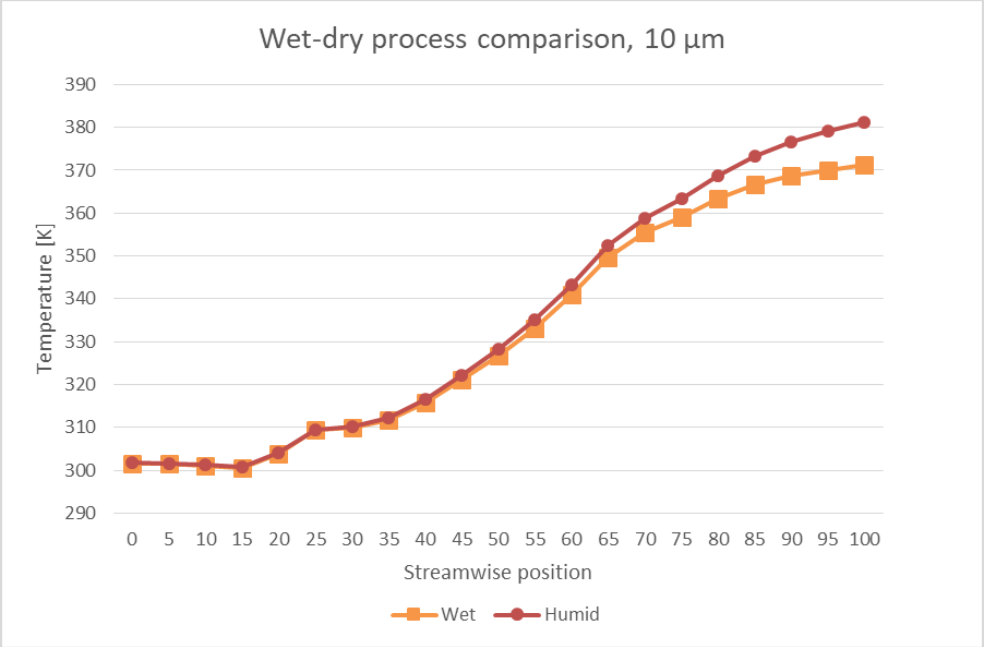

Figure 7.34. *Temperature rise through the impeller, 10 µm droplets injection and dry compression comparison.*

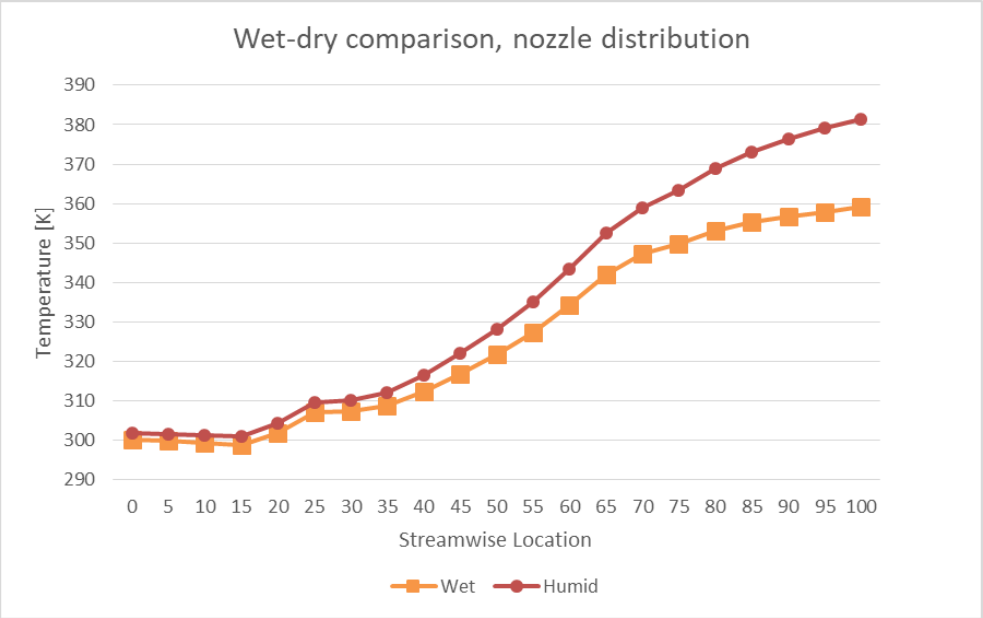

Figure 7.35. *Temperature rise through the impeller, nozzle injection and dry compression comparison.*

The temperature profile, as it occurs with the pressure one, is initially characterized by a small decrease in proximity of the leading edge, where local acceleration of the flow affects the parameters calculated on surface n. 15; then, as the fluid enters the passage between the blades, a rapid increase of both temperature and pressure occurs, due to the blades action. Then, the rise proceeds gradually towards the trailing edge. After the blade passage, pressure keeps increasing, while the temperature rise is reduced: evaporation continues in this region, water vapour increases and provides more cooling effect.

The same trend can be observed in the following figures, 7.36 and 7.37, where the difference between the dry and the two wet cases analysed is plotted, in terms of pressure and temperature respectively. The different slope of the lines is clear and their shape resembles the absolute rise seen in the previous figures.

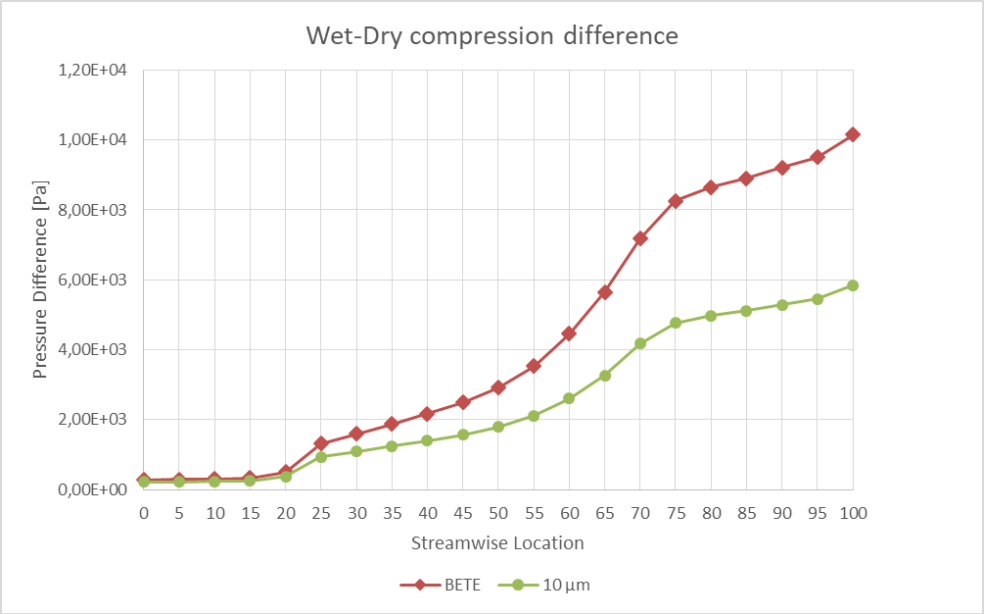

Figure 7.36. *Pressure difference between dry and wet cases across the impeller.*

Figure 7.36 shows a small difference at the inlet, as different vapour content in the mixture is present; then, the effect becomes more significant inside the impeller, where pressure mostly increases. The region downstream is characterized by an increased difference between the three cases. The final increase is about 3% for the 10 micrometre case, and 5% using the BETE distribution.

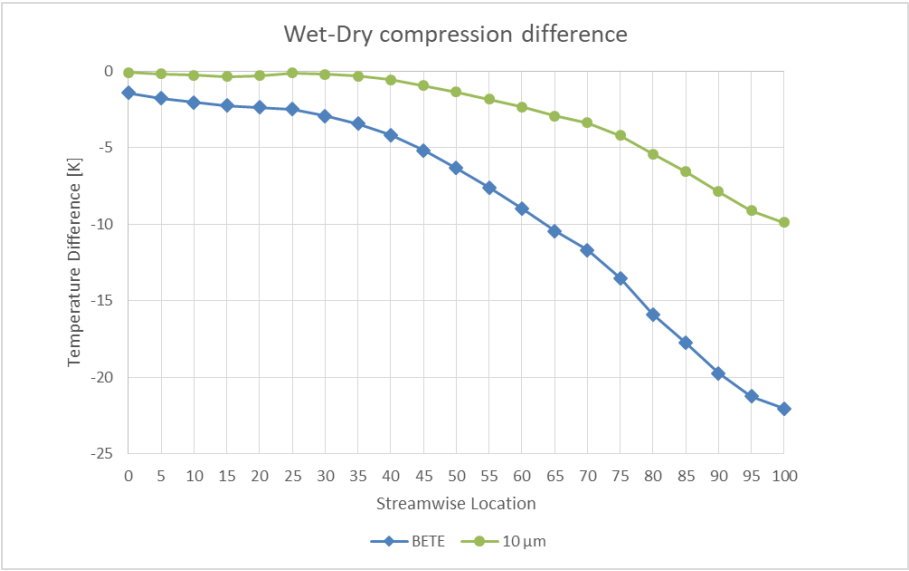

Figure 7.37. *Temperature difference between dry and wet cases across the impeller.*

Looking at Figure 7.37 it can be noticed how the 10 micrometre droplets do not provide any improvement in the first part of the path, while inside the impeller and after the cooling effect is present and increases streamwise. The nozzle distribution, however,

shows a lower temperature (even if just 1-2 K lower) since the beginning, and then cooling becomes larger through the impeller and especially after the trailing edge. At the outlet of the domain the temperature reduction is about 22 K in the nozzle case, and around 10 K for the other case.

7.3.4 Injection rate influence

A bigger amount of evaporated water changes not only the overall effect, but also the position where the thermodynamic parameters vary significantly. The evaporation depends not only on the droplets size but also on the injection rate. Hence, it is interesting to describe its influence on the variation of thermodynamic variables through the stage. The nozzle case, using 1.4% injection rate, is analysed.

The vapour mass fraction is plotted in Figure 7.38. Its variation along the streamwise direction can be analysed referring to the inlet section, the blade passage and the outlet region. The diagram shows that a higher injection rate changes the vapour mass fraction from the first location, and then the curves diverge as a natural consequence of the different amount of water injected in the machine. On the other side, it should be kept in mind that increasing the injection rate, the efficiency of the evaporation decreases, therefore less water participates in the process improvement, and the lines look more close than they could be if the same percentage of water took part in the phase change.

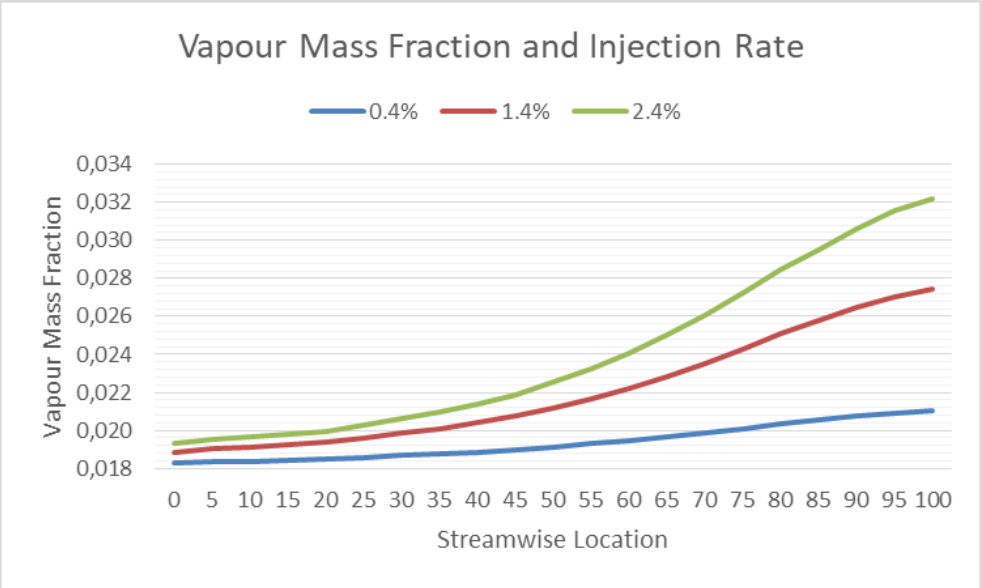

Figure 7.38. *Vapour mass fraction through the impeller, injection rates comparison.*

In addition, the same three regions are used to investigate where the bigger vapour increase happens inside the machine. As shown in Figure 7.39, the share on the total vapour increase changes with the injection rate, as different regions are responsible for more or less evaporation.

The inlet contributes only in a small part, and its contribution decreases with more water injection: the reason can be found in the fact that, without any blade action, the amount of water that can be evaporated is small, and increasing the water mass flow rate this amount becomes even smaller in terms of share. The values are given in Table 7.20 and Table 7.21 in terms of vapour mass fraction (partial increase), and share on the total increase.

Table 7.20. *Water vapour, mass fraction increase.*

	Injection rate		
	0.4%	1.4%	2.4%
Inlet increase	0,0002	0,0004	0,0004
Impeller increase	0,0014	0,0043	0,0063
Outlet increase	0,0011	0,0039	0,0061
Total increase	0,0027	0,0086	0,0128

Table 7.21. *Water vapour, local increase on the total.*

	Injection rate		
	0.4%	1.4%	2.4%
Inlet increase	5,80%	4,38%	3,36%
Impeller increase	52,49%	49,95%	48,93%
Outlet increase	41,71%	45,67%	47,71%

A higher injection rate leads to higher vapour generation, with a small decrease on the total evaporation share inside the impeller; at the same time the downstream region percentage increases, as shown in Figure 7.39 by the red and green bars.

This evaporation shift towards downstream positions is probably due to the fact that higher injection rates lead to lower evaporation efficiency, therefore not only in the whole domain, but also in the impeller, the amount of water vapour generated is higher, but a higher amount of water does not evaporate as fast as in the 0.4% case. Hence, more water (considering the share on the injected quantity) can be found in the liquid phase and its partial evaporation is shifted afterwards, in the region downstream.

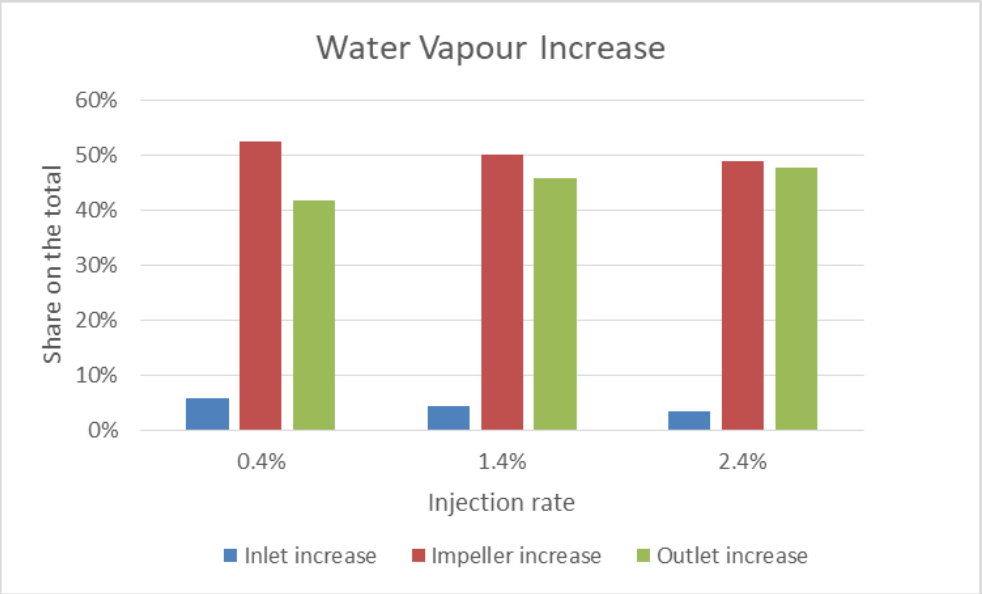

Figure 7.39. *Local increase of water vapour mass fraction on the total.*

The same phenomenon can be analysed taking the Sauter Mean Diameter variable, and plotting its decrease through the stage. Figure 7.40 shows for the three injection rates a similar decrease in the first section, but after the surfaces n. 20-25 the higher injection rate leads to a bigger particle mean diameter, as evident in proximity of surface n. 60, where the values are 1.48 μm, 1.64 μm, 1.76 μm respectively, for the 0.4%, 1.4% and 2.4% cases.

Downstream the position n.60, the difference becomes even more evident, although it occurs where the unexpected diameter increase happens. Nevertheless, the final value follows the same trend, with the values 1.42 μm, 2.07 μm, 2.56 μm, listed in order of increasing injection rate.

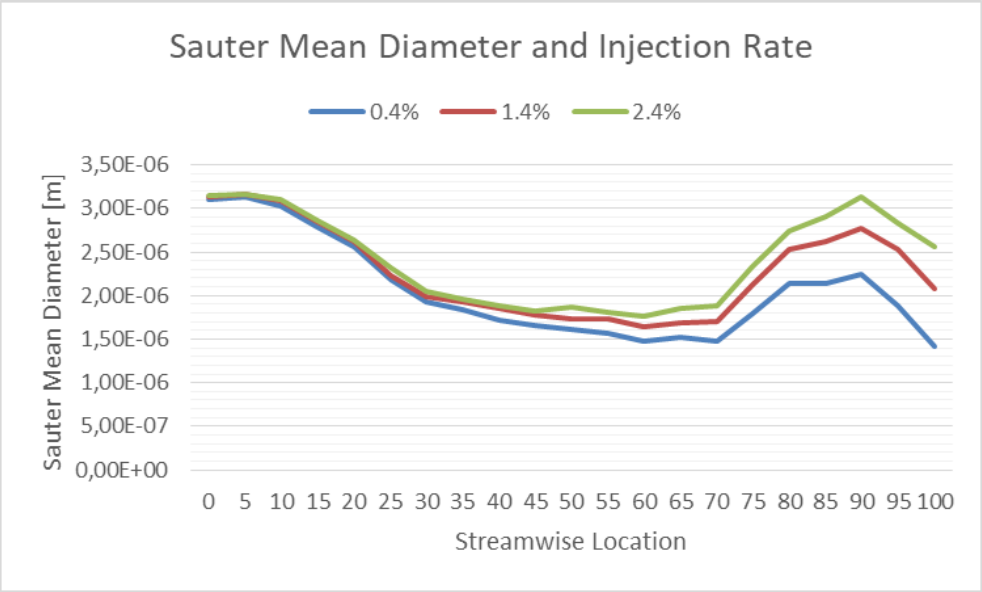

Figure 7.40. *Injection rate influence on the mean droplet diameter change through the impeller.*

The analysis can be completed describing the evaporation influence on pressure and temperature across the domain.

The use of higher injection rates lead to a higher final value of pressure, but inside the impeller the difference is smaller, as it can be seen in Figure 7.41: the curves start to diverge only in the last part of the blade section, and the difference increases downstream the leading edge.

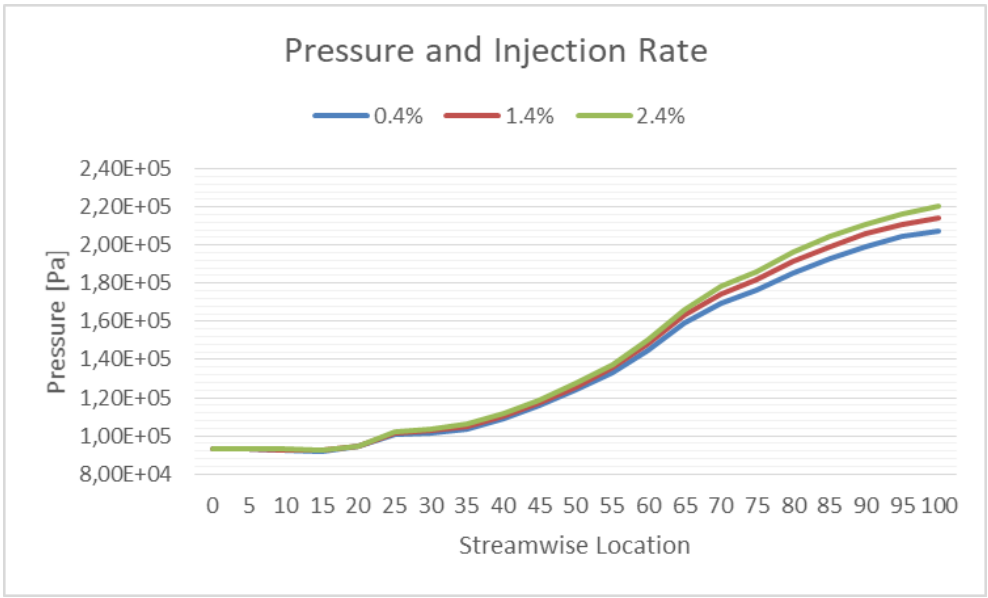

Figure 7.41. *Pressure rise through the stage, injection rate influence.*

Moreover, the data show the same distribution of the pressure variation through the machine, as reported in Table 7.22, the values are almost the same.

Table 7.22. *Local pressure increase on the total.*

	Injection rate		
	0.4%	1.4%	2.4%
Inlet increase	-0,81%	-0,74%	-0,69%
Impeller increase	67,71%	67,74%	67,56%
Outlet increase	33,09%	33,00%	33,13%

Analysing the effect on temperature, two aspects should be noticed.
The cooling effect inside the impeller is clear (see Figure 7.42), and starts from the first locations at the inlet; then it becomes more relevant as the compression goes on. Lastly, the effect is very strong in the outlet region, where no blade action (and fluid heating source) is present, and the evaporation effect prevails, lowering the temperature in a significant way when the water injection is considerable.

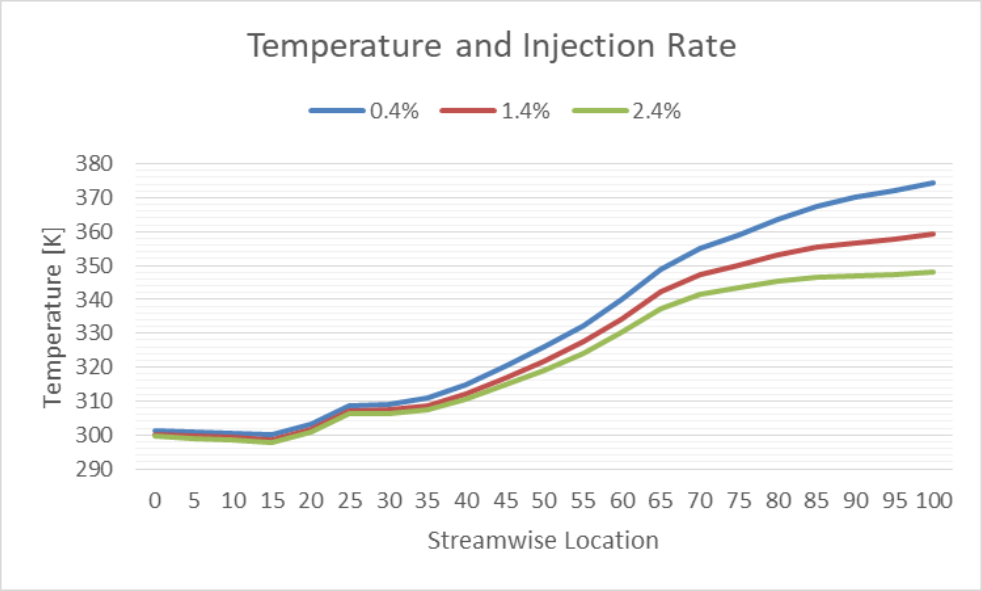

Figure 7.42. *Temperature rise through the stage, injection rate influence.*

Moreover, this aspect can be examined more in depth considering where the temperature increase occurs and how it is influenced by the water quantity. Figure 7.43 draws attention to the difference introduced by the injection rate used. In the outlet region the temperature increase share on the total decreases, due to the higher amount of water available to be evaporated after the impeller; on the other hand, as a consequence of the cooling effect, the impeller is responsible for a higher percentage when the injection rate is bigger. This also depends on the higher power consumption required, but is influenced by the single case behaviour.

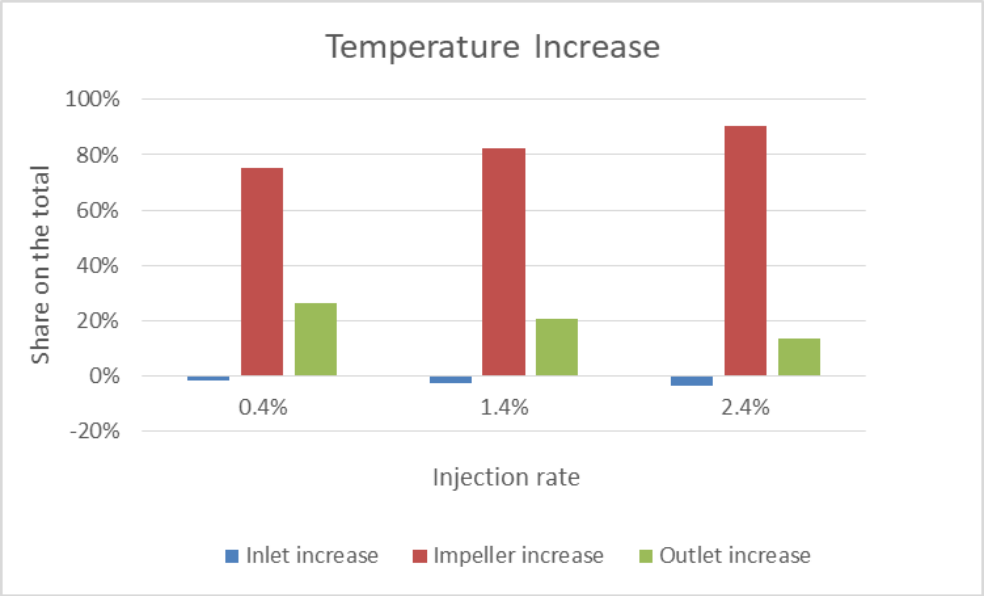

Figure 7.43. *Local temperature variation on the total.*

The corresponding values are reported in Table 7.23.

Table 7.23. *Local pressure increase on the total.*

	Injection rate		
	0.4%	1.4%	2.4%
Inlet increase	-1,61%	-2,79%	-3,59%
Impeller increase	75,14%	82,33%	90,39%
Outlet increase	26,47%	20,47%	13,20%
Total increase [K]	73,01	58,94	48,46

Conclusion

The present investigation focused on the overall effect of water droplets injection in an air compressor stage, considering two main aspects that influence the machine performance: the droplet size and the amount of water injected.

The droplet diameter influences the thermodynamic parameters in a strong manner, as shown first of all in the analysis of the evaporated water according to the particle size. Smaller particles enhance evaporation thanks to their smaller mass and smaller surface area/volume ratio, providing a higher cooling effect inside the stage. The best performance in terms of temperature reduction and pressure rise is obtained using 5 micrometre droplets, whereas bigger particles such as 20 and 50 micrometre ones do not produce significant improvement.

The injection rate as well produces a strong effect, as increasing the amount of water injected leads to a bigger amount of evaporated water mass, though the percentage (evaporation efficiency) on the total amount decreases.

The compressor power analysis is influenced by the boundary conditions, which let the outlet parameters free to vary, except the gaseous mass flow rate; these model settings lead to a comparison between different performances and require a suitable parameter to describe the improvement obtained.

As the common efficiency definition cannot be applied in a wet compression process, the isothermal efficiency is introduced to evaluate and compare the different cases analysed. Moreover, the polytropic index is added as second parameter for the evaluation.

For both parameters a general trend is highlighted, showing a correlation between the evaporated water inside the machine and the process improvement obtained in terms of efficiency increase/polytropic index decrease: a stronger evaporation leads to a stronger cooling effect, improving the machine performance.

The investigation is carried out using also a discrete nozzle droplet distribution, whose result resembles the 5 micrometre case, while in other aspects give a slightly lower improvement.

In general, the highest injection rate and the smaller droplet size show a specific work reduction around 4.9%, which can be compared to what Abdelwahab pointed out in his numerical investigation using a comparable droplet size and injection rates up to 3%.

In addition, this work provides a through-the-impeller analysis, in which the comparison between the 10 micrometre and the nozzle distributions shows that a different droplet size influences not only the overall machine behaviour, but also the

location where evaporation begins. This aspect leads to a variation of droplet diameter, vapour mass fraction and temperature that becomes significant in earlier locations when smaller droplets are injected in the machine.
Finally, the injection rate influence has been examined inside the impeller, and a higher effect on temperature emerges as more water is injected; at the same time, a smaller decrease of the droplet mean diameter is observed, due to the lower evaporation efficiency assessed with higher injection rates.

The model implemented in this work provides further knowledge on the topic, with a low computational cost and some simplifying hypothesis. One of these is the frictionless approach, which led to a different mesh structure and slightly different results in the dry air case performance. Future work can be done to set a model able to compute in a fast and efficient way the particles physics that play a great role in increasing the solver instability and the computational time.
A second aspect is related to the behaviour of the droplets and their interaction with the walls: in this model a rebounding wall is set, while particles would tend to stick to the walls and form liquid films. The model can be developed introducing a specific feature to simulate the wall sticking and to understand if water sheets are formed and cause secondary droplets, which represent a remarkable concern for the machine, as their size is bigger and they can be responsible of unacceptable erosion inside the stage.
Lastly, an interesting improvement of the model could be achieved with the insertion of a particle spectrum analysis, in order to examine how the droplet diameter varies through the impeller, providing more understanding about it, as the use of the Sauter mean diameter cannot provide a detailed analysis of this aspect.

Bibliography

[1] M. Obermüller, K.-J. Schmidt, H. Schulte, D. Peitsch, *Some aspects on wet compression – physical effects and modelling strategies used in engine performance tools*, Deutscher Luft- und Raumfahrtkongress, 2012

[2] Reece V. Hensley, *Theoretical performance of an axial-flow compressor in a gas-turbine engine operating with inlet water injection*, NACA, March 1952

[3] William L. Beede, Joseph T. Hamrick, Joseph R. Withee, Jr., *Evaluation of centrifugal compressor performance with water injection*, National Advisory Committee for Aeronautics, Washington July 18, 1951

[4] Qun Zheng, Yufeng Sun, Shuying Li and Yunhui Wang, *Thermodynamic Analyses of Wet Compression Process in the Compressor of Gas Turbine*, ASME Turbo Expo 2002

[5] A. J. White and A. J. Meacock, *An Evaluation of the Effects of Water Injection on Compressor Performance*, ASME Turbo Expo 2003

[6] R. Bhargava, C. B. Meher-Homji, *Parametric analysis of existing gas turbines with inlet evaporative and overspray fogging*, ASME Turbo Expo 2002

[7] J. P. Schnitzler, I. von Deschwanden, S. Clauss, F. K. Benra, H. J. Dohmen and K. Werner, *Experimental determination of a four stage axial compressor map operating in wet compression*, ASME Turbo Expo 2014

[8] Lanxin Sun, Qun Zheng, Yijin Li and Rakesh Bhargava, *Understanding effects of wet compression on separated flow behavior in an axial compressor stage using cfd analysis*, *J. Turbomach* 133(3), 031026 (Feb 28, 2011)

[9] Jobaidur R. Khan and Ting Wang, *Three-dimensional modeling for wet compression in a single stage compressor including liquid particle erosion analysis*, *J. Eng. Gas Turbines Power* 133(1), 012001 (Sep 27, 2010)

[10] Lanxin Sun, Qun Zheng, Mingcong Luo, Yijin Li and Rakesh Bhargava, *On the behavior of water droplets when moving onto blade surface in a wet compression transonic compressor*, *J. Eng. Gas Turbines Power* 133(8), 082001 (Apr 07, 2011)
[11] Oyvind Hundseid, Lars E. Bakken, Trond G. Grüner, Lars Brenne and Tor Bjorge, *Wet gas performance of a single stage centrifugal compressor*, ASME Turbo Expo 2008

[12] Matteo Bertoneri, Simone Duni, David Ransom, Luigi Podestà, Massimo Camatti, Manuele Bigi and Melissa Wilcox, *Measured performance of two-stage centrifugal compressor under wet gas conditions*, ASME Turbo Expo 2012

[13] Ahmed Abdelwahab, *An Investigation Of The Use Of Wet Compression In Industrial Centrifugal Compressors*, ASME Turbo Expo 2006

[14] Anish Surendran and Heuy Dong Kim, *Effects of wet compression on the flow behavior of a centrifugal compressor: a CFD analysis*, ASME Turbo Expo 2014

[15] ANSYS CFX 18.0, CFX-Solver Modeling Guide, 2017

[16] Sebastian Schuster, Friedrich-Karl Benra, Hans Josef Dohmen, Sven König and Uwe Martens, *Sensitivity analysis of condensation model constants on calculated liquid film motion in radial turbines*, ASME Turbo Expo 2014

[17] Sebastian Schuster, Friedrich-Karl Benra, Dieter Brillert, *Droplet deposition in radial turbines*, European Journal of Mechanics - B/Fluids Volume 61, Part 2, January–February 2017

[18] Hai Zhang, Bin Jiang, Mingcong Luo, Xiangkun Liu, Shuangming Fan, Lu Yang and Qun Zheng, *Investigation of water film formation on blade surfaces of a wet Compression transonic compressor rotor*, ASME Turbo Expo 2015

[19] Tjark Eisfeld, *Experimentelle Untersuchung der Aerodynamik einer mit Wassertropfen beladenen Luftströmung in einem ebenen Verdichtergitter*, Hamburg 2011